Processing and Interpretation of Near-Earth Satellite Magnetic Data

Luc André Georges Antoine

A thesis submitted to the Faculty of Science,
University of the Witwatersrand, Johannesburg,
in fulfilment of the requirements for the
degree of Doctor of Philosophy.

Johannesburg, 1990.

Abstract

The processing of near-earth satellite magnetometer data towards extracting an improved lithosphere anomaly map is addressed. The two aspects of the data reduction route where data quality has been compromised most by contemporary methods is researched, namely: (1) correcting for the variable altitude of the survey platform and (2) removal of the ionospheric field effects. New algorithms are developed using computer simulations and are successfully implemented on Magsat data. The altitude correction is based on a robust (median) regression of the amplitude versus altitude. It also serves as a noise preprocessing filter and requires no *a priori* assumptions of magnetisation. After removal of the core and ring current field effects, using published procedures, application of the median regression filter with different local time and geographical constraints produces two magnetic field maps, viz.: (1) ionospheric and (2) ionosphere-contaminated lithospheric maps. The target lithospheric signal is extracted with a new two-dimensional data adaptive filter where the ionosphere and ionosphere-contaminated lithosphere signals are input. This process is applied for two local times (dawn and dusk) and, to optimise noise cancellation, the two lithospheric maps are input to a data adaptive filter structure which, using a method of converging operations, results in the final lithospheric anomaly map.

The southern African region is selected to implement this new data reduction approach on Magsat data and the ensuing map is interpreted. This region is selected because (1) it is a focal point of Gondwana reconstructions and (2) both continental and oceanic magnetic anomaly types are present. The anomaly map is image-processed and composite images (Magsat with Seasat and bathymetry data) are presented to aid the interpretation. This anomaly map shows a marked improvement on previously published maps in terms of resolution and correlation with geological provinces. A north-south oceanic anomaly bordering the west coast of southern Africa is now recognised. Continental anomalies are found to be localised within major tectonic provinces. The increase in magnetisation is interpreted to be the result of the Hopkinson effect of a thickened crust in a higher geothermal gradient. The oceanic anomalies (i.e. the intense Walvis Ridge and Agulhas anomalies) are interpreted to represent remanently magnetised (during Cretaceous Quiet Times) thickened crust. The Agulhas anomaly is the remnant 'scar' of the process that led to the fragmentation of Gond-

wana. It is hypothesised that Gondwana was fragmented by an upwelling of hotter than normal asthenosphere centred directly below the Agulhas anomaly.

Declaration

I declare that this thesis is entirely my own work, except where explicitely stated in the Preface. It is being submitted for the degree of Doctor of Philosophy in the University of the Witwatersrand, Johannesburg. It has not been submitted before for any other degree or examination in any other University.

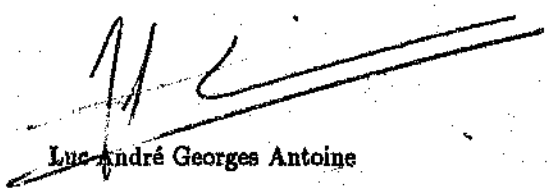

Luc André Georges Antoine

This 13th day of June, 1990.

Dedication

To Wendy, Guy and Jacques

Contents

List of Figures

List of Tables

Preface

The realisation of the digital geological map of Gondwana (de Wit et al., 1988) has given impetus to the concept of creating a multidisciplinary geoscientific database of Gondwana (Wilsher et al., 1989). It is a long-term objective of the Geological Department of the University of Cape Town in collaboration with other institutions to achieve this goal by co-registering geological, geochemical and geophysical datasets of Gondwana. This database has been given the acronym of GO-GEOID (Gondwana-Geoscientific Indexing Database).

Two doctoral research theses were initiated as fundamental steps towards achieving this end, namely: (1) "Distribution of selected transition elements within mineral deposits across Gondwana, with geodynamic implications" by Wendy Wilsher of the University of Cape Town and (2) this study. The latter research is motivated on the principle that satellite altitude magnetometer data constitutes, in the short-term, a complete global dataset, albeit of low resolution, and can be co-registered with an equally complete gravity dataset (Geosat, Seasat and regional continental data). These datasets will serve as precursors to later, higher resolution, magnetic and gravity compilations for a Gondwana Atlas.

The thesis addresses the processing of satellite-borne magnetometer measurements towards extracting an improved signal orginating from remanent and induced magnetisation in rock forming minerals of the crust. Magnetometer measurements made from a satellite-based platform constitute a total response of signal components originating from various sources, viz.: (1) the earth's core, (2) the magnetosphere and (3) the target crustal magnetisation. Although, the signal separation has been achieved since 1975 (Regan et al., 1975), there are several aspects of the data reduction which compromises data resolution and quality and these are addressed in this study.

This thesis is structured so as to encapsulate the broad spectrum of topics which require to be covered. Chapter 1 provides the background and research objectives while Chapters 2 and 3 review the geomagnetic field and external fields, respectively. Chapter 4 addresses the problem of the variable altitude of the survey platform and presents an effective, simple, robust, linear regression technique, as an adequate solution to the problem. Removal of magnetic field effects originating from the ionosphere are investigated in the following Chapter. Here a novel data adaptive filter is developed to facilitate separating the ionospheric field

from the target crustal field. All algorithms were developed using synthetic data. In Chapter 6 the newly developed procedures are implemented using a selected Magsat dataset of the southern African region. The resultant magnetic anomaly map is image-processed and interpreted in Chapter 7. These results provide a new insight into magnetisation of continental and oceanic crust and, into geodynamic processes.

A preliminary interpretation of the Agulhas Magsat anomaly from previously processed Magsat data was presented by the author on August 3 at the IAGA, 6th Scientific Assembly, Division I (Geophysical anomalies of Gondwana), Exeter, 1989. A paper was subsequently submitted to Tectonophysics for a special issue of the proceedings. The paper is co-authored with A.B. Moyes whose contribution is to the geology of Antarctica and to the reconstruction of Gondwana; and which is, in part, incorporated in Chapter 7. As a consequence of the newly processed results the interpreted remanent polarisation vector of the probable source of the Agulhas Magsat anomaly has changed but not the inferred geodynamic processes.

Acknowledgements

I wish to thank friends and colleagues whose contributions helped in the successful completion of this work. I express my appreciation for the help, guidance and criticism offered by my supervisors Branko Corner, Maarten de Wit and Deon Kühn.

I thank Artur Cichowicz, Cas Lötter, Ray Durrheim and Gordon Cooper for sharing many hours of enlightening discussions.

Tiens Hattingh introduced me to data adaptive filters and their uses. I am grateful for his help and for reviewing those aspects of the thesis.

To Paul Versnel and Alistair Lamb many thanks for their help and cheerful co-operation with the image-processing. This processing was performed on the I²S image-processing facility of Gold Fields of S.A. to whom I am grateful.

I express my appreciation to Peter Sutcliffe for his review of the external fields section.

Lastly, but not least, I thank Ingrid Turton, Sonia Bunge and again Gordon Cooper for their help with the many computing problems.

Chapter 1

Introduction

Satellite observation of the earth's magnetic field began in 1958 with the Sputnik 3 satellite. Since then several satellites were launched to study the near-earth geomagnetic field, for example: Vanguard 3 (1959), OGO-2, 4 and 6 (1967-1971) (Taylor et al., 1983). The most recent of the near-earth magnetometer satellites is Magsat, launched in 1979. The Magsat d[illegible]e unique in that for the first time three-component vector measurements were made. To augment the three-axis fluxgate magnetometer data, a Caesium vapour magnetometer was also included for high resolution scalar measurements. Unfortunately, this scalar magnetometer malfunctioned and could only be used for in-flight calibration purposes.

Magnetic measurements made from satellite-based platforms were originally directed towards magnetospheric studies. First confirmation that crust or lithosphere magnetic anomalies could be detected from satellite magnetometer data was made by Regan et al. (1973) with the identification of, the now well known, central African Bangui anomaly. The first global crustal magnetic anomaly map was published by Regan et al. (1975), processed from POGO (OGO-2,4 & 6) satellite measurements. The successful generation of crustal anomaly maps from POGO was a strong motivating force for the undertaking of the Magsat mission. Magsat was specifically designed for optimum main field modelling and for crustal magnetic anomaly detection. Following the successful completion of the mission there has been a steady stream of publications mostly related to crustal magnetic field studies (Langel and Benson, 1987). More than half of the research from the Magsat data is directed towards crustal studies, while some 30 % is equally spread in external field and main field studies. These publications bear testimony to Magsat having met its objectives.

The term *lithosphere* will be used, in preference to *crustal*, for discussion of satellite-derived magnetic anomaly maps. The reason for the choice is to conform with present usage, since it is now being argued that a substantial part of the 'crustal' signal may originate from the subcrustal part of the lithosphere (although this point is still contentious). More importantly the term 'lithosphere' gives a perspective of the spatial resolution of present near-earth satellite data which is, at best, a wavelength of 250 km (Sailor et al., 1982).

This work addresses the processing of near-earth satellite magnetometer data towards extracting improved lithospheric anomaly maps. It was decided to use Magsat data in this work because it is a superior dataset and because it has been adopted by most investigators. Results may therefore readily be compared with other studies. This Chapter discusses mission design, spatial resolution of near-earth satellite data and briefly outlines existing processing routes towards generating magnetic anomaly maps. With this background the research objectives are presented.

1.1 The Magsat mission

Magsat was placed into a twilight, sun synchronous, near-polar orbit with an inclination of $96,76^0$. The orbit's apogee and perigee, from the earth's surface, were 561 km and 352 km respectively. The near-polar orbit was designed to provide an almost complete geometrical coverage of the earth for main field modelling and for the preparation of lithospheric anomaly maps. The satellite was placed into orbit on 30 October, 1979 and remained in orbit until 11 June, 1980. An explicit account of the mission, design, instrumentation and data acquistion is given in Langel et al. (1981 and 1982b). This information is summarised here for the sake of completeness and continuity.

The instruments were designed and constructed as two separate modules; a base module and an instrument module. The instrument module consisted of: (1) the attitude determination systems for the satellite and for the vector magnetometer and, (2) the magnetometer sensors fixed to a platform on an extended 6 m magnetometer boom. The base module contained all the supporting systems. The scalar magnetometer was a Ceasium vapour type with an accuracy of 1,5 nT. However, this magnetometer malfunctioned soon after launch and was rendered unusable other than for in-flight calibration of the vector magnetometer.

error source	scalar (nT)	vector (nT)
instrument	1,5	3,0
position and time	1,0	1,0
digitisation	0,5	0,5
attitude control		4,8
spacecraft fields	0,5	0,5
r.s.s.	1,96	5,8

Table 1.1: Magsat survey noise. (After Langel et al., 1982b).

The vector magnetometer was a three-axis fluxgate type with an accuracy of 3 nT in each axis. This instrument showed a slight drift of some 20 nT over the entire mission. The sampling rates for the scalar and vector magnetometers were 8 and 16 samples per second, respectively.

Magsat's survey specifications required that the magnetic field orientation be known within 20 arcsec. Fine attitude control was achieved with the use of two star cameras, a sun sensor, a pitch gyro and the attitude transfer system. Survey specifications of the satellite's position required a tracking accuracy of less than 60 m radial and 300 m horizontal to maintain an error below 1 nT.

The survey noise for the vector data is approximately 6 nT r.s.s. as detailed in Table 1.1.

1.1.1 The data set

The Magsat data that were employed in this study, to produce the anomaly map of the southern African region, were obtained from a suite of tapes containing a culled data set, the INV-B format, provided by NASA (Langel et al., 1981; Abrams and Gilson, 1982). The INV-B tapes contain a five second sample interval. In addition, some necessary and useful information are included, viz.: geocentric position, a mean value from samples within the 5 s interval, predicted fields from the spherical harmonic model MGST 4/81, the MGST 4/81 model coefficients, the Kp magnetic activity index, dip latitude, universal time, magnetic local time and Dst coefficients.

1.2 Magnetic lithosphere signal resolution

It is important to take note of system limitations so that the significance of interpretations of lithospheric anomaly maps may be assessed in context. A substantial amount of magnetic data has been acquired on the earth's surface and at aircraft altitudes ranging from several metres to some 1 to 2 km. If one considers marine surveys then magnetic observations have been extended to source-to-sensor separations of up to 6 km. There is a total defficiency of magnetic data in the large gap between these terrain clearances and those of near-earth satellite data (ca 400 km). Some successful attempts have been made to fill this gap with atmospheric balloon surveys at altitudes of 40 km (Cohen et al., 1986). The Geopotential Research Mission (GRM) is intended to fill this gap with an intended survey altitude of 150 km (Taylor et al., 1983; Yionoulis and Piscane, 1985; Webster et al., 1985; Taylor et al., 1989). The limiting factor to resolve magnetic signatures of structures is the altitude of observations; in this respect Magsat data suffer the coarsest resolution of the above datasets.

The ability to resolve magnetic signatures may be considered in several ways, for example, Sailor et al. (1982) determined from the Magsat data, using spectral analysis, the wavelength passband of lithospheric anomalies. Webster et al. (1985) define resolution "as the ability to distinguish, as separate entities, two bodies of equal magnetisation and shape separated and surrounded by material of different magnetisation". Sailor et al. (1982) have shown that an absolute minimum resovable along-track wavelength of 250 km may be obtained from Magsat data. Coherence analysis, for the Southeast Indian Ocean region, showed that Magsat data are repeatable for track-to-track wavelengths greater than 700 km; therefore a spatial resolution in the order of one (along-track) to four (track-to-track) degree spherical tesserae may be deduced for this region.

Webster et al. (1985) through forward modelling attempt to quantify resolution. They consider a model comprising two 200 by 200 km crustal blocks (40 km thick) separated by 150 km having a magnetic susceptibility contrast of 0,0005 in a 57000 nT ambient field (cgs units). The resolution parameter R is quantified as

$$R = (A_1 + A_2)/2 - B \tag{1.1}$$

where A_1 and A_2 are the peak anomaly amplitudes while B is the trough amplitude separating the anomaly peaks (Fig. 1.1).

The emphasis of their work was to demonstrate that the most dominant effect on resolution is the altitude of observation. Figure 1.1 serves to illustrate that anomalies from geolcgical structures, such as the given model, are at the limits of the resolving capabilities of Magsat. Also, the effect of increased source to sensor separation is to provide an integrated (bulk) magnetisation image of the crust/lithosphere.

1.3 Processing of near-earth magnetometer data

The total magnetic field as observed by a near-earth satellite magnetometer comprises several contributing sources, viz.: (1) the main core field produced by the geodynamo, (2) the lithospheric field from the distribution of induced and remanent magnetisation in rock forming minerals, (3) the external magnetic fields originating from the magnetosphere and the ionosphere and, (4) the internal induced magnetic fields from electromagnetic induction of the lower mantle by temporal variations of the external fields. The contributory sources and relative signal strengths are summarised schematically in figure 1.2.

The target component field in this study is the lithospheric field. The processing route since the early work of Regan et al. (1973), towards extracting the lithospheric anomaly field, has not deviated fundamentally from the following generalised procedures, namely:

- A main field model is defined by a truncated (degree and order 13) spherical harmonic series of the global data set.
- The main field model is subtracted from the total field. The residual from this operation contains ring current, ionospheric and lithospheric components.
- A ring current model is defined by a first-degree zonal harmonic function. This function takes into consideration the internal induced component.
- The ring current model is subtracted. The remaining signals contain primarily ionospheric and lithospheric contributions.

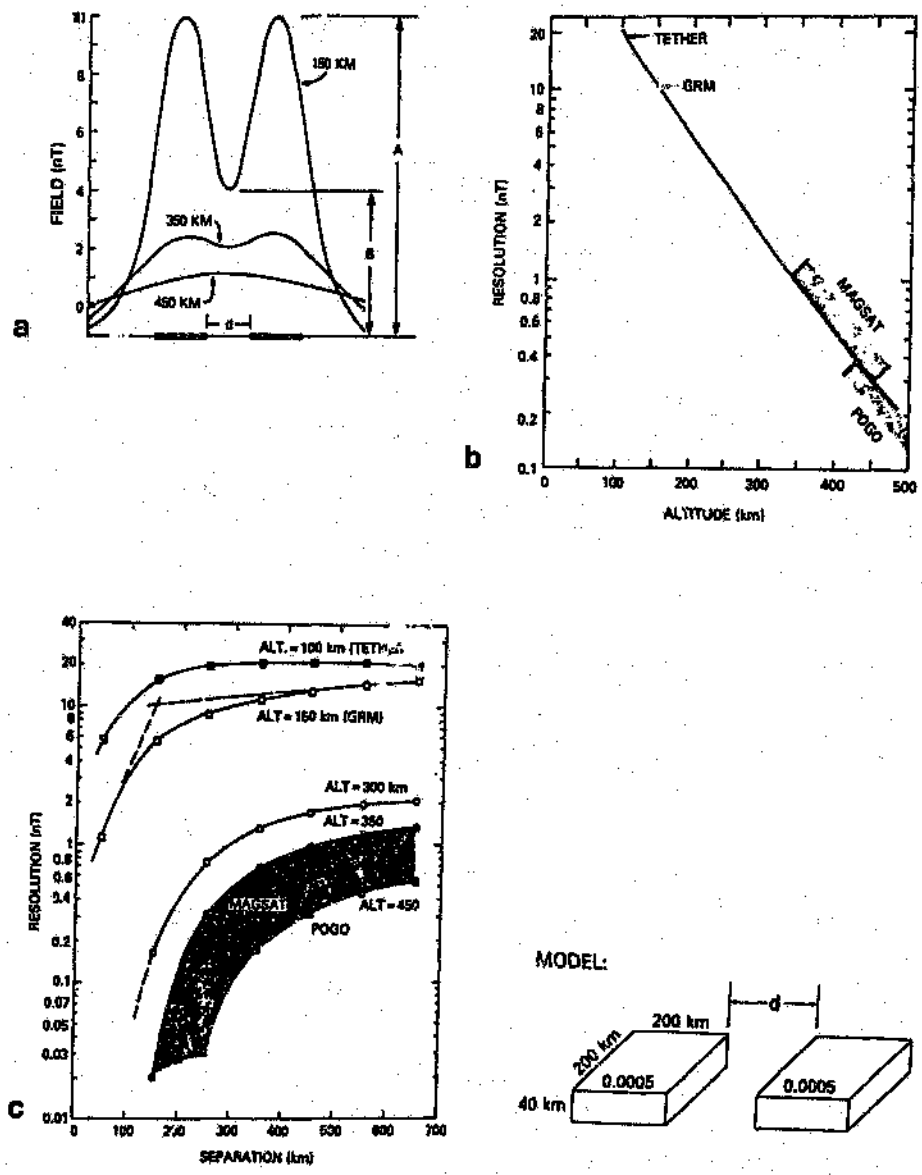

Figure 1.1: Geological model and related graphs illustrating aspects of resolution. (a) East-West profiles for different altitudes; (b) Resolution (R) as a function of altitude and; (c) Resolution (R) as a function of block separation. (After Webster et al., 1985).

- Hereafter, the procedures to separate the remaining signals differ widely amongst investigators. The most common practice is to fit and remove, arbitrarily, a 'regional' from each satellite track.

In detail, the processing route has evolved according to specific needs and requirements. Not mentioned in the above outline are the effects of variation of sensor altitude during data acquisition. Some investigators ignore the effect while others correct for this variation.

The above processing steps are discussed seperately below.

1.3.1 Removal of the core field

Separation of the core from the lithospheric fields remains a difficult and an unresolved problem. Analyses of the spherical harmonic power spectra show a distinct change in slope at degree 13. This discontinuity in the power spectrum has generally been interpreted as representing the change from dominance of core field (below degree 14) to a dominance of crustal field (see e.g. Langel and Estes, 1982). Although there are numerous spherical harmonic models, the only viable solution to date for the core-crustal field separation is to truncate the spherical harmonic series at the point of change in slope (degree and order 13; Langel et al., 1982). The problem, however, is in the spectral overlap of the contributory component fields (e.g. Mörner, 1986; Benton and Alldredge, 1987). This approximate separation creates a problem in long-wavelength anomalies in the wavelength-band around 3000 km. There is a conflict of opinion, on mineralogical grounds, as to whether or not upper-mantle is magnetised (Wasilewski, 1987; Toft and Haggerty, 1988). The debate is fueled by the inversion problem, which in many cases requires that upper-mantle be magnetic, and may well be closely associated to the question of spectral overlap. Most Magsat investigators have standardised to the truncated model MGST 4/81 (Langel et al., 1981) and it was decided to adopt the same standard in this study.

1.3.2 Removal of ring current field effects

The effect of the equatorial ring current manifests as a substantial (30 nT) V-shaped response, symmetrical about the dip equator. It is assumed that the gross latitude-dependent geometry of the response is due to the ring current and that the perturbations from this shape are

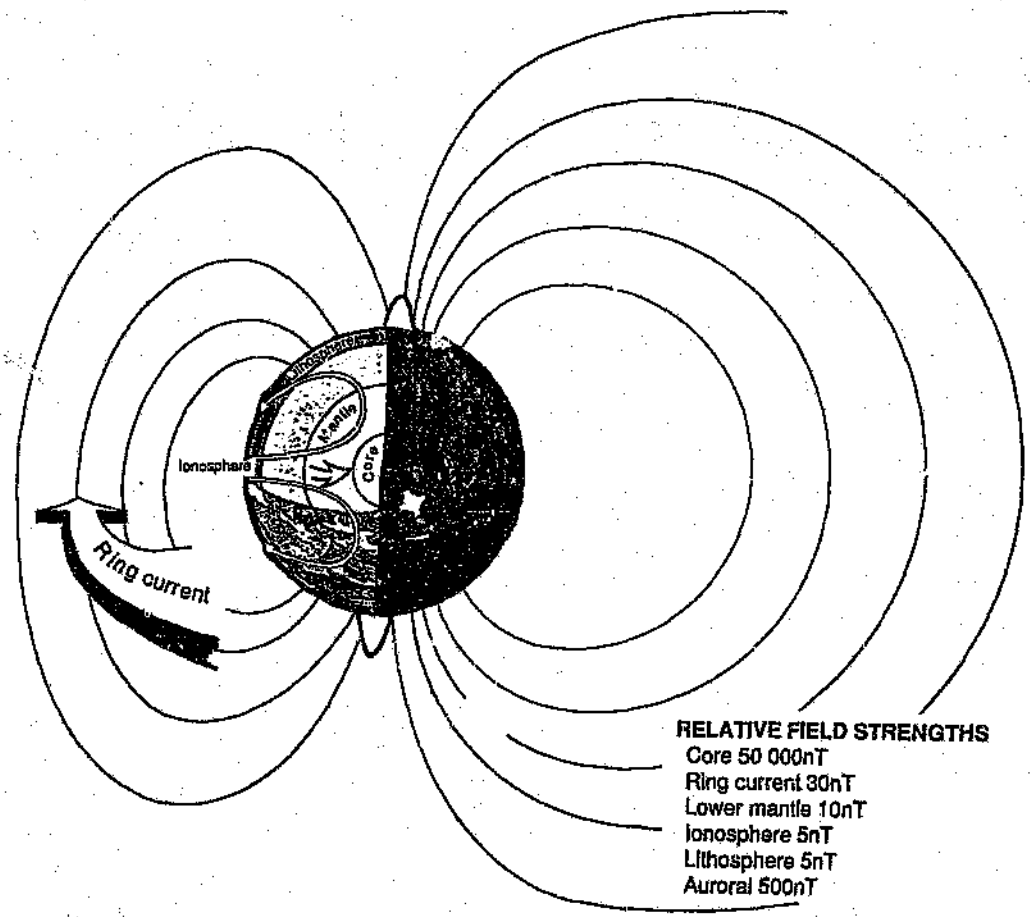

Figure 1.2: Schematic illustration of the contributory source regions of field components observed by a near-earth satellite magnetometer. Relative field strengths of each source are also indicated.

related to the lithospheric anomaly field and the ionospheric field. The ring current can be approximated by a simple zonal harmonic function which considers both the external as well as the internal induced components (Langel and Sweeney, 1971). This correction has been adopted by most investigators, the coefficients of which are given in the INV-B tapes. Alternative techniques consist of fitting a quadratic function or band-pass filtering (e.g. Arkani-Hamed et al., 1985). The standard correction is however inadequate for the southern African region. An improved solution is achieved by fitting the function for dip latitudes calculated at 3 R_E rather than those at the satellite's altitude (Zaaiman and Kühn, 1986).

1.3.3 Removal of ionospheric field effects

Satellite data, corrected for the main field and ring current, show strong path-to-path inconsistencies. It is assumed that this reflects ionospheric Sq effects contaminating the sought after lithospheric anomaly field. Mayhew (1979) had noticed this effect in POGO data and although the Magsat polar, twilight orbit was designed to remove the Sq effects, this was not achieved. This path-to-path inconsistency is manifest as a long-wavelength trend in individual passes. Removal of the trend is made (by most workers) with the use of arbitrary linear, quadratic or higher order polynomial functions and is known as the path-to-path correction. Yanagisawa and Kono (1985) introduce the concept of defining a mean ionospheric field determined by a process where the lithospheric field component is treated as random noise and produces a more objective and repeatable correction. Taylor and Frawley (1987) adopt a different approach. Only dawn and dusk passes which intersect are selected. In order to minimise intersection point discrepancies, they adjusted these profiles by solving for the coefficients of a set of polynomials (one polynomial for each orbit) using a generalised least-squares method.

1.3.4 Correcting for altitude variations

In order to provide a lithospheric anomaly map from a moving platform of variable altitude it is necessary to fix an altitude datum. Many attempts have been made to broach this problem with as many resultant solutions. This reduction is usually incorporated as a final step for the display of the anomaly maps and may preceed, follow or be combined with the gridding

procedures (the details of which are given in Chapter 4). For example, the most popular method is the equivalent source technique (Mayhew, 1979) where preprocessing is required (i.e. gridding; data within a particular cell is averaged to give a mean value and respective mean altitude) and an assumption must be made that magnetisation is entirely induced.

Because of the global nature of the data, the final total-field anomaly map will contain a variable anomaly response, that is dependent on geographical position, as a result of the varying ambient-induced polarising field. Radial reduction to the pole is sometimes applied to provide an easier interpretation map (e.g. von Frese et al., 1987).

1.4 Objectives

It is the aim of this thesis to research aspects of processing of near-earth satellite magnetometer data towards generating improved lithospheric anomaly maps. Altnough, the core field and ring current corrections are not entirely satisfactory, the procedures are standard amongst investigators and accepted as reasonable approximations. The process of path-to-path reductions are however arbitrary, subjective and non-repeatable. Also, the altitude reduction procedures fail in several respects, in that they are either applied after some preprocessing or with an *a priori* assumption of the magnetisation and, often, both are applied or assumed.

In salient form this thesis aims to:

- Introduce an ionospheric field correction that may be applied ubiquitously and objectively.
- Consider an altitude reduction that attempts to minimise preprocessing and *a priori* assumptions of the magnetisation.
- Test these algorithms on synthetic data.
- Process Magsat data over a selected geographical region (southern Africa) using existing procedures which are deemed suitable, together with the newly developed algorithms for those procedures prone to inaccuracy and ambiguity; the aim being to create an improved dataset better suited to quantitative interpretation.

- Assess the derived Magsat anomaly map in terms of previously published work and conduct a qualitative and quantitative interpretation.

Chapter 2

The geomagnetic field

Magnetometer measurements made from ground- or satellite-based observations in a source- and disturbance-free environment will comprise contributing components from the earth's fluid core, solid crust and from large-scale current systems known to exist at the boundaries of the magnetosphere, in the magnetotail and in the magnetic quiet (ring current) (see e.g. Regan and Rodriguez, 1981). In addition to the large-scale external fields there are smaller, localised fields from the equatorial and auroral electrojets and field-aligned current concentrations.

The *ground state* or *baseline* magnetosphere is to a certain degree an elusive concept (Stern, 1988). The external fields are mostly studied by their temporal variation, particularly in times of strong magnetic activity, while the baseline magnetosphere is defined by selecting magnetically quiet days in the analysis of the geomagnetic field (see Campbell, 1987).

For a near-earth satellite the total-field measured by the magnetometer is assumed to be in a source free region[1] such that the divergence and the curl is zero. The field may be derived from a potential function that satisfies Laplace's equation, viz.

$$\nabla^2 V = 0 \tag{2.1}$$

The spherical harmonic expansion

$$V = a\sum_{n=1}^{N}\sum_{m=0}^{n}\left\{\left[g_n^m \cos m\phi + h_n^m \sin m\phi\right]\left(\frac{a}{r}\right)^{n+1} + \left[g_n^m \cos m\phi + s_n^m \sin m\phi\right]\left(\frac{r}{a}\right)^{n}\right\} P_n^m(\theta) \tag{2.2}$$

[1]This assumption is not strictly valid since the satellite is orbiting within a low density plasma.

is one solution to Laplace's equation (Langel and Sweeney, 1971), where: a is the mean earth radius, r is the geocentric satellite altitude, θ and ϕ are respectively, the colatitude and longitude, and $P_n^m(\theta)$ are Schmidt quasi-normalised Legendre functions. The magnetic field is represented by the gradient of the potential

$$\vec{B} = -\nabla V \tag{2.3}$$

The terms comprising the g and h coefficients describe fields of an internal origin with respect to the satellite's orbit. The converse holds for the terms comprising the s and q coefficients. The external fields, being strongly time-varying in nature, may induce currents within the conductive portions of the lower mantle and thus contribute to the internal coefficients.

The common problem faced by both the solid- and liquid-earth geomagnetists is the separation of the two internal component fields. Either of these fields (i.e. the core or lithospheric) are regarded as contaminants to the external source-field under investigation and *vice versa*. In this Chapter modelling of the geomagnetic field is discussed, considering the problem of the core/lithospheric field component separation, followed by a discussion of rock magnetism pertinent to satellite altitude data. Because we are able to separate the geomagnetic field model into internal and external components and because the physics is subsantially different we will treat the external field effects separately in the proceeding Chapter.

2.1 The geomagnetic spectrum

Modelling of the internal components of the geomagnetic field is generally approached by selecting a suitable data set over several magnetically quiet days to minimise external field effects. Data from the high latitudes ($\geq 50^0$) are rejected to avoid field-aligned currents that distort the field (Meyer et al., 1983; Langel and Estes, 1982). A global geomagnetic field model (MGST 10/81) to degree and order 23 was derived by Langel and Estes (1982) from Magsat data for the purpose of analysing the power spectrum.

The spatial power spectrum (Lowes 1966, 1974) is the mean square value of the topology of the geomagnetic field intensity produced by harmonics of a given degree n and is expressed as

$$R_n = (n+1)\sum_{m=0}^{n}\left[(g_n m)^2 + (h_n m)^2\right] \tag{2.4}$$

Figure 2.1 is the power spectrum for model MGST 10/81. The dominant feature of this spectrum is the linear decay with increasing n and a sharp 'knee' around $n = 14$. The dipole term stands alone (asterisk in Fig. 2.1). Langel and Estes (1982) interpret the turn in the spectrum to reflect data originating from separate sources and not noise; a generally accepted interpretation (see e.g. Lowes, 1974; Hahn et al., 1984; Mörner, 1986; Benton and Alldredge, 1987; Cain et al., 1989a).

Benton and Alldredge (1987) compared spectra from two separate high-degree Magsat models (one of which is the MGST 10/81) and found good agreement to $n = 15$. Although, the agreement between the spectra remains uncertain towards the higher harmonics, an analysis of the noise, and primary and secondary spectral features led, the authors to reject the possibility that the high-degree flat region of the spectrum reflects a dominating influence of error in model determination. They then tested the hypothesis that the break-in-slope of the spectrum reflects dominance of core sources over lithospheric sources by modelling the spectrum using simple arrays of dipoles and current loops. Two ranges of source depths were found to adequately model the spectrum (one crustal the other core) and consequently support the hypothesis.

2.2 Core-lithosphere separation

The complexity of separating the component fields originating from the core and the lithosphere lies in the spectral overlap. Benton and Alldredge (1987) show by modelling that the shallow lithospheric sources contribute significant power in the lower harmonics. Similarly, the power spectrum contains a significant contribution from the deep core sources in the higher harmonics ($n = 16 - 18$). The point in the spectrum where the energy densities of the core and lithospheric components are equal is at $n = 14,2$ (Cain et al., 1989b); a value obtained from a high degree spherical harmonic analysis (up to $n = 63$). Lithospheric field components completely dominate the spectrum for $n \geq 15$ (see figure 2.1). For this and the above reasons, it is accepted amongst Magsat investigators to separate the field components by defining the core field with a truncated spherical harmonic model of degree and order 13

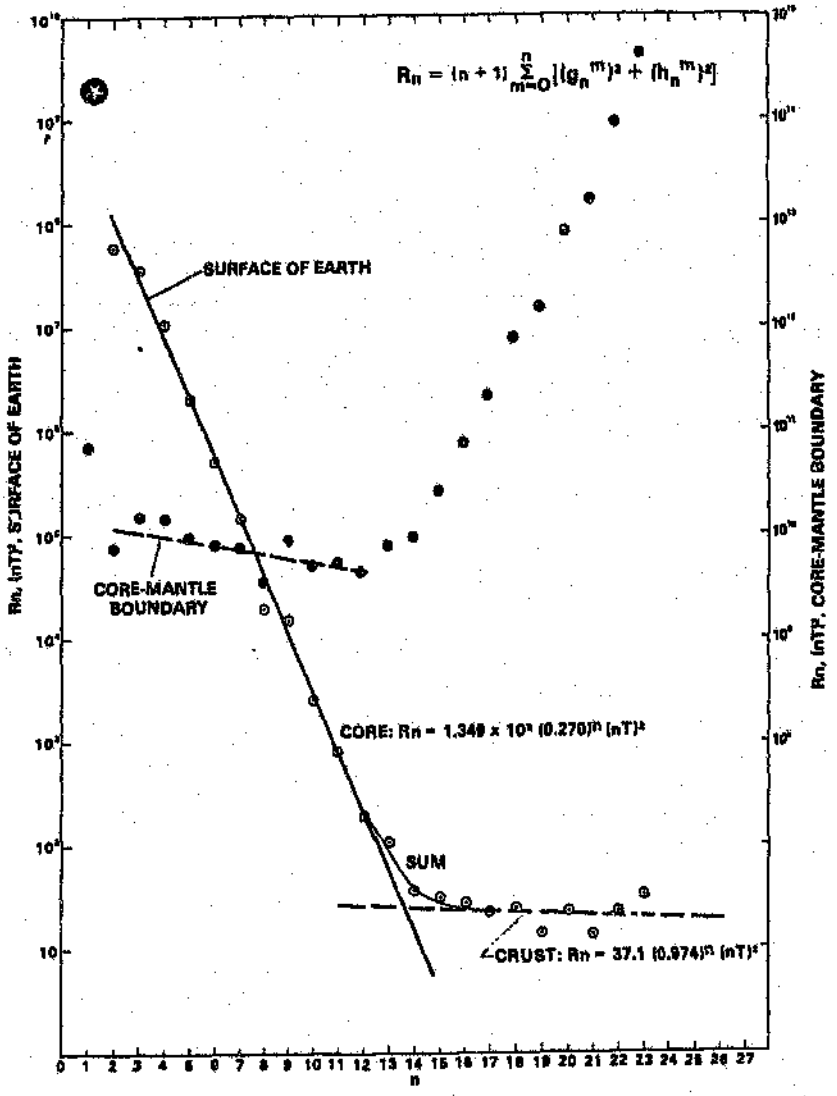

Figure 2.1: Geomagnetic field spectrum from the MGST 10/81 model. R_n is the total mean square contribution to the vector field by all harmonics of degree n. Open circles are the satellite-altitude results, solid circles represent extrapolation to the core-mantle boundary. (After Langel and Estes, 1982).

(MGST 4/81, Langel et al., 1981).

Use of a degree and order 13 spherical harmonic model as an approximation to the core field is not entirely satisfactory. Harrison et al. (1986), using spherical harmonic coefficients above degree 13 in two different representations to approximate the lithospheric field, have shown that there is little latitudinal variation of magnetic signatures. A latitudinal variation is expected if the lithospheric magnetisation is entirely induced. This may reflect the fact that they never test the stability properties of their solution such that the corresponding variance may completely mask any latitudinal variations (von Frese, pers. comm.).In addition, an expected continent/ocean contrast in magnetisation was not observed. By progressively using the higher degree coefficients latitudinal variation became evident as well as an increase in contrast between continental and oceanic crust. The conclusion reached is that the intermediate wavelength signal believed to be of lithospheric origin may in fact reflect an origin within the core and that the lithospheric portion of the signal is limited to harmonics between $n = 19$ and $n = 53$ (see also Arkani-Hamed and Strangway, 1985). At present, however, there is no clear alternative method to the truncation of the spherical harmonic series at a degree and order 13.

2.3 The lithospheric geomagnetic field

The term *lithospheric* is being used in preference to *crustal* to impress that magnetisation within the solid upper regions of the earth is not necessarily constrained to the crust but may be sub-crustal. Mörner (1986) describes the lithospheric field in terms of permanently locked, temporarily locked and induced components (see figure 2.2). The permanently locked component is the remanent magnetisation which will not change with time unless by tectonic reorientation, overprinting or stress-induced piezomagnetic variations in intensity (see e.g. Counil and Achache, 1987). Temporarily locked magnetisation originates in regions where thermal changes and phase boundary transitions lock and unlock magnetisation in response to various geodynamic changes.

As discussed in section 1.2 the limiting factor in resolving the magnetic signature of structures in the crust and lithosphere is the altitude of observation. At satellite altitude the effective observed magnetisation is a bulk magnetisation subject to the system resolution.

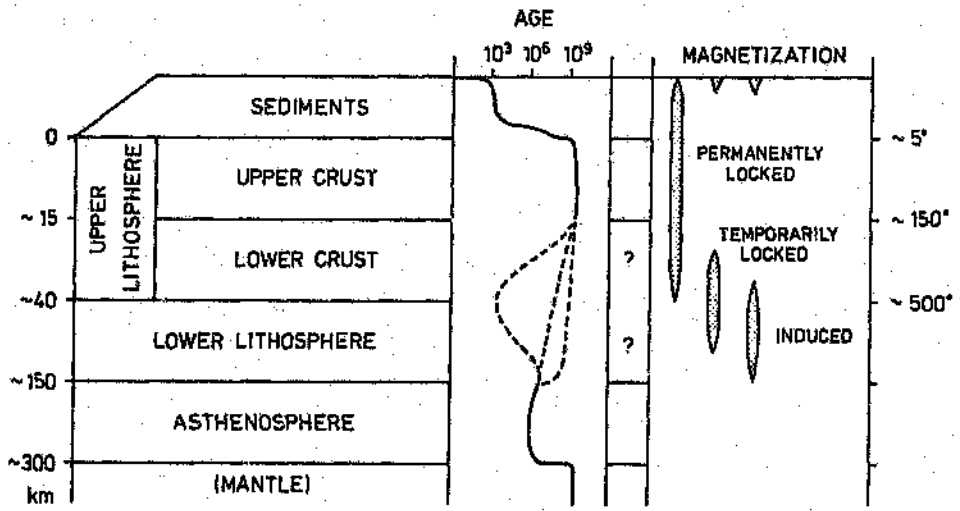

Figure 2.2: Approximate magneto-lithostratigraphic subdivision of the lithospheric anomaly field in a typical craton (Fennoscandian Shield). Approximate ages and ranges of magnetisation are given. The Moho is a phase boundary that moves in response geodynamic processes, hence locking and unlocking the magnetisation in that region and giving these transition rocks an anomalously young effective age. (After Mörner, 1986).

Thus, when interpreting satellite altitude magnetic data the system limitation to resolve magnetic structures must in turn limit the frame of reference. For example, two dipoles separated by two degrees in mid-latitudes (200 - 300 km) cannot be resolved at an altitude of 400 km.

2.3.1 What is the base of the magnetic crust ?

While Harrison et al. (1986) and Arkani-Hamed and Strangway (1985) postulate that higher degree harmonics (≥ 13) are dominated by field components originating from the core, Mörner (1986) postulates that lower degree harmonics are dominated by a long-wavelength lithospheric field component whose source is sub-Moho. Wasilewski et al. (1979) postulate that the Moho is also a magnetic boundary. By analysing mantle-derived xenoliths (of dunite, peridotite and eclogite) and reviewing the literature they provide evidence that metals and primary Fe_3O_4 are absent and that complex Cr, Mg, Al, Fe spinels dominate the oxide mineralogy. These spinels would be non-magnetic at mantle temperatures. The crust/upper-mantle transition is thus interpreted as a magnetic mineralogy transition where the mantle contains non-magnetic refractory spinels and the crust the FeTi spinels. According to Wasilewski et al. (1979) and Wasilewski (1987) the base of the *magnetic crust* is the crust-mantle boundary, where it exists as a magnetic mineralogical discontinuity, except where the Curie isotherm ($\sim 550^0C$, Buddington and Lindsley, 1964) is above the Moho.

In contrast, Toft and Haggerty (1988) also analysing mantle derived xenoliths propose, for magnetic modelling of cratonic lithosphere, that magnetisation should not be confined to depths shallower than the Moho. Magnetisation could extend to 95 km depth but most probably to upper-mantle depths of 70 km. This conclusion is based on a debatable point as to the abundance of metal phases in the upper-mantle. Magnetic susceptibility and NRM are due to $\leq 0,1$ vol. % of fine-grained metal derived from the decomposition of garnet and ilmenite plus magnetite, possibly as a result of metal oxidation. The model includes T and P transitions of magnetite and iron metal, along with silicate equilibria, oxidation states, and geothermal gradients (see figure 2.3). The native iron concentrated at crystal edges and cracks is believed by the authors to reflect a ubiquitous low oxidation state for the lower-crust and upper-mantle generally. This free iron, with a high Curie temperature (770^0C), may be

a source of the long-wavelength lithospheric anomalies.

Griffin and O'Reilly (1987) propose that the Moho and the crust-mantle boundary may rarely coincide in cratonic areas. These authors used high-pressure xenoliths to construct geotherms and stratigraphic profiles as lithological and physical parameter constraints for the interpretation of geophysical data. In areas of high heat flow the Moho, as defined by seismic refraction data, may lie deeper than the crust-mantle boundary. Clearly, the question of *"what constitutes the base of the magnetic crust ?"*, remains an important point in the interpretation of the lithospheric anomaly field, and is as yet unresolved.

2.3.2 Magnetisation of crustal rocks

Magnetisation of the crust above the Moho is perhaps slightly better understood. The few kilometers of the upper-crust, including supracrustal rocks and crystalline basement may contain an original remanent magnetisation modified by thermal overprints producing variable remanent vector orientations. With increasing depth, conditions for coherent regional magnetisation are enhanced (Wasilewski et al., 1979). Viscous remanent magnetisation is enhanced with increasing temperature, and pressure provides additional viscosity enhancement. Also, susceptibility increases with increasing temperature particularly in the region $100 - 150^0C$ below the Curie point[2]. These aspects of crustal magnetisation according to Wasilewski et al. (1979) account for anomalous magnetisation of the middle-to lower-crust. The thickness of crust above 400^0C and below the Curie isotherms may vary in thickness from 5 to 20 km. This region of the crust could be the most magnetic and the thickness of this layer could provide the source of the long wavelength anomalies (Wasilewski and Mayhew, 1982).

Several uplifted terranes are regarded as unique crust-on-edge sections exposing deep crustal rocks (for example: Ivrea Zone, Italy; Lofoten and Vesterålen, Norway; Kapuskasing, Canada; Vredefort, South Africa and; the Vema fracture [illegible] Atlantic). Few of these sections, however, extend in equivalent crustal depths beyond 25 km, and are thus more

[2]The Hopkinson effect on studies of high-grade metamorphic samples from Lofoten and Vesterålen indicate that magnetic susceptibility is nearly constant, gently increasing with temperature by 5% near the Curie temperature. Schlinger (1985) is of the opinion that this effect is not an important phenomenon and magnetisation enhancement at depth is probably not as a consequence of the Hopkinson effect. Results from this study would indicate that the Hopkinson effect is important (see section 7.2.3).

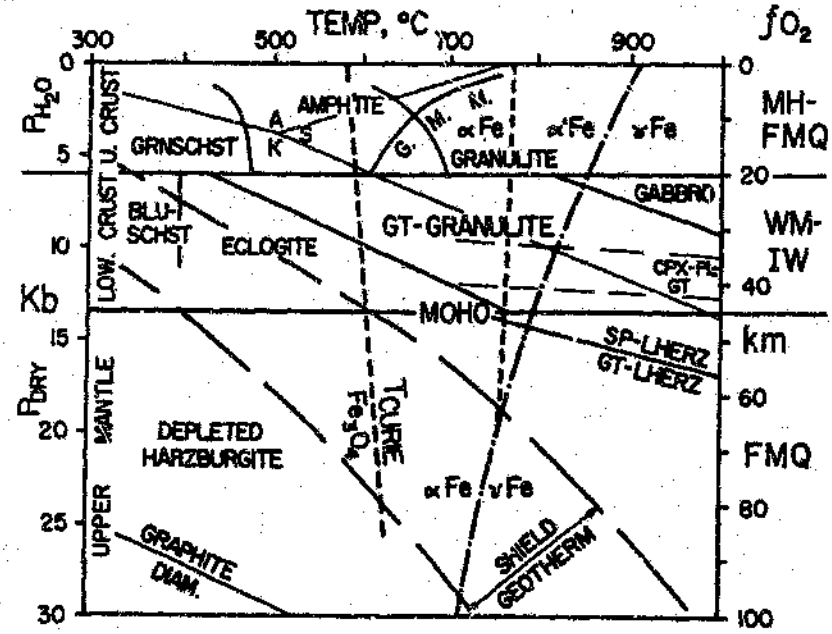

Figure 2.3: Model of the cratonic crust and upper-mantle. Most boundaries are diffuse zones but the $Fe_3\ O_4$ and iron melt transitions are well constrained and their interrections with a shield geotherm window, along with fo_2 controls, suggests a maximum depth for lithospheric magnetisation of 95 km. In the presence of both magnetite and iron metal and an average geotherm, the best estimate for the maximum thickness of magnetic lithosphere is 70 km. (After Toft and Haggerty, 1988).

representative of mid-crustal sections. Further, with the exception of the last-cited example all are continental sections. Nevertheless these represent a unique access to deep crustal rocks for petrophysical property studies. The oceanic Vema section (Auzende et al., 1989) is at present a synthesised geological section only (oceanic crust and upper-mantle from samples collected and visual observations made using the French submersible *Nautile*).

The most comprehensive petrophysical/petrographic study of one of these terranes is that of Schlinger (1985) of the Archean and Proterozoic gneisses and intrusive rocks of northern Norway. This study portrays the lower-crust as an extensive and highly magnetic region of the crust which is defined by granulite facies metamorphic grade and by a Curie isotherm of 575^0C (magnetite). The magnetisation is parallel to the polarising geomagnetic field because significant NRM is mostly viscous. The average susceptibility is 4×10^{-2} (SI) while in the deepest high-grade region it is 6×10^{-2} (SI). Granulite facies rocks have, on average, five times higher susceptibility and NRM than their amphibolite facies equivalents. Most of the NRM is viscous in nature.

2.4 Conclusion

The general model, for the magnetisation of crustal rocks, gained from the literature is that magnetisation increases from mid- to lower-crust (with increasing metamorphic grade). Most of this magnetisation probably originates from mafic and ultramafic rocks of the lower-crust and may have total magnetisations in up to 5 A/m (for granulites, Schlinger, 1985). This is consistent with the interpretation of long wavelength anomalies of stable continental crust (e.g. Schnetzler and Allenby, 1983; Corner and Cooper, 1989). Hahn et al. (1984) provide a magnetic model of the earth's crust for modelling the Magsat lithospheric anomaly field. The model consists of 16 crustal types in columns of 2^0 by 2^0 tesserae. Crustal sections consist of two or three layers with assigned magnetisations according to surface geology and seismic information. The resultant crustal model does not fit the Magsat anomaly field satisfactorily. They found that the average model magnetisations were insufficient to account for the Magsat anomalies (by a factor of 2). These authors postulate that the discrepancy may be due to layer-like magnetic units in the crust with lateral extents in excess of 2000 km. These units should be regarded as quasi-homogenous part of the total magnetisation of the earth's crust

in a particular area.

The discrepancy between modelled geological sections with assigned magnetisations and the observed magnetic field from satellite altitudes continues to manifest itself. For example, Mayhew et al. (1985) could not model the U.S.A. Kentucky body alone when using Magsat anomaly data and had to introduce an extensive magnetic source region with magnetisations of 4,2 A/m through most of the crustal thickness. The problem of magnetisation defficiency (if known magnetisations are assigned to geological units) with respect to the observed satellite anomaly field is thus currently dealt with in several ways, viz.: (1) by assuming magnetisation of the upper-mantle (e.g. Toft and Haggerty, 1988) or (2) by introducing remanent magnetisation (e.g. Fullerton et al., 1989a). A solution to this problem could perhaps be found by the careful analysis and interpretation of the magnetisation contrast (the lack thereof) between continental and oceanic crust in satellite altitude anomaly data. With the exception of a few localities on the globe, published satellite anomaly maps do not show a contrast in magnetisation between oceanic and continental crust. This could be closely related to the problem of spectral overlap and the core-lithospheric field separation procedure (Hayling, unpublished preprint; Harrison et al., 1986). Hayling (unpublished preprint) used several magnetisation models to simulate the lithospheric anomaly field at Magsat altitude over the North and South Atlantic Ocean. The three models are given in figure 2.4 which assume: (1) induced magnetisation and TRM or (2) induced with viscous remanent magnetisation or (3) induced magnetisation plus TRM and a magnetised upper-mantle. A subjective comparison was made of the various simulations, from which he concluded that the last model of a magnetised upper-mantle best explained the observed Magsat anomaly field.

This debate, on whether or not the upper-mantle contributes to the total integrated magnetisation as observed at satellite altitudes, will continue. The problem is closely interlinked to the truncation of the spectrum in the core/lithosphere separation procedure (e.g. Arkani-Hamed and Strangway, 1985; Mörner, 1986).

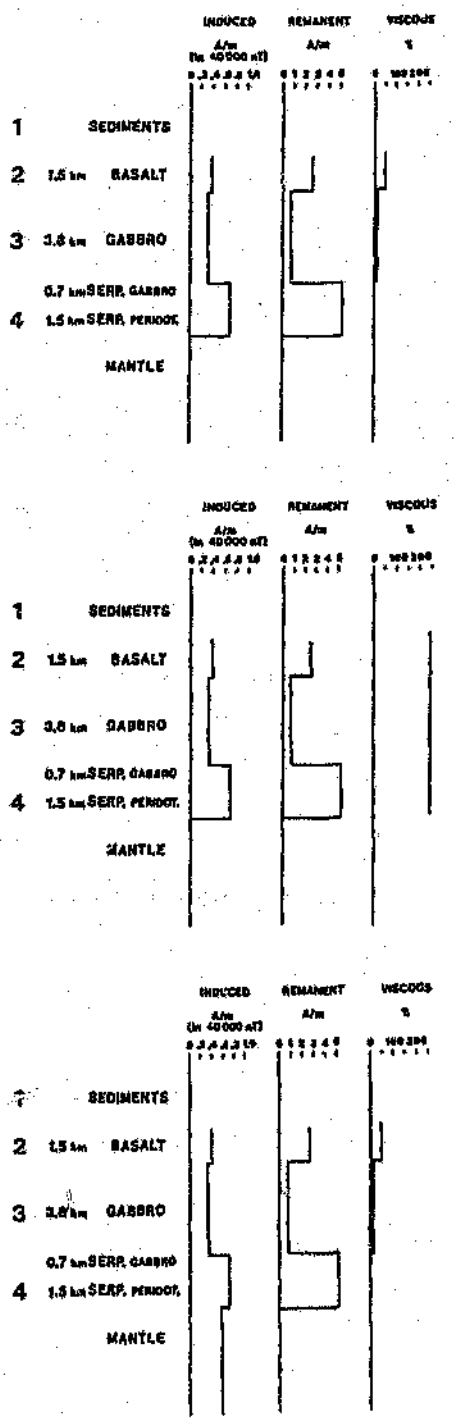

Figure 2.4: Magnetisation models of the oceanic lithosphere used for computer simulations of the oceanic to continental contrast anomaly field. (After Hayling, unpublished preprint).

Chapter 3

External magnetic fields

Definition of the *baseline* magnetosphere is difficult because of the strong temporal nature of the observed field effects. The geomagnetic field interacts with the solar wind and becomes stretched into an almost cylindrically shaped region extending into interplanetary space. This interaction creates a large, rather complex, magnetohydrodynamic electrical generator. There are several current systems that are created which in turn generate magnetic fields. The general structure of the magnetosphere and related current systems is described, focussing on those fields that affect the near-earth satellite-borne magnetometer measurements. A major proportion of the material of this Chapter was obtained from Hones (1986), Hargreaves (1979), Parkinson (1983) and, Regan and Rodriguez (1981). Because of the review nature of the Chapter and the frequency of use, these sources are acknowledged here in preference to citing them specifically .

In addition to the direct effects of the temporal variations of the external fields strong inductive responses also result from the interaction with the electrically conductive regions of the earth. It is necessary, therefore, to also consider the electrical structure of the earth and the effects thereof pertinent to near-earth satellite magnetometer measurements.

3.1 The magnetosphere

The geometry of the magnetosphere is modified by the solar wind (and resultant current systems) as it moves away from the sun and collides with the geomagnetic field. The magnetosphere begins at the magnetopause where a current system is established (magnetopause current, see Figs 3.1 and 3.2). The compressed, sunward side of the magnetopause is situ-

ated some 10 R_E (earth radii) from the earth while the leeward side is stretched downstream (some 1000 R_E) to form the magnetotail (diameter of approximately 50 R_E). This magnetotail consists of two oppositely magnetised lobes. In the mid-plane region where oppositely polarised field lines meet there is a narrow zone of zero field, termed the *neutral sheet*. This same zone is the locus for the sheet current that flows across the mid-plane and loops around both the north and south lobes.

Plasma regions

Some of the solar-wind plasma penetrates the magnetosphere's sunward regions (mostly at the polar cusps) some of which is found to accumulate in the surface regions of the tail (plasma mantle). In terms of plasma density the magnetosphere can be devided into two regions. The inner 4 R_E region comprises relatively cold, low energy plasma and is known as the *plasmasphere*. The plasmasphere rotates with the earth and is comparatively protected from interference from the solar wind. The boundary, the plasmapause, varies in postion from 3,5 R_E for disturbed conditions to 6 R_E for quiet conditions. Outside the plasmasphere the plasma is considerably lower in density, hotter and of higher energy. This plasma drifts through the lobes to concentrate in the mid-plane known as the plasma sheet. There are also a few very energetic particles forming what is known as the *Van Allen belt* or the *trapped radiation belt*. They exist inside as well as outside the plasmasphere. The plasma is strongly affected by interaction with the solar wind which is one of the factors that can contribute to sudden changes in plasma density across the plasmasphere.

Within the plasmasphere the plasma is trapped by those magnetic field lines that rotate with the earth and are confined to a region fairly close to the earth. Magnetic field lines beyond the plasmapause are controlled by convection caused by interaction with the solar wind. The magnetic field lines are dragged into the magnetotail and by their interaction with the interplanetary magnetic field (IMF) lose plasma. This process results in a one way flow of plasma from the higher latitudes away from the earth, termed the *polar wind*.

Magnetic reconnection

Magnetic *reconnection* or *merging* is the process by which regions of opposed magnetic field lines come together. The magnetosphere's field lines interact with those of the IMF. As a result of reconnection the magnetotail has three types of magnetic field lines, viz.:

- The field lines in the lobes connected to the earth (open field lines).
- The field lines on the earthward side of the neutral sheet where all field lines of the two lobes have reconnected (closed field lines).
- The field lines on the distant leeward side of the neutral line that have reconnected but are disconnected from the earth and are open downstream into interplanetary space (interplanetary field lines).

Magnetic reconnection is one mechanism by which plasma can be injected into the magnetosphere.

Current systems

In the magnetosphere the magnetohydrodynamic (MHD) process generates electricity at two different locations. One of these arises as a consequence of magnetic reconnection at the sunward side of the magnetopause. There the solar wind and IMF encounters the the earth's magnetic field, merge (this process is seemingly at random) and become earth-tied. The solar wind plasma moving through this earth-tied magnetic field completes the basic elements of the MHD generator. Polarised charges are deflected around the magnetopause establishing a lateral electric field across the magnetosphere in the dawn to dusk direction. A current system results across the neutral sheet. The circuit is completed over the surface of the tail, so that the tail is confined within a pair of current solenoids.

The conductive ionosphere[1] constitutes a low-resistance external circuit by which polarisation charge, from the solar wind, can flow. At low latitudes some solar-wind plasma penetrates the closed lines of the earth's magnetic field. This plasma moving at right angles

[1]The ionosphere is located at an altitude of some 90 to 400 km above the earth's surface. The upper atmosphere is ionised by electromagnetic radiation of the sun. Once polarised charges are produced they tend to recombine, however a minor net imbalance remains giving rise to the ionosphere.

to the magnetic field creates conditions for MHD power generation with a polarisation discharge path through the ionosphere. Lines of force, for a fixed observation point, maintain their identity down to the ionosphere. Because the ionosphere rotates with the earth it causes co-rotation of the low-latitude magnetic force lines. At the polar regions the open field lines are fixed relative to the midnight meridian. In these latitudes two whorls of current termed the *field aligned currents* are established through the discharge of polarisation currents. The current pattern they produce constitutes a polar diurnal variation of the observed magnetic field (S_q^p).

An important current source results from the gradient of the magnetic field. The motion of an ion will circumscribe a circle in the equatorial plane whose radius is inversely proportional to the magnetic flux. The orbit of this ion is a circle (only in a uniform field). The radius of curvature of the path of the ion is greater away from the earth than closer to the earth. This differential radius of curvature makes the positive ions drift westwards and the electrons eastwards. This drift contributes to a net westward current known as the *ring current* which occupies the equatorial regions of the near-dipolar field below 7-9 R_E.

3.2 Magnetic disturbances

Through the MHD process the solar wind generates electric currents in the geomagnetic field and shape the earth's magnetic field lines. These current systems produce magnetic field perturbations that are additional to the main geomagnetic field and are manifested as either regular or as impulsive temporal variations. Since the magnetopause current results from the reconnection process of the IMF with the geomagnetic field variations in solar wind pressure may alter the reconnection process resulting in the propagation of wave motions in the magnetosphere. These effects can either be coherent oscillations of the magnetic field with periods of seconds to minutes or impulsive with no distinct periodicity.

Such sudden major changes in solar wind pressure thus give rise to a magnetic storm, which is a period of rapid, irregular, transient fluctuations of the magnetic field greater in magnitude, more irregular, and of higher frequency than diurnal variations (Sheriff, 1984). These storms occur on average about once or twice a month. Much more frequently there occur intervals of disturbance without all the manifestation of a storm and in which the

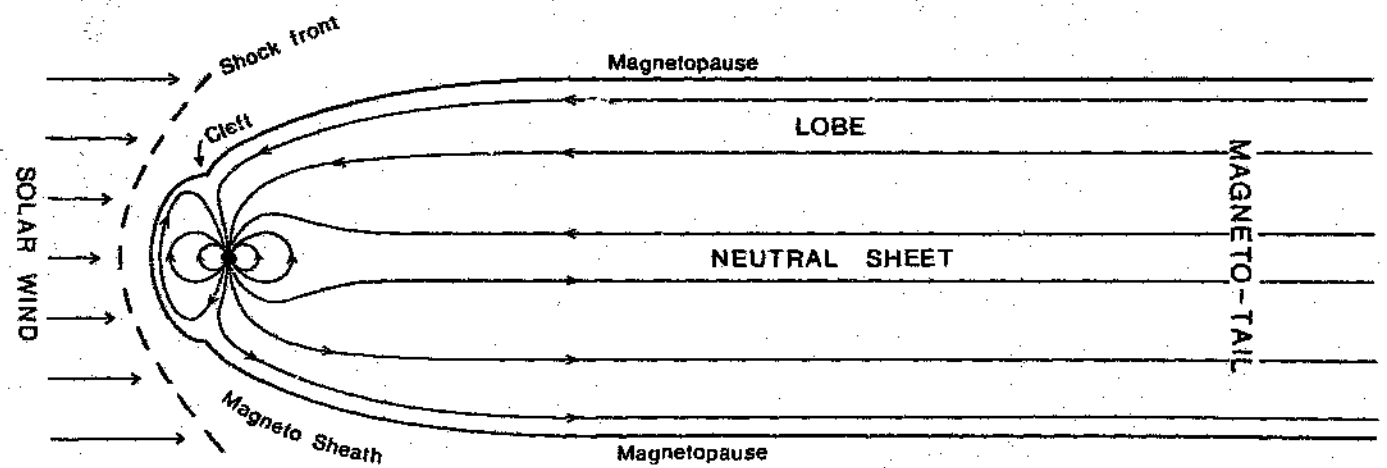

Figure 3.1: Illustration of magnetic field lines and structure of the magnetosphere. (After Parkinson, 1983).

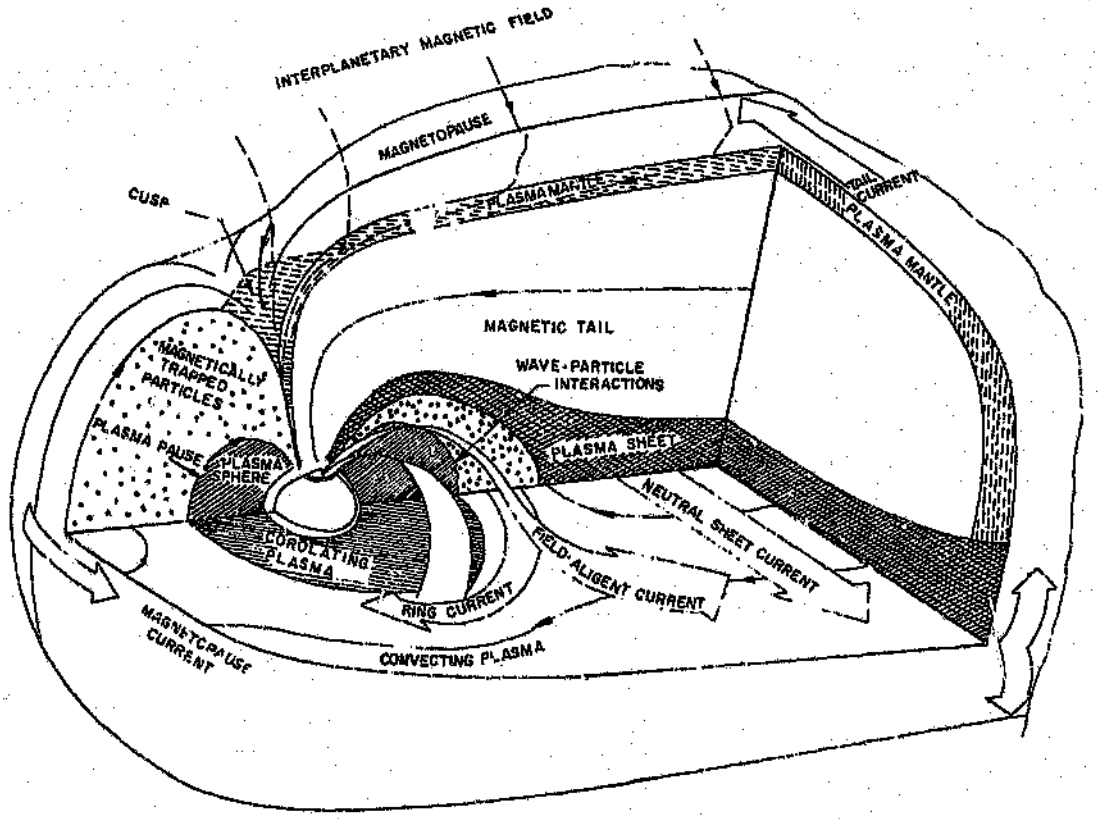

Figure 3.2: Schematic illustration of the structure of the magnetosphere, magnetospheric regions and current systems. (After Regan and Rodriguez, 1981).

strongest disturbance is confined to auroral latitudes. These are termed *magnetic substorms*. Parkinson (1983) believes that the irregular fluctuations of a storm are, in part, simply a series of substorms. For this reason the generation of a magnetic substorm is discussed first.

3.2.1 Magnetic substorms

Magnetic substorms and associated aurora are believed to originate from instabilities in the magnetotail neutral sheet current. At the onset of a substorm a new neutral line is created at a closer distance from the earth (of some 15 R_E) because of extreme tailward stretching of magnetic field lines beyond 7 R_E. This stretching results from an increased rate of field line reconnection at the magnetopause, hence an increased transfer of energy from the solar wind to the magnetotail. The new neutral line disrupts the sheet current, the cross-tail current is reduced, the magnetic field lines in response become less stretched and collapse earthward becoming more dipolar in shape (see Fig.3.3). This collapse increases the injection of high energy plasma into the polar regions of the ionosphere. This causes ionisation and increased conductivity along the auroral oval. Also, atmospheric molecules are excited and result in the auroral lights. The cross-tail current is short circuited by the field-aligned currents and auroral oval thus forming auroral electrojets.

At the site of the new neutral line the newly merged magnetic field lines form shortened closed field lines. This results in a form of a 'boudin' of magnetic field lines (they form closed loops) between the newly created neutral line and the pre-substorm position. This structure of closed loop magnetic field lines enclosing hot plasma is known as a *plasmoid*. After its formation the open field lines of the lobes reconnect and propel the plasmoid downwind. The new neutral line remains in its near-earth position for a period of half an hour to two hours before rapidly retreating to the original distant position.

3.2.2 Magnetic storms

The position of the magnetopause is determined by a balance between the kinetic solar wind pressure and the magnetic pressure of the field of the magnetosphere. The pressure balance equation, to a first approximation, is given by

$$B^2/2\mu_0 = Knmv \tag{3.1}$$

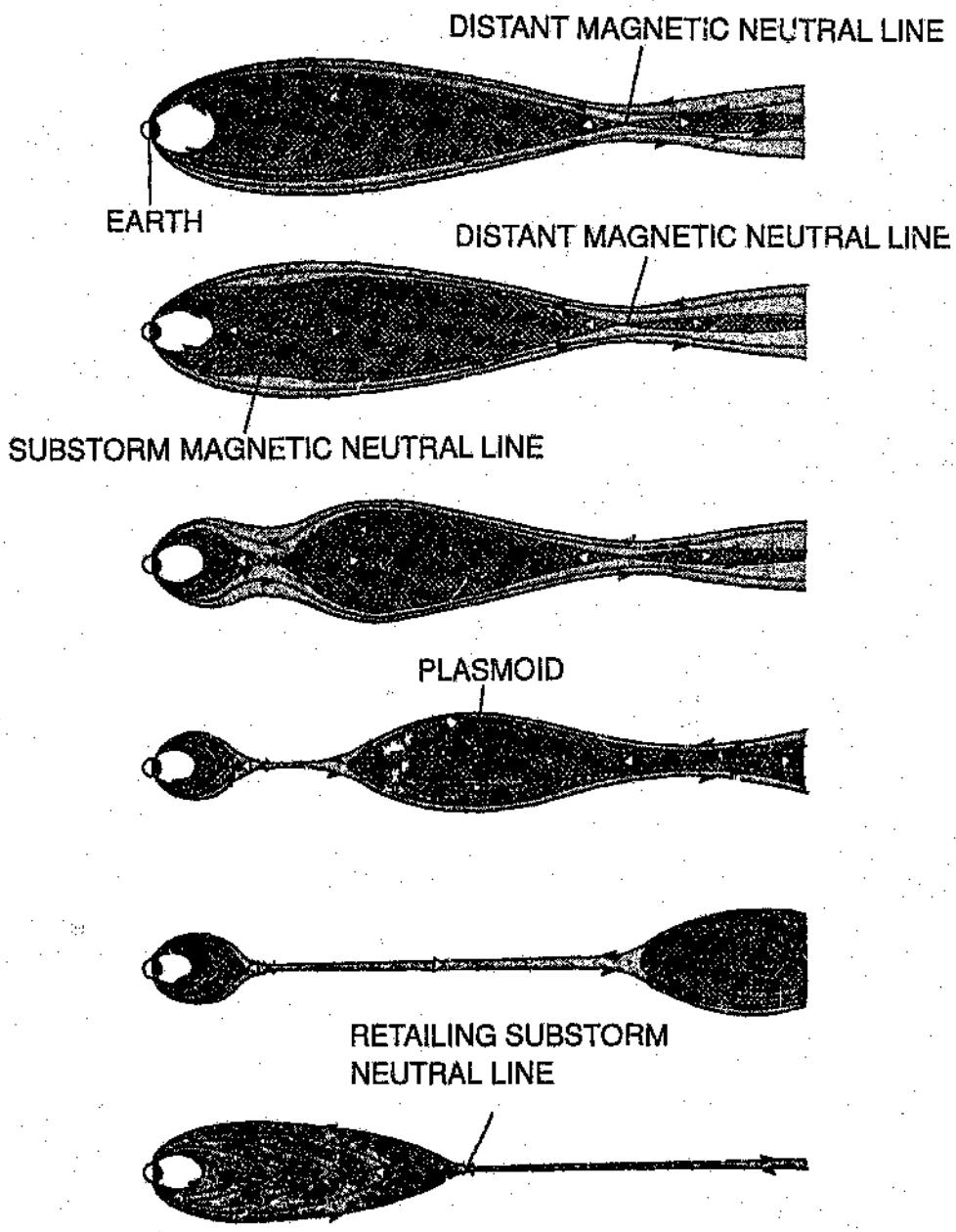

Figure 3.3: The magnetosphere model showing the merging of field lines and the creation of a plasmoid. This is one way the magnetotail releases energy and one explanation of the initiation of a substorm. (After Hones, 1986).

where B is the magnetic flux density, μ_0 is the magnetic permeability of free space, K is a constant, n is the density of solar wind particles, m is the particle mass and v is the particle velocity.

An increase in either plasma density or solar wind velocity will manifest as an increase in B; entectively compressing the entire magnetopshere. This compression has the effect of increasing the measured horizontal magnetic component at the earth's surface or from a near-earth satellite platform. A sudden compression of this type is known as a *sudden impulse* (SI). A SI may start a period of increased disturbance leading to a substorm or a storm (which is believed to represent, in addition to complex magnetohydrodynamic wave reverberations propogated through the magnetosphere, a series of substorms), in which case the SI becomes a SSC (*sudden storm commencement*).

Magnetic storms are manifested by substantial variations and irregular fluctuations in the observed magnetic field intensities. Effects of magnetic disturbances are best illustrated using magnetograms. For example, the magnetogram of figure 3.4 was recorded at the Hermanus Magnetic Observatory (12-13 September, 1957) and shows a typical magnetic storm in progress begining with a SSC at 0047h UT.

There are several indeces available to allow a quantitative measure of magnetic disturbance. The most commonly used index and adopted for the Magsat INV-B tapes is the planetary K-index (Kp) (Langel et al., 1981). This planetary magnetic activity index provides a measure of the average intensity of magnetic disturbance (of 12 observatories), on a 27 digit scale, in 3 hourly intervals. It is usually expressed in thirds of a unit on the scale of 0 to 9, i.e. 0_0, 1_-, 1_0, 1_+, 2_- ... 9_-, 9_0.

3.3 The ionospheric field

The previously discussed magnetic field perturbations encompass the irregular fluctuations of impulsive origin and have sources originating from several magnetospheric and high-latitude ionospheric current systems. In addition to these disturbances there are coherent diurnal fluctuations of the external magnetic field which affect magnetic observations of satellite-based platforms. The diurnal fluctuation of particular concern to near-earth satellite measurements is that originating from a current system in the ionosphere, the solar-quiet (Sq) current sys-

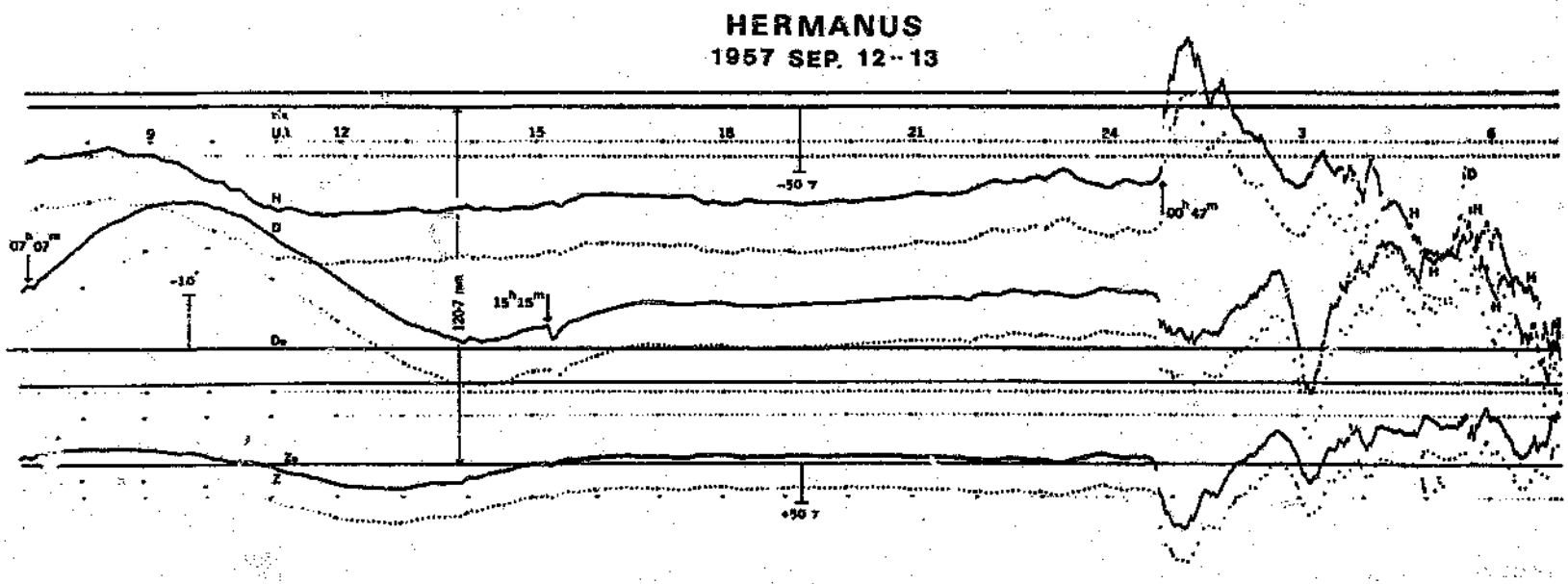

Figure 3.4: Magnetogram from the Hermanus observatory showing principal temporal features: the solar quiet day variation followed by a solar flare effect (1515h) and a magnetic storm commencing at 0047h.

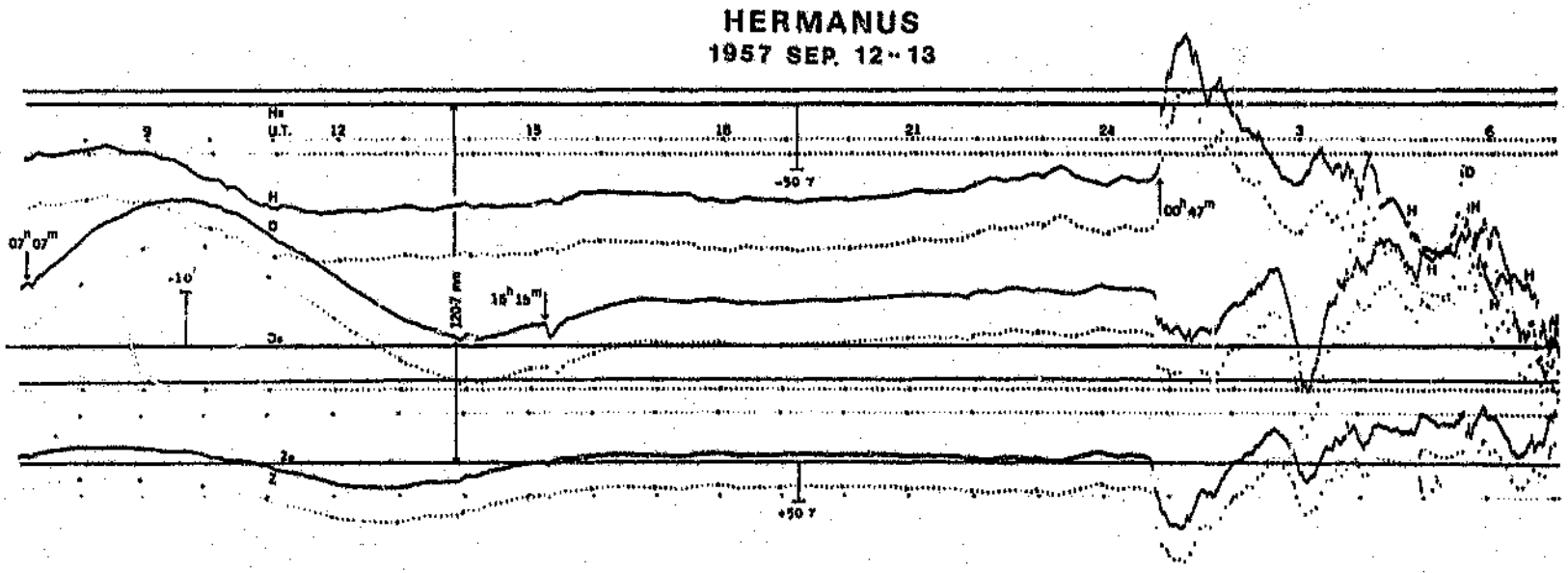

Figure 3.4: Magnetogram from the Hermanus observatory showing principal temporal features: the solar quiet day variation followed by a solar flare effect (1515h) and a magnetic storm commencing at 0047h.

tem.

Seasonal variations of ionospheric equivalent Sq current systems are given in figure 3.5 which show a variable but systematic pattern. The pattern consists of two current systems of opposite directions centred in each hemisphere arising from the heating effect of the sun on the ionosphere. The currents are focussed about the mid-latitudes of 30^0 and the summer hemisphere currents are more intense. The foci remain almost static with respect to the sun, centred on 1200h *LT*. Magsat's sun-synchronous, twighlight, polar orbit was designed so as to minimise Sq effects. The 0600h and 1800h local times indicate the approximate Magsat path with respect to this model.

In addition to the Sq system there is a secondary effect due to atmospheric circulation from the gravitational attraction of the moon, the *L* effect. The resultant field is small (by a factor of 25 relative to Sq), difficult to isolate and complex since it depends on lunar phases and seasons.

At the level of the magnetic dip equator there is a 600 km wide belt of increased Cowling conductivity of the ionosphere, thereby channeling an eastward current within this region; the *equatorial electrojet*. The electrojet produces total field amplitude responses of 12 to 26 nT of near-earth satellite magnetometer observations (400 km altitude) (Cain and Sweeney, 1973). Cain and Sweeney (1973), using POGO data, mapped the position of the electrojet which is reproduced in figure 3.6. Although the electrojet follows the magnetic dip equator generally, it does show small but significant excursions. They found that there were instances when the equatorial electrojet was absent or weakly westward. Maeda et al. (1982) by analysing Magsat data observed an anomalous variation in declination (not observed at ground-based observatories), viz.: (1) it appears on the low-latitude dusk side, (2) it is antisymmetric about the dip equator and (3) the amplitude of the response (5 to 25 nT) depends on longitude and altitude. They concluded that a meridianal current system exists in the equatorial ionosphere which is associated with the equatorial electrojet.

It should be noted that diurnal quiet variations also occur at high latitudes similar to Sq but termed S_q^p (see section 3.1; field aligned currents).

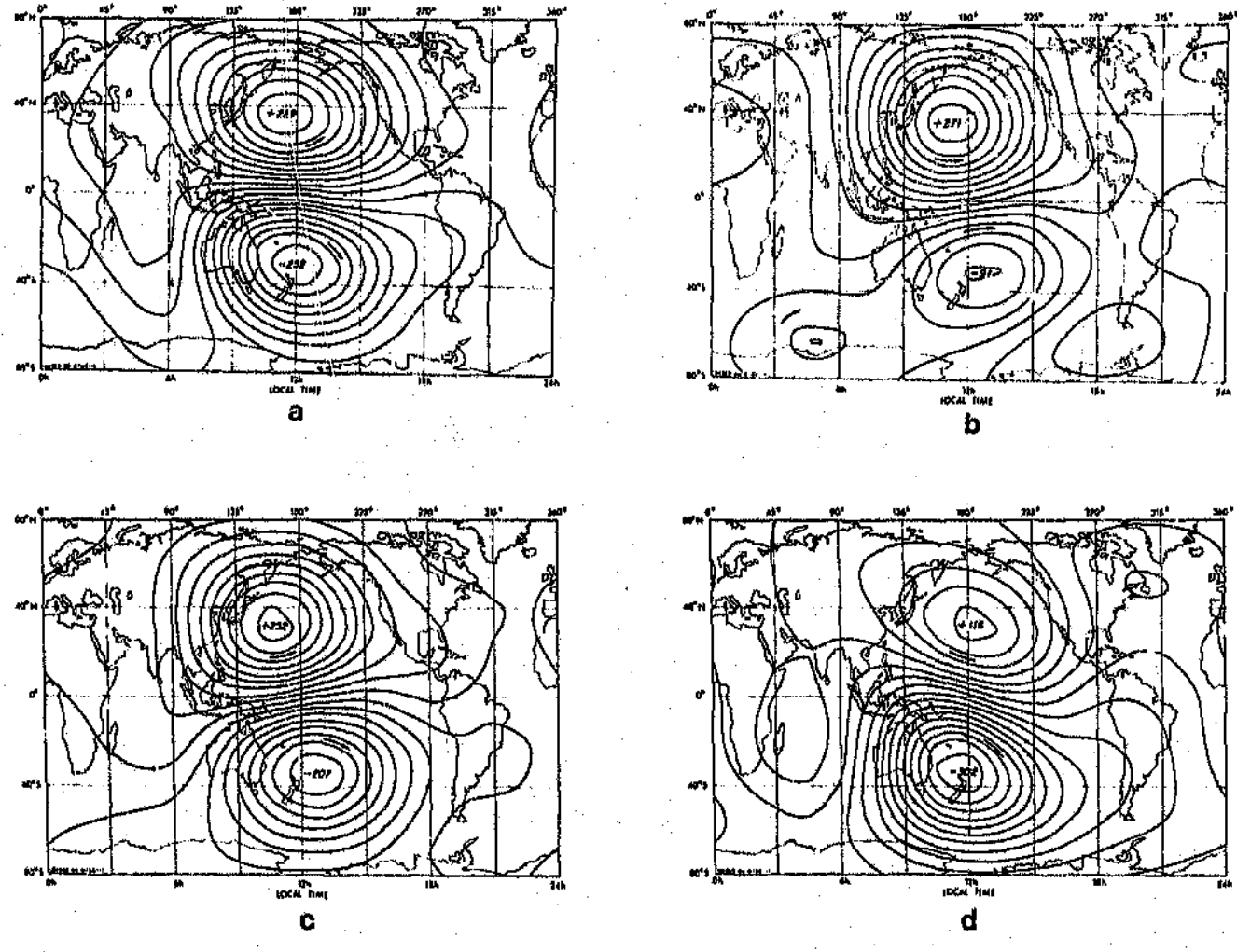

Figure 3.5: Equivalent current system of Sq variation at 0000h UT for March equinox (a), June solstice (b), September equinox (c) and December solstice (d). 0600h and 1800h local times are Magsat's approximate twighlight path with respect to the Sq current system. (After Parkinson, 1983).

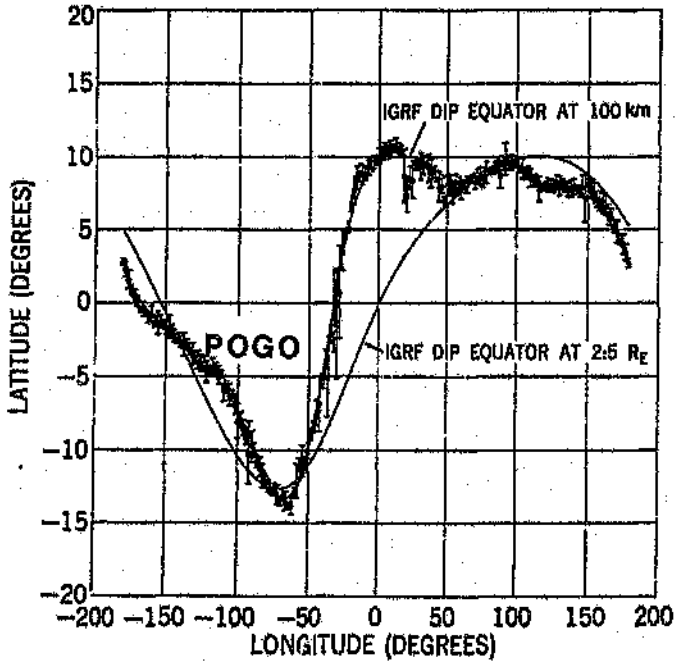

Figure 3.6: Average latitude of equatorial electrojet from observations made by POGO satellites. The centres are compared with the IGRF (epoch 1970.0) dip equator at 100 km and 2,5 R_E altitudes. (After Cain and Sweeney, 1973).

3.4 Modelling of External field effects

The above phenomenological synopsis gives an insight of the complexity of the structure of external magnetic fields and their temporal behaviour. In order to model the geomagnetic field and magnetospheric field, magnetic quiet days are selected. The magnetic potential may be represented by the spherical harmonic series of equation 2.2 where the coefficients s and q describe fields of external origins.

The strongest magnetospheric field effect that is manifest on the ground or from a near-earth satellite at low to mid-latitudes is that of the equatorial ring current with lesser contributions from other magnetospheric sources. The ring current and magnetospheric fields may be represented adequately by the first-degree and zero-order zonal function of equation 2.2 (Langel and Sweeney, 1971). Because of temporal variations of Dst (the storm time field) a siginificant internal contribution is obtained from inductive components within the earth. Details of this model are dealt with explicitly in Chapter 6.

The ionospheric sources are modeled from ground-based observations using spherical harmonic analysis. However, the problem for Magsat data is different in that the data are restricted to dawn and dusk local times, which in theory were meant to eliminate ionospheric field contributions. This proved not to be entirely correct. A method proposed by Yanagisawa (1983) allows the determination of an average ionospheric field by simply stacking observations for a specific local time. Details of this problem are addressed explicitly in Chapters 5 and 6.

3.5 Conductivity structure of the earth

The temporal nature of the external ionospheric and magnetospheric source fields induce eddy currents within the conductive regions of the earth, i.e. the oceans and lower mantle. The spectral responses from these conductive regions are used to determine the underlying electrical structure. Resistivities encountered in the crust range from less than 0.25 Ohm m (the value of seawater) to 10^6 Ohm m or more for dry crystalline rocks. Most estimates of global conductivity (using Sq and Dst variations) as a function of depth indicate a sharp rise at a depth of 400 to 600 km (at the level of the mantle transition zone). The conductivity

below this depth can, for most purposes, be considered to be at the inductive limit; this global conductive region is termed the *conductosphere*. Figure 3.7 illustrates several conductivity profiles determined over oceanic and continental crust. The main difference between the oceanic and continental profiles seems to be that the discontinuity is shallower below the oceans.

With regard to near-earth satellite magnetometer observations the concern is to ascertain the significance of the induced earth currents on the magnetic fields arising from the oceans and the conductosphere. Hermance (1982) by model simulations addressed two important questions, viz.: (1) are induction effects significant for near-earth satellite observations and (2) what are the effects of lateral differences in the gross conductivity structure of the earth at satellite altitudes? He noted that for the distant magnetospheric sources the induced component of a conductive mantle in a spherical earth may contribute as much as 34% of the external source field amplitude; larger at satellite altitudes than the target lithospheric magnetic anomalies. For short period fluctuations of the inducing field (200 s to 1 hr) the response of the oceans is at the inductive limit. The induced contribution at satellite altitudes may be as much as 42% of the source field.

Hermance (1982) then considered the position of the satellite (400 km) with respect to the two possible inducing field sources, namely, magnetospheric ($\sim 3\ R_E$) and ionospheric ($\sim$ 150 km). The total response (horizontal component) for magnetospheric sources above the satellite is close to twice that of the source field strength. For sources beneath the satellite the fields observed at the satellite tend to cancel and the total field is almost zero. A lateral conductivity change in the crust or lithosphere (e.g. continent to ocean contrast) may generate a magnetic response of an order of magnitude smaller than the source field, whose shape is complicated by the position of the observation platform with respect to the primary field. The anomalous response is significant for sources originating below the satellite only (i.e. the ionosphere). A disturbance of say 100 nT over a lateral resistivity change from 30 Ohm m to 15 Ohm m would manifest a horizontal magnetic field inductive response of 5 nT, which is well within the resolution of Magsat.

The study of Hermance (1982) serves to demonstrate that measurements made during magnetic disturbances could be used to investigate gross electrical properties of the litho-

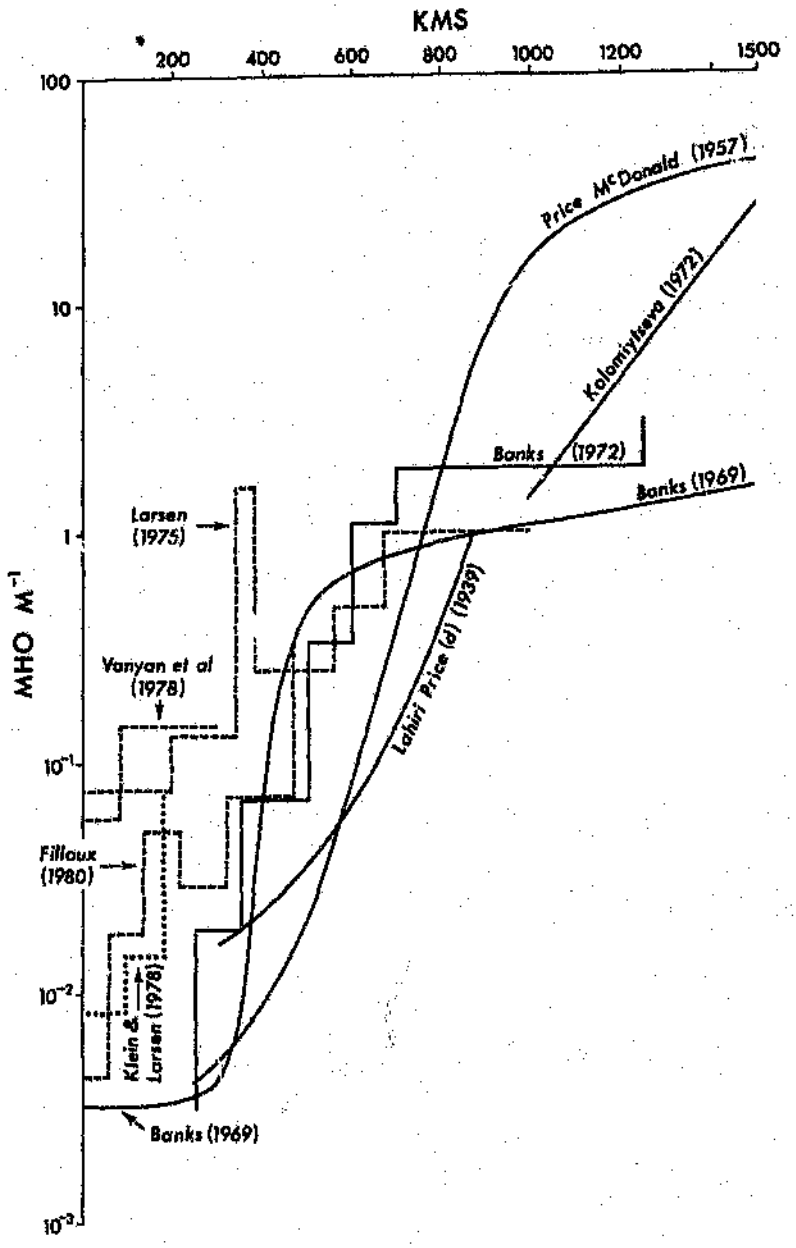

Figure 3.7: Earth conductivity estimates as a function of depth. Solid lines refer to continental crust while the dashed lines refer to oceanic crust measurements. (After Parkinson, 1983).

sphere as a useful complement to magnetic investigations. Didwall (1984) using a database derived from POGO satellite magnetic measurements estimated an electromagnetic response function. Best estimates of this response function indicate an upper-mantle conductivity of 10^{-2} Mho m^{-1}. For the purpose of generating lithospheric anomaly maps inductive effects are minimised by selecting magnetically 'quiet' data, typically with a magnetic activity index of $Kp \leq 2_+$[2]. In the final analysis the most significant contribution originates from the Dst variations.

[2]A magnetic activity index of 3_+ represents a disturbance, peak to peak, of 24 nT at ground level at the Hermanus observatory (Kühn and Zaaiman, 1986).

Chapter 4

Altitude reduction

Processing magnetic measurements to account for the variable altitude of the satellite tracks is an unresolved problem, to-date. Attempts towards a solution have and continue to be made with varying degrees of success. The approach, rationale and methodology to correct for the variable altitude covers a wide spectrum. In this chapter the various techniques that have been used are reviewed and results of this research towards finding a solution to the problem are presented.

4.1 Review of methods

Corrections to account for the variable altitude of the satellite tracks varies widely amongst users. The effect of the variation of the satellite altitude is complex, because it is manifested not only as a change in amplitude but also in a spatial sense. These effects are demonstrated graphically in section 4.2. In many instances the problem is coarsely dealt with, for example, by simple stacking of magnetic data within selected cells. A mean magnetic amplitude and altitude is thus obtained for the selected cells within the area under investigation (Coles et al., 1982; Ritzwoller and Bentley, 1982). The supporting philosophy being that, although the variation is still largely unaccounted for it is minimised, resulting in losses of both the amplitude and detail of anomalies, but the gross features are maintained. This may be acceptable for qualitative appraisals of the data but, not so, for quantitative interpretations.

Other more exacting methods have been considered to reduce satellite magnetometer measurements to a common datum. A review of some of these procedures is given by Regan (1979); those and other methods are described below.

4.1.1 Equivalent source

Inherent of potential fields is the ambiguity in describing the source distribution from field values outside the source region. The magnetic potential due to a magnetic distribution $m(\alpha,\beta,\gamma)$ at a point $P(x,y,h)$ above the distribution is

$$U(x,y,h) = \nabla_0 \int_0^\infty \int_{-\infty}^{\infty} \int_{-\infty}^{\infty} \frac{m(\alpha,\beta,\gamma)}{[(x-\alpha)^2+(y-\beta)^2+(z-\gamma)^2]^{\frac{1}{2}}} d\alpha d\beta d\gamma \qquad (4.1)$$

where ∇_0 is the directional derivative in the direction of magnetization (Gunn, 1975). The concept provides a means of variable surface continuation of the magnetic field (Dampn ., 1969; Mayhew, 1979; Mayhew et al., 1980).

In practice the equivalent source method is performed by modelling the anomaly field with respect to an arbitrary surface distribution (an array) of dipoles. The anomaly field is computed at discrete points

$$a_j = \sum_{i=1}^{k} p_i F_{ij} \quad , j = 1,2,3,\ldots,n \qquad (4.2)$$

where k is the total number of dipoles and p_i is the magnetic moment of the ith dipole. F_{ij}, the dipole source function is given by Mayhew (1979).

The magnetic dipoles are constrained to a regular latitude, longitude grid with an inclination and declination defined by a degree 13 spherical harmonic expansion (Mayhew and Galliher, 1982). A solution for the moments is made using least squares. Having determined the parameters, these may be used to compute the anomaly field at any position above the equivalent source distribution.

4.1.2 Spatial gradients of the equivalent source

A method was presented by Bhattacharyya (1977) where the spatial gradients of an equivalent magnetic dipolar source distribution are used to perform a variable upward continuation of the field. The formulation of the technique was developed by Bhattacharyya and Chan (1977) and extended to take into consideration the spatial variation of the main field in the case of satellite data.

The method is applied after some preprocessing. Arithmetic means of both amplitude and altitude of measurement are calculated from a selected dataset for 1^0 by 1^0 longitude and

latitude cells. This procedure is based on the assumption that the amplitude of the magnetic field at satellite altitudes decays linearly with respect to altitude.

Dipoles (of moment p per unit area) on the equivalent source surface S are assumed to be polarised in a direction normal to S. The total field at a point $P(x, y, h)$ above the surface in a direction t defined by the direction cosines (l,m,n) may be expressed as

$$T = -\int\int_s \mu \frac{\delta}{\delta n}\frac{1}{r} ds \tag{4.3}$$

where $\mu = (t \cdot \nabla_0)p$, and represents the gradient of magnetisation along the direction t of the geomagnetic field.

Considering the limiting case where the point P approaches the surface S along a normal to S, equation 4.3 reduces to a Fredholm integral of the second kind and relates the observed total field T to the spatial gradients of magnetisation of an equivalent dipole source (Bhattacharyya and Chan, 1977). The total field can thus be calculated for any point above S if the spatial gradients of $p(\frac{\delta p}{\delta \alpha}, \frac{\delta p}{\delta \beta})$ are known. Satisfactory results can be achieved only if the direction of the geomagnetic field that is used to compute (continue) a new point is in the same direction as modelled by the gradients of the equivalent dipole source distribution surface (i.e. induced magnetisation must be assumed).

4.1.3 Fourier series modelling

The method proposed by Henderson and Cordell (1971) uses finite Fourier harmonic series approximation to reduce variable altitude potential field data to a common datum. The method may be applied to regular or irregularly spaced data in two- or three-dimensional space.

The magnetic field may be approximated by a finite number of linear, independent harmonic functions of the form

$$T(x, y) = A_0/2 + \sum_{k=1}^{M} e^{2\pi k(z/\lambda)} \cdot [A_k \cos 2\pi k(x/\lambda) + B_k \sin 2\pi k(x/\lambda)] + \varepsilon_M(x, z) \tag{4.4}$$

where λ is the fundamental wavelength, $2M + 1$ is less than or equal to the number of data points and $\varepsilon_M(x, z)$ is the error of approximation.This functional represents a finite Fourier series if the data were on the plane $z = 0$ and were equally spaced. The proposed method fits the function to the data and solves for the coefficients using least squares. The harmonic

modelling technique has been used on satellite-borne magnetometer data by, for example, Regan (1979).

4.1.4 Multiple linear regression

The method presented by Lötter et al., (1986) models the data as in the previous case but, assumes a linear dependance of variables. The approximation is of the form

$$T = S_0 + S_1 h + S_2 \theta + S_3 \phi \tag{4.5}$$

where T is the anomaly field, h the altitude of measurement and θ,ϕ are the respective longitude and latitudes of measurement.

The coefficients $S_0, S_1 \ldots, S_3$ are solved for, using least squares (Lötter and Kühn, pers. comm.). The principal assumption is that, for satellite altitudes and for a cell of 1^0 by 1^0 or less the magnetic gradients may be regarded as linear.

4.1.5 Schwarz-Christoffel transformation

Wendorff (pers. comm.) developed the Schwarz-Cristoffel method (Parker and Klitgord, 1972) to correct satellite data to a common datum. If the measured field is on a level plane, continuation to an irregular plane is straightforward (Henderson, 1970). The irregular satellite track problem can be converted into the simpler form by using the theory of functions of a complex variable. Let every point of a satellite's half orbit be represented by a complex number given by $z = x + iy$. The complex z domain is now mapped with an analytic function into another complex region given by $w = u + i$ such that each point (x, y) in the one domain is represented by (u, v) in the other (Fig. 4.1).

If an analytical function g(z) maps the satellite track onto a straight line in a domain equivalent to the w domain, then the sought after simplification is achieved. To begin with, the mapping between the z and w domains is implemented with (cf. Fig. 4.1)

$$w = i\frac{z+1}{z-1} \tag{4.6}$$

where the satellite's position is given by the phase. Figure 4.2 illustrates this mapping for Magsat half orbit 402. To utilise the inverse Schwarz-Cristoffel transformation[1] (SCT)

[1]The Schwarz-Cristoffel transform provides a simple means to map the region above and including the

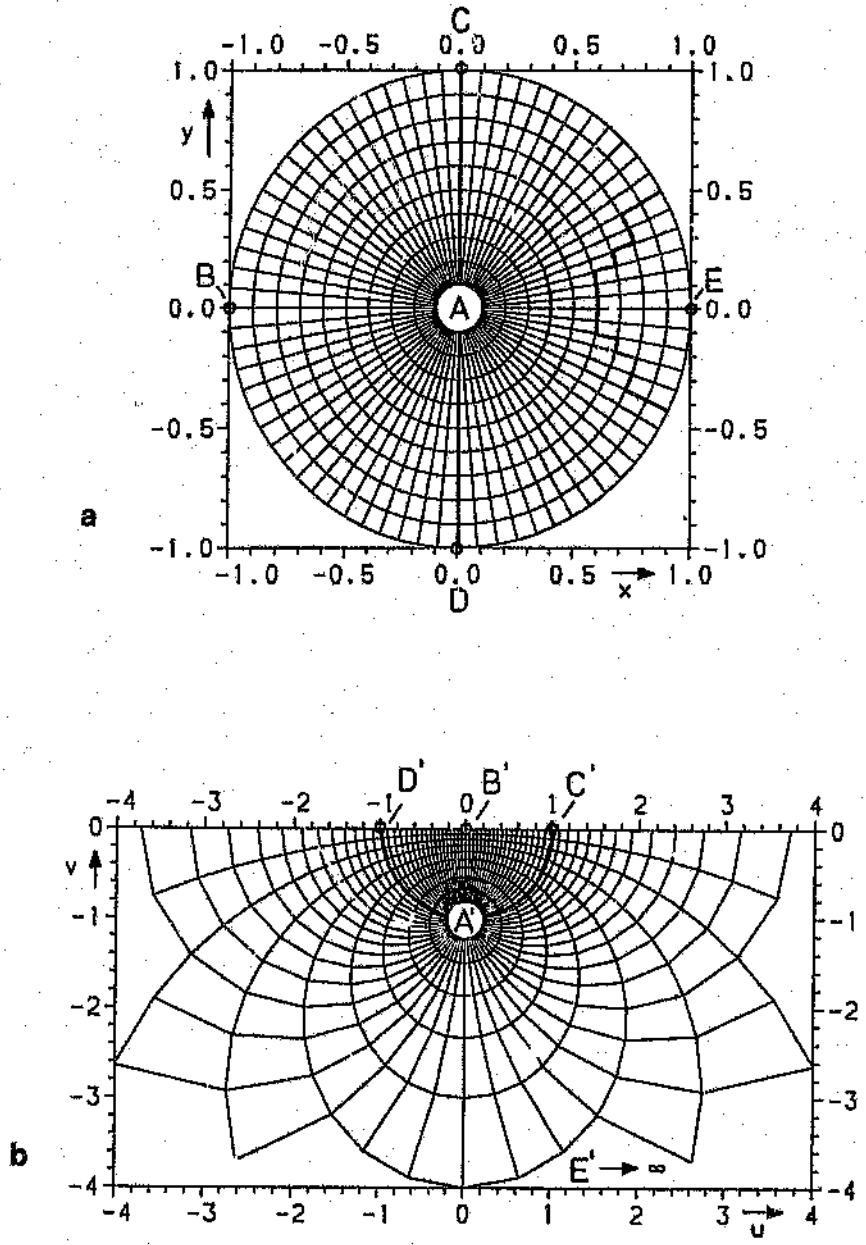

Figure 4.1: Example of a mapping between the complex regions $z = x + iy$ (a) and $w = u + iv$ (b). A satellite's half orbit D to C via B (z domain) maps onto the real axis of the w domain (D'B'C'). After Wendorff (pers. comm.).

$$g(w) = C_1 \int_{w_0}^{w} \prod_{j=1}^{n} (\hat{w} - u_j)^{\alpha_j} d\hat{w} + C_2 \quad , -1 < \alpha_j < -1 \qquad (4.$$

the satellite passes are approximated by a polygonal track; the tolerance corresponding to about 10km at the earth's surface. Applying the inverse SCT, the polygonal curve L' is transformed to L"(Fig. 4.3). Upward continuation is performed on this mapping (Fig. 4.4).

4.1.6 Discussion

The altitude corrections exploit two principles, namely:

1. Implicit modelling where a function is modelled to fit the anomaly field and corrections applied by interpolation. This process endeavours to make the functional respond implicitly to the behaviour of the potential field without *a priori* knowledge.
2. Explicit modelling where the knowledge of the field and of potential theory is used either to model the source or to extrapolate the field by analytical means.

The Fourier series and linear regression methods attempt to conform to the former rationale of implicit modelling. To successfully implement this method the variables must be linearly independent. Also, it is assumed that the function is sufficiently flexible to represent the topology of the field. The three-dimensional linear regression method makes an erroneous assumption that the magnetic field decays linearly with altitude (Lötter et al., 1986). A similar assumption is made by Bhattacharrya (1977) at the preprocessing stage with regard to the equivalent-source spatial gradients method. Both authors believe that this assumption is reasonably valid for the altitude range of a near-earth satellite.

With respect to the latter principle, the equivalent source, the spatial gradients and the Schwarz-Cristoffel transform methods are used to continue the magnetic anomaly field with *a priori* information. The ambiguity of the potential field to discriminate source distribution is effectively exploited by the equivalent source methods. However, in order to continue the field to an altitude datum, it is assumed that the magnetic polarisation of the anomaly field is parallel to the main field. Although this assumption is almost universally made there is

real w axis into the interior and edge of a polygon (Parker and Klitgord, 1972).

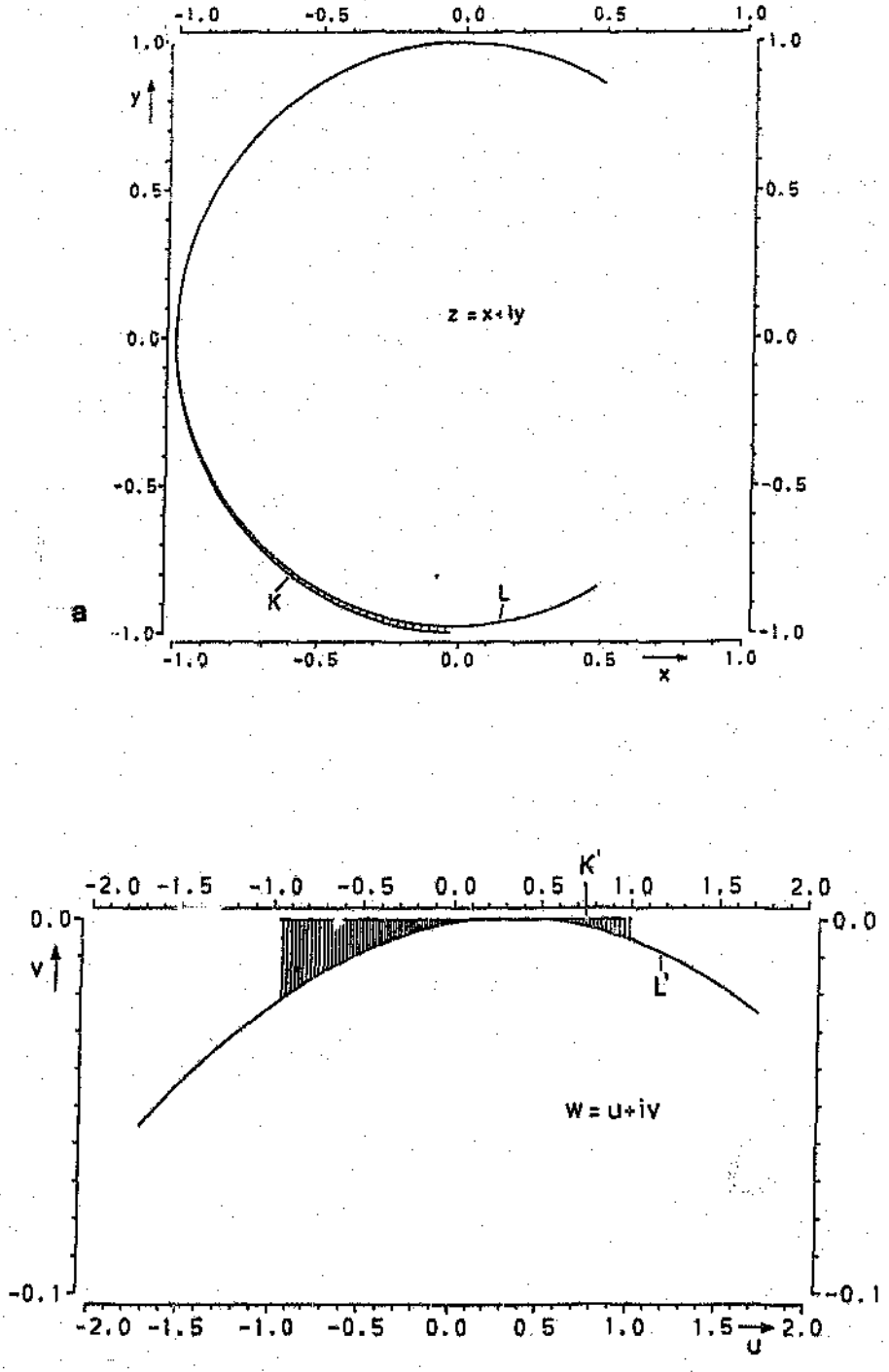

Figure 4.2: Example of the mapping of Magsat half orbit 402 in the z (a) and w (b) domains i.e. circle to plane. After Wendorff (pers. comm.).

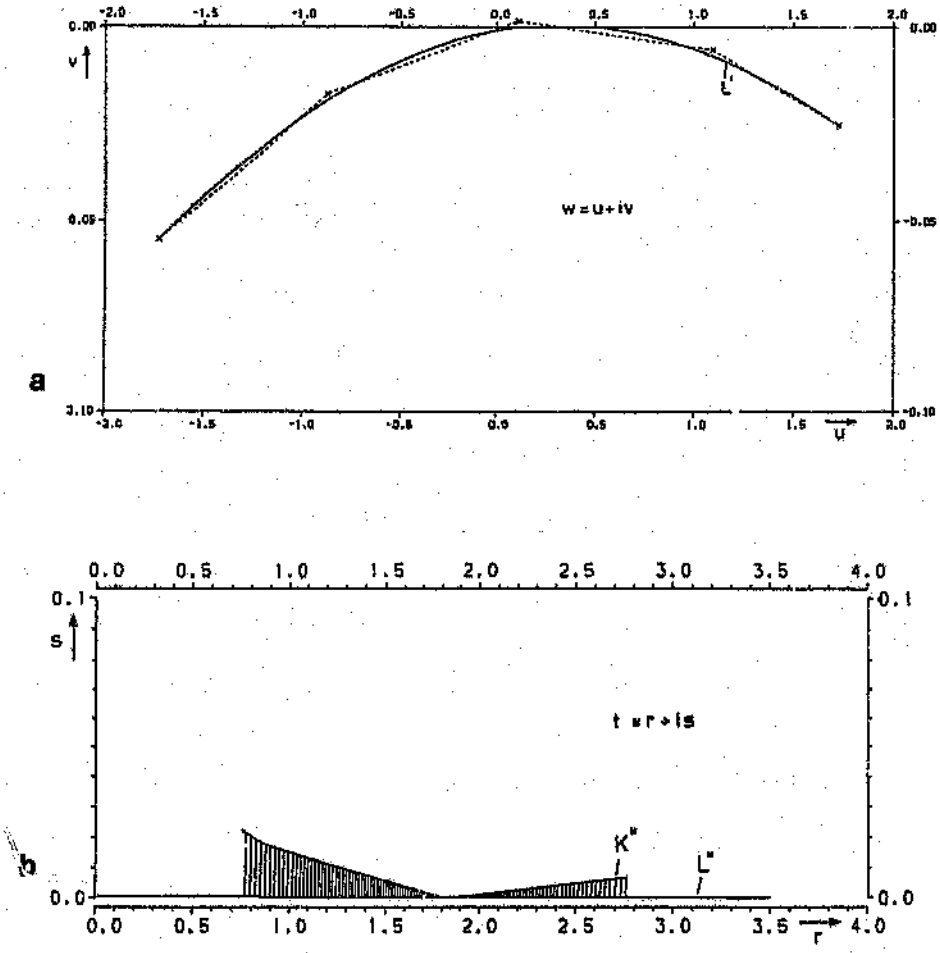

Figure 4.3: Example of the polygonised satellite track (a) and the applied inverse Schwarz-Cristoffel transformation (b). After Wendorff (pers. comm.).

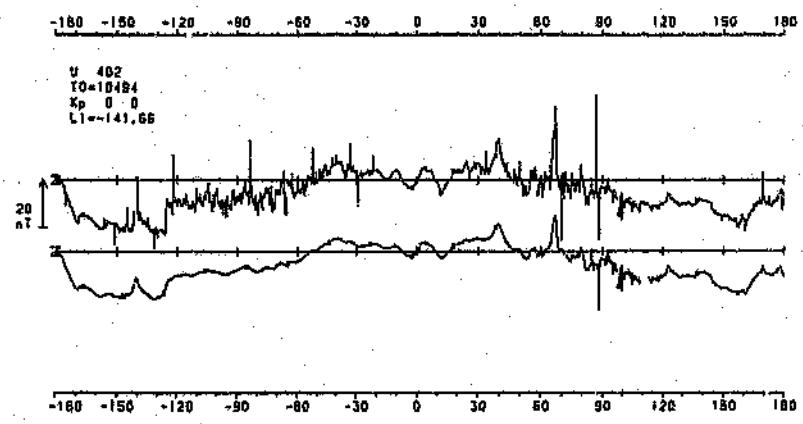

Figure 4.4: Results of upward continuation after SCT . The top curve is the original data, the bottom the continued data. After Wendorff (pers. comm.).

growing evidence that non-viscous remanent magnetisation[2] is observed at satellite altitudes (Toft and Haggerty, 1986; Antoine, 1989). Remanent magnetisation components may be combined vectorially to develop accurate equivalent point source operators (von Frese et al., 1981). The problem however, is to derive a suitable equivalent source distribution for processing.

The advantages and disadvantages of implementing the various methods are far reaching and need to be considered. The concept of implicit modelling is appealing, in that, no *a priori* information is required. The Fourier series three-dimensional regression method should have superior qualities to the three-dimensional linear regression of Lötter et al., (1986) since the latter method represents the anomaly field as a linear function. The approximation is partially valid for the horizontal gradients (for the scale at which it is implemented, i.e. one degree cells) but erroneous in the case of the amplitude decay with respect to altitude. Implementation of the Fourier series method however faces certain constraints. The development of the method in a rectangular coordinate system is a limitation with satellite data. The method was used by Regan (1979), over a central African region covering an area of 20^0 in longitude and in latitude, and produced reasonable results. Regan, however, showed preference to the Bhattacharyya (1977) equivalent-source spatial gradients approach.

Bhattacharyya's technique, although meeting many of the theoretical requirements, will produce errors in several regards: (1) the assumed linear decay of amplitude with altitude at the preprocessing stage, (2) the process requires downward continuation (a highly unstable process) thus requiring additional low pass filtering, and (3) the continuation assumes induced magnetisation. Similarly, the equivalent source technique is implemented with some preprocessing by simple stacking within selected latitude, longitude cells. Induced magnetisation is most commonly assumed. The process is more stable since the continuation is away from the source distribution. The equivalent source spatial gradients method is computationally more efficient (Regan, 1979).

The Schwarz-Cristoffel transformation method although attractive as a variable continuation tool, has substantial limitations for satellite applications. To begin with, the process assumes two-dimensionality of the source; an assumption that is mostly not strictly valid.

[2]It is generally argued that, for the purpose of inverting or interpreting satellite magnetic anomaly maps, VRM predominates. On this basis, induced magnetisation may be assumed (e.g. Johnson, 1985).

The mapping procedures are in themselves passive. The analytical continuation also imposes the problem of induced magnetisation. In addition, the method is based on upward continuation to the satellite orbit apogee. The process is also computationaly intensive (Wendorff, pers. comm.).

4.2 Implicit modelling

The processing and digital manipulation of the data are not ends in themselves but first steps in the process of model construction and hypothesis testing (Mayhew and LaBrecque, 1987). The emphasis here is to ameliorate the reduction process towards improving data quality, suitable for quantitative assessment. Because of the substantial limitations of the present altitude reduction methods, it is necessary to test alternative methods. In order to achieve the objective of improved data quality, model constraints should be kept at a minimum.

As previously discussed, the process of fitting a function implicitly to the potential field is appealing, particularly, if assumptions are kept to a minimum. The purpose is to interpolate, from the irregularly sampled field, the representative value of that field for a fixed point in space. If a numerical method is applied within a small sector say 1^0 by 1^0 latitude, longitude cells it may be possible to achieve altitude reduction at a stage equivalent to the preprocessing stages of the above mentioned techniques.

The weakness of most of the altitude corrections begins with the statistical averaging of the randomly sampled data within a selected bin. The results, i.e. average amplitude and altitude for the bin, are then used to apply the various altitude corrections. This process, in all cases, assumes that the magnetic anomaly field decays linearly with respect to altitude, an assumption which is shown to be invalid in figure 4.6. It is also assumed that the horizontal gradients are linear, an assumption that is almost correct for the cell sizes used at satellite altitudes. Finally, to implement satellite magnetometer data processing and reduction effectively, procedures should be computationally efficient. Overall computational efficiency can be improved by integrating the altitude correction with stochastic noise filtering at an early stage in the processing route.

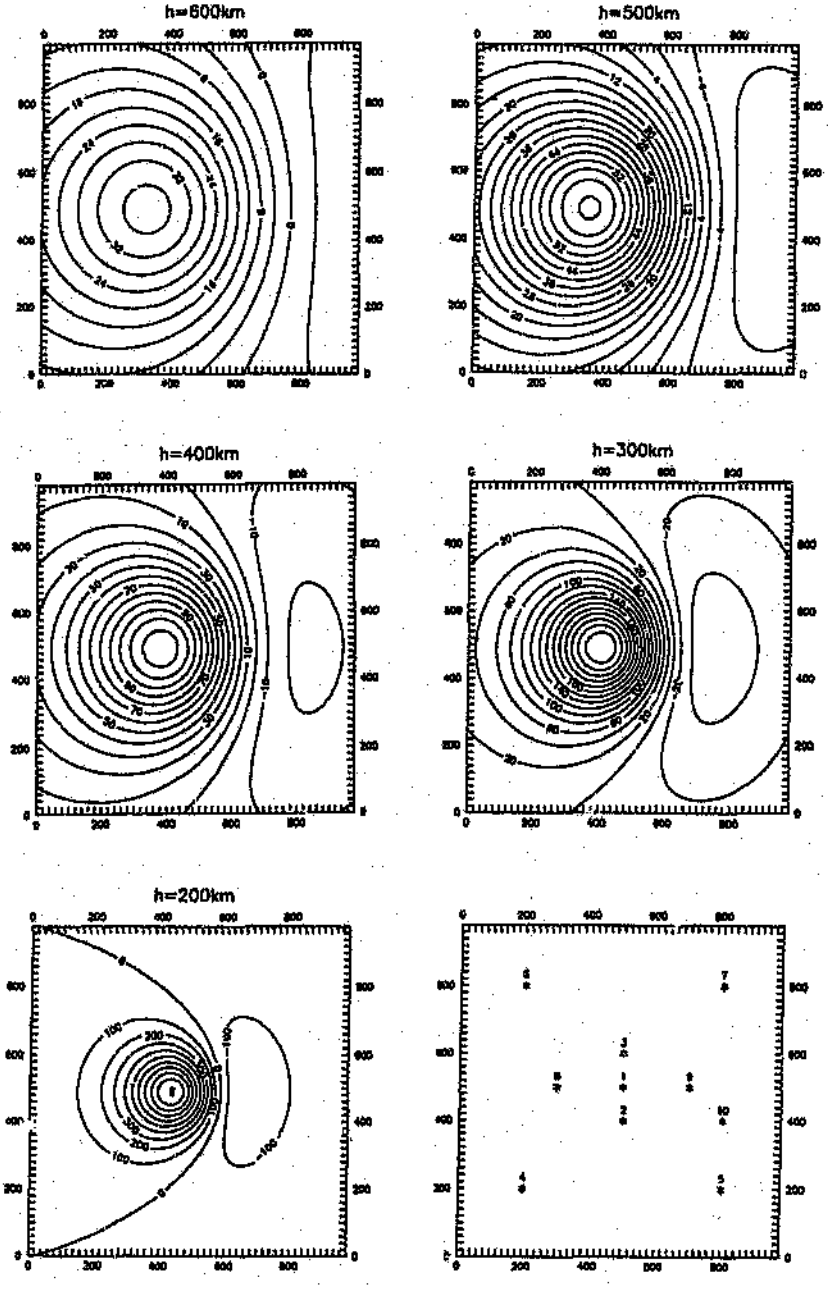

Figure 4.5: Model dipole anomaly field for various satellite altitudes. Magsat's perigee and apogee was 350 and 561 km, respectively. The lower right box shows the locality of selected points used to illustrate the amplitude versus altitude graphs of figure 4.6.

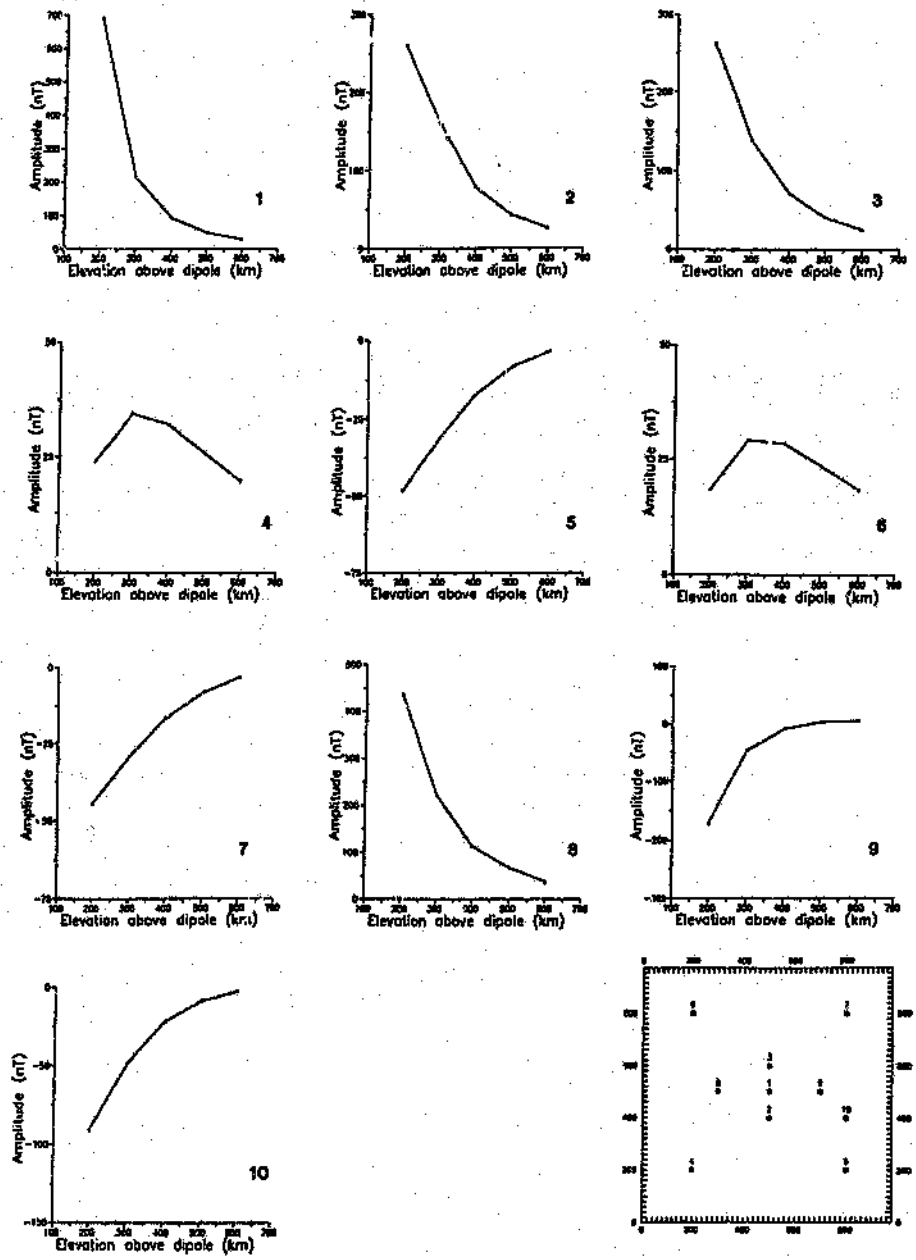

Figure 4.6: Graphs of magnetic amplitude versus satellite altitude for selected points within the near-field and far-field of the model dipole. The lower right box shows the locality of points with respect to the dipole field of figure 4.5. Magsat's perigee and apogee was 350 and 561 km, respectively.

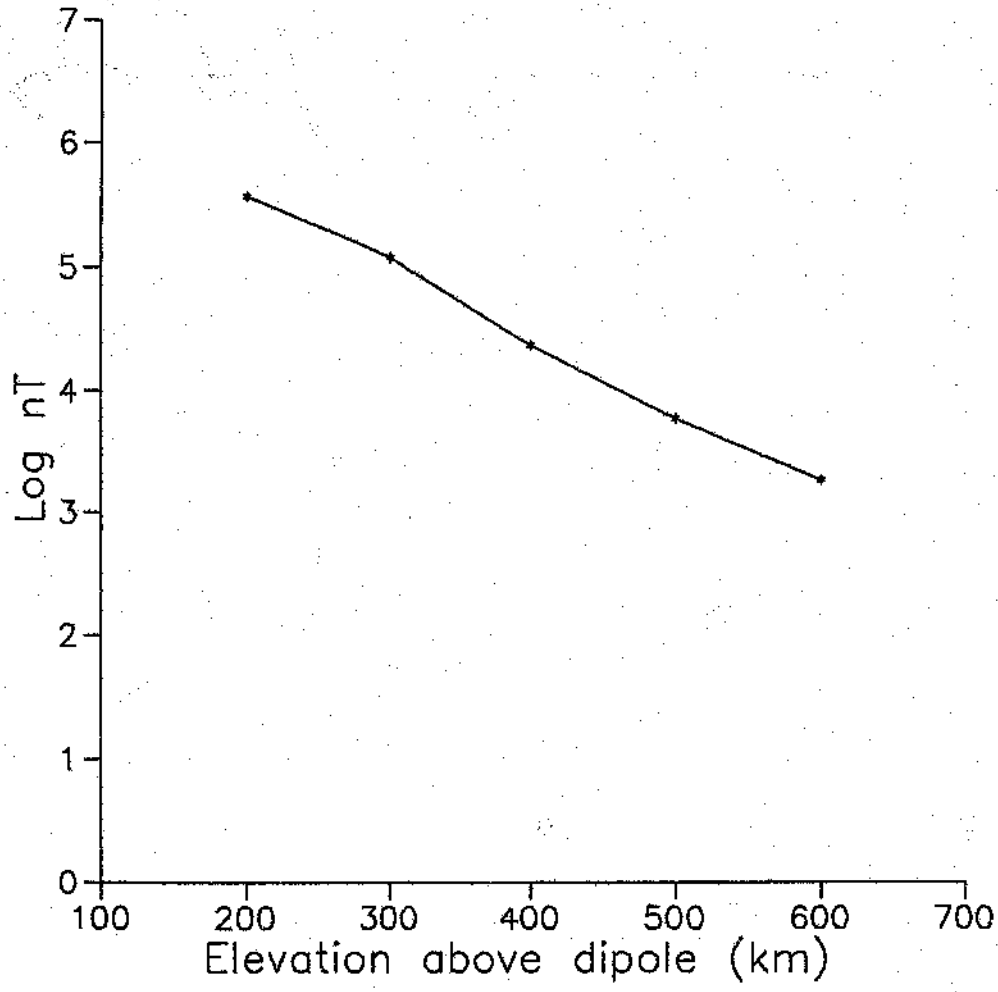

Figure 4.7: Graph of the logarithm of amplitude versus altitude for a location (position 2, Fig. 4.6) in the near field of the model dipole.

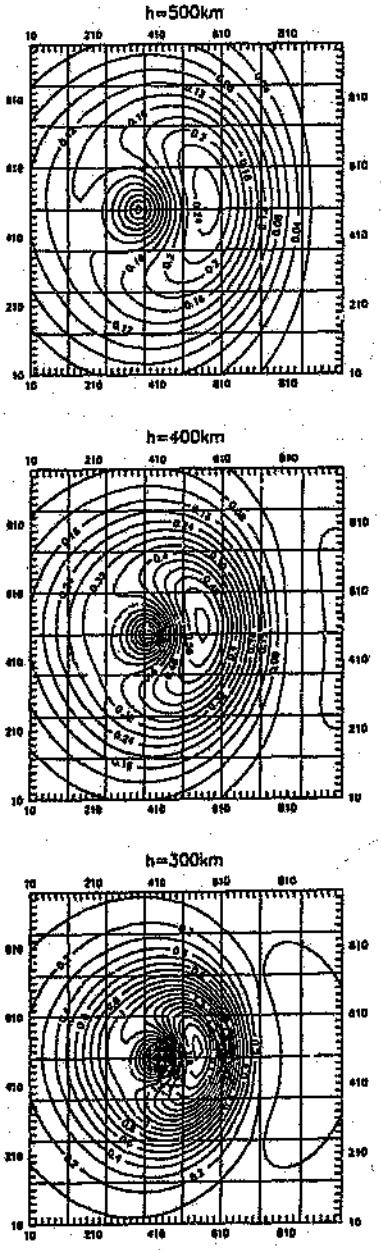

Figure 4.8: Amplitude of the horizontal gradients over the dipole anomaly field for various satellite altitudes.

4.2.1 Quadratic least squares regression

The three-dimensional linear regression of Lötter et al., (1986), although it imposes a rigid limitation on the function with respect to the morphology of the field, has the essence of the properties sought after in this research. As discussed above the horizontal gradients can be regarded as linear if the scale at which the reduction is made is small with respect to the wavelength of the anomaly field. The method is severely limited in the regions of change in slope of gradients (troughs and peaks). The concept of performing an altitude reduction at an early stage, incorporated with stochastical noise filtering, is encapsulated in the three-dimensional linear regression method of Lötter et al., (1986) and is tested in this study with necessary modification to overcome the discussed problems of linear regression. Change in slope direction of the horizontal gradients can be catered for simply by increasing the order of the polynomial.

A quadratic function of the form

$$f(x,y,h) = s_0 + s_1x + s_2y + s_3h + s_4xy + s_5xh + s_6yh + s_7x^2 + s_8y^2 + s_9h^2 \qquad (4.8)$$

was decided upon; where x, y, and h are, respectively, the latitude, longitude and altitude. The reason for selecting a quadratic function rather than a higher order function is three-fold, namely: (1) although the function is an imperfect representation of the altitude decay as presented, it is not if the amplitude decay could be made approximately linear by assuming logarithmic functionality, (2) the horizontal gradients at the scale at which it is to be implemented (approximately one to four degree cells in mid latitudes) will be well represented by a quadratic even in the regions of change in slope direction and, (3) the 'stiffness' of the function will act as a smoothing function (additional noise filtering). The amplitude decay for different sources have different fall off rates, usually obeying a power law, which may be approximated by exponential decay with respect to altitude (see Fig. 4.6). By taking the logarithm the problem is approximately linearised (Fig.4.7); satisfying point (1) above. The quadratic function is tested below, by computer simulations, with and without linearising the amplitude decay.

A single dipole source at the earth's surface was used as a synthetic model to test the validity of the reduction processes that are tested or implemented in this study. The dipole

was chosen because it describes a three-dimensional anomaly field. Figure 4.5 illustrates the dynamic spatial and amplitude[3] range of the anomaly field, for a dipole source (in mid latitudes) viewed from a fixed 1000 by 1000 km window at various satellite altitudes. Figure 4.6 shows the decay of anomaly amplitude with respect to altitude for selected points in the far-field and near-field of the dipole. Clearly, the assumption of linear decay is erroneous. The horizontal gradients (scalar gradient) over the dipole field for typical satellite altitudes are illustrated in Figure 4.8.

4.2.2 Least squares solution using singular value decomposition

The least squares solution of a quadratic function is a set of ten coefficients. Depending on the cell size, rejection criteria and the latitude of the cell, the number of data points may be less than but in general will be greater than the number of coefficients. Thus the problem under consideration is that of an overdetermined (or rarely underdetermined) set of linear equations. Also, for the routine application of the reduction algorithm, it is necessary that the algorithm be robust. The singular value decomposition is a robust method to solve linear least squares problems of this kind.

The problem may be formulated as a set of simultaneous equations

$$A \cdot x = b \tag{4.9}$$

where x is the solution vector. The general least-squares solution is

$$x = [A^T A]^{-1} \cdot A^T \cdot b \tag{4.10}$$

Singular value decomposition may be defined as any $M \times N$ matrix A whose number of rows M is greater than or equal to its number of columns N, and can be expressed as the product of an $M \times N$ column-orthogonal matrix U, an $N \times N$ diagonal matrix W with positive or zero elements and the transpose of an $N \times N$ orthogonal matrix V

$$A = U \cdot W \cdot V^T \tag{4.11}$$

where U and V are eigenvector matrices.

[3]For the convenience of operating with the various graphic facilities and for general presentation purposes the dipole moment was chosen so as to exagerate typical satellite anomaly amplitudes by a factor of 10.

The decomposition of equation 4.11 can always be made no matter how singular the matrix is (Press et al., 1988). The robustness of the method is further exploited by the ability to diagnose and rectify ill-conditioning or singularity of the matrix. For an underdetermined set of linear equations the matrix A is simply augmented with zeros.

The inverse of the matrix A is

$$A^{-1} = V \cdot [diag.(\frac{1}{W_j})] \cdot U^T \tag{4.12}$$

Thus the least squares solution vector x is given by

$$x = [A^T A]^{-1} \cdot A^T \cdot b = V \cdot [diag.(\frac{1}{W_j})] \cdot U^T \cdot b \tag{4.13}$$

where W_j are the squares of the eigenvalues of $[A^T A]$ (Jackson, 1972).

4.2.3 Results of the quadratic regression

In order to test the response of the method with a fairly complex field morphology it was first tested over an area (1000 by 1000 km) covering a dipole source at the earth's surface with a range of altitudes as indicated by Figure 4.5. Depending on the results the method would then be extended to the scale of implementation, that is, one to four degree cells. In order to approximate the problems of variable altitude a set of some 45 data points of random altitude (range, 200-600 km) were selected randomly over the dipole source (Fig. 4.9). The quadratic regression algorithm was then applied to that data and used to interpolate the dipole field for specific altitudes (300, 400 and 500 km) above the dipole source.

Figure 4.10 shows the results of the altitude reduction using the quadratic regression for some 45 data points covering the dipole source (cf. Fig. 4.9). These results are unsatisfactory. The method shows a close prediction of anomaly amplitudes in the central region for the mean altitude of 400 km only (Magsat's mean altitude). The function does not, however, make a fair attempt to follow the topology of the field. In comparison, a cubic function was also tested on the same data. The results of that trial, which are not included here, showed that the interpolation was far too susceptible to sampling. The interpolated field morpholgy was strongly controlled by the distribution of the sample points.

Although the results of the above experiment were not satisfactory, the next phase of implementation was nevertheless attempted, i.e. simulating the 1^0 by 1^0 cells. This was

undertaken on another synthetic data set. Here the area over the dipole source (1000 by 1000 km) was gridded on 20 km centres. The amplitude of the anomaly field is given by a randomly generated altitude (in the range 200 km to 600 km) (Fig. 4.11). The quadratic regression algorithm was then applied to a moving cell whose dimension (window) is larger than the increments. The cell's midpoint is interpolated to the required altitude datum. The resultant grid represents the altitude corrected dipole field.

Results of this work are disappointing. Several attempts were made using various window sizes and increments with insignificant improvements. Figure 4.12 is an example of the altitude reduction (400 km) for a 120 by 120 km moving window with 60 km increments. Clearly these results are unacceptable. By excluding the linearisation procedure (i.e. by not taking the logarithm) of altitude decay from the algorithm its influence was assessed. This had a marginal effect. The above tests serve to illustrate the inadequacy of quadratic regression. They do, however, suggest that the answer to an effective altitude reduction algorithm may lie in the statistical modelling process rather than in manipulating the independent variables.

4.2.4 Median linear regression

Having established that the modelling by least squares may be the reason in part[4] for the poor results obtained with the linearised-decay surface quadratic function, an alternative robust modelling method was attempted. For experimental data that cannot be guaranteed free from 'flyers', modelling in the L_1 norm provides superior results than from those obtained by the traditional least-squares method (Barrodale, 1968).

The horizontal gradients within the area in which the reduction is to be made are assumed linear and the amplitude decay with altitude is linearised. The problem is thus simplified from a surface quadratic function to a simple straight line regression. The approximation to a straight line lends to efficient computation.

The problem may be expressed as

$$y(h) = a + bh \tag{4.14}$$

where the amplitude of the anomaly field $y(h)$ is given by the altitude.

Fitting of the line is achieved by minimising the L_1 norm

[4]It is recognised that the source function used may also in part be responsible for the poor results.

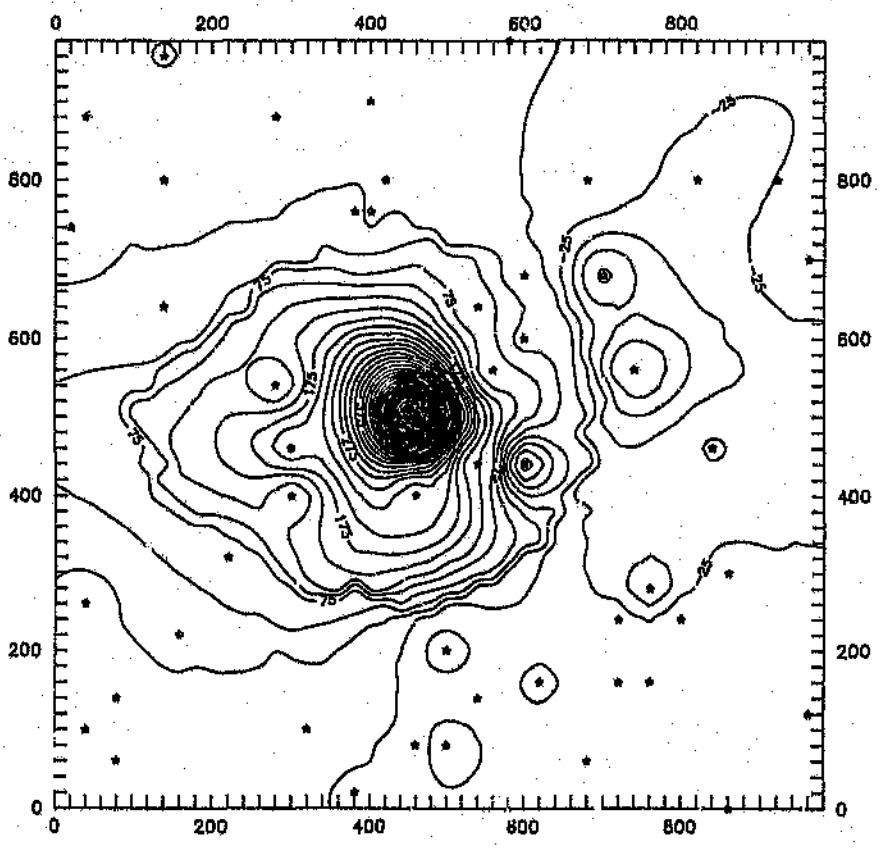

Figure 4.9: Simulated effect of variable altitude over a dipole source. Data points are represented by an asterisk. Amplitudes were calculated for altitudes randomly generated in the range 200 km to 600 km.

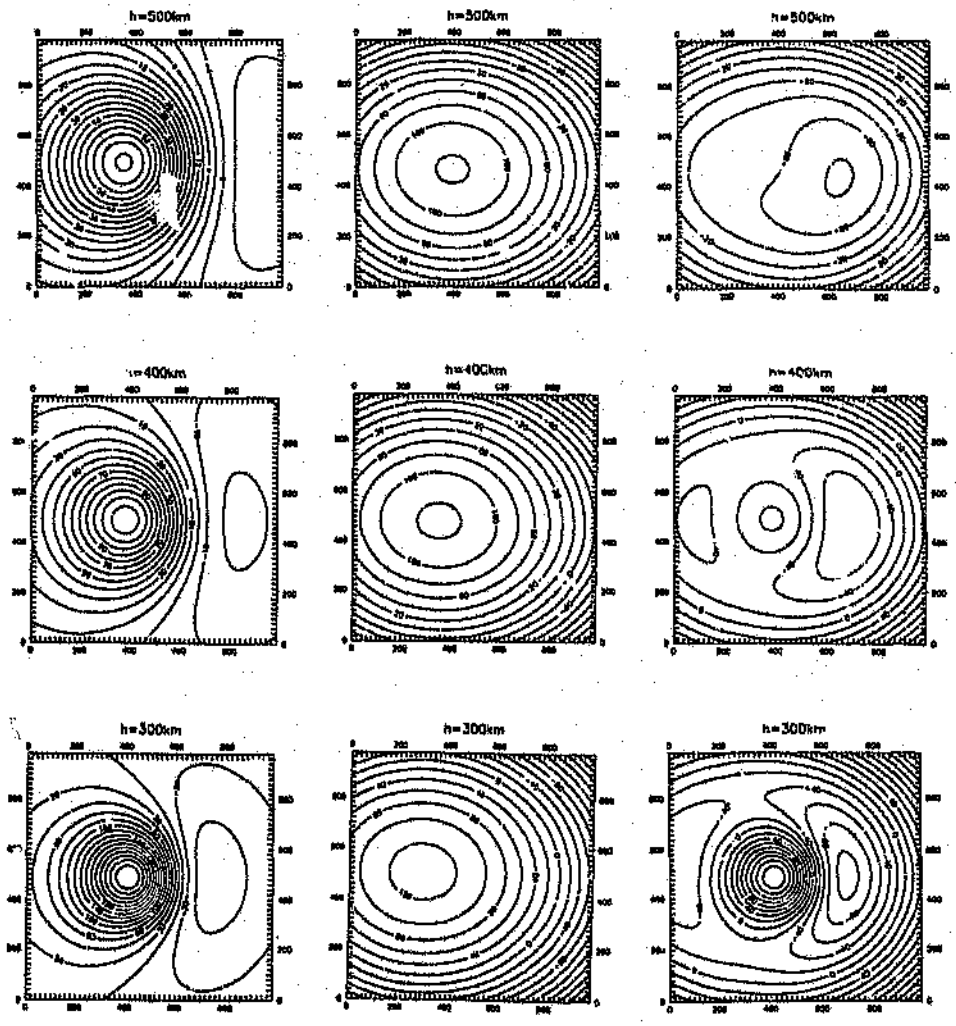

Figure 4.10: Altitude reduction using the quadratic regression method over the dipole source. From left to right, columns illustrate the original dipole anomaly field, the interpolated field and residual, respectively. The rows indicate the appropriate altitudes of interpolation.

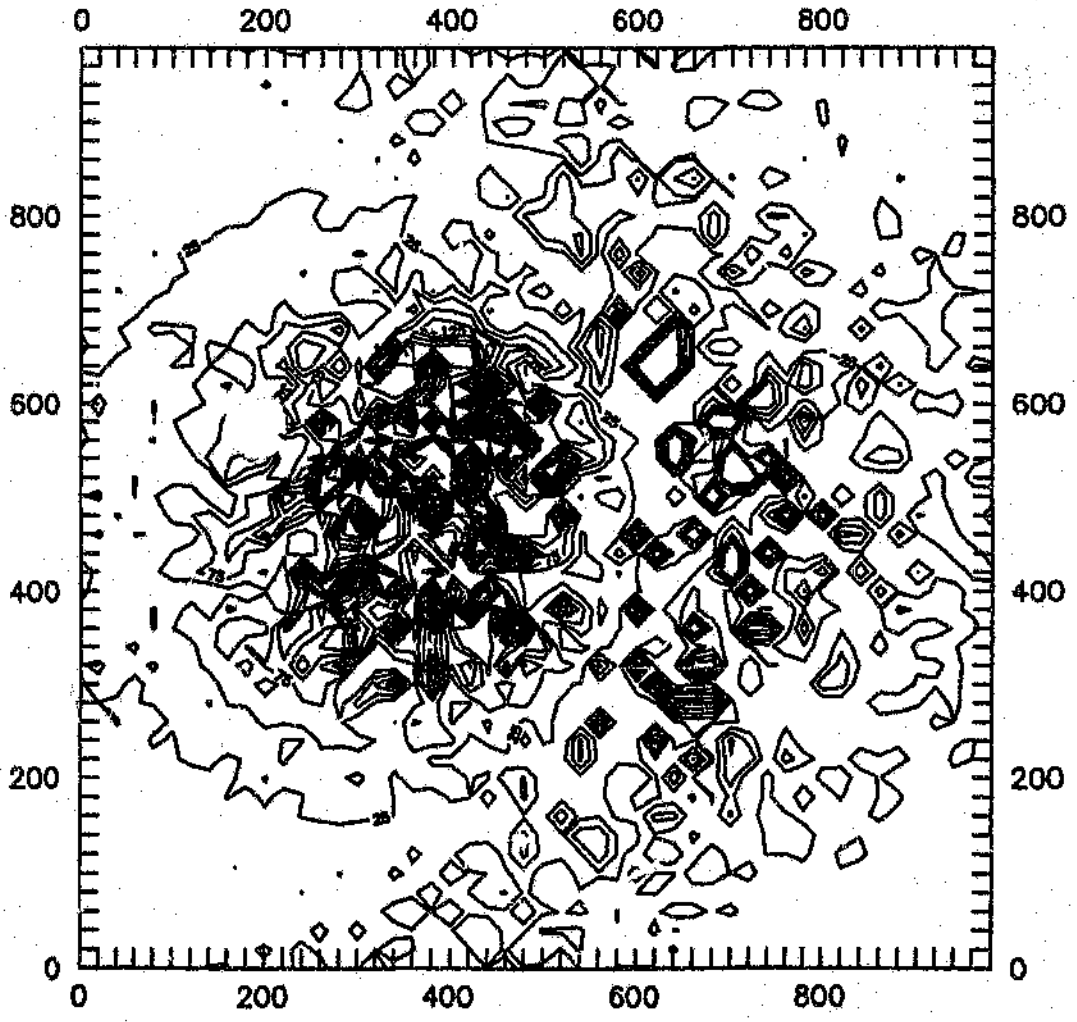

Figure 4.11: Simulated variable altitude effect of the dipole anomaly field. The data are on a 20 km grid spacing. Amplitudes are given by the altitude, in the range 200-600 km. Contour interval is 25 nT. The anomaly field is far too noisy to annotate contours.

$$\sum_{i=1}^{N} |y_i - a - bh_i| \tag{4.15}$$

The simplification of the merit fun tion with respect to the least squares method is based on the median. The median C_M of a set of numbers C_i is also that value which minimises the sum of the absolute deviations

$$\sum_i |C_i - C_M| \tag{4.16}$$

For a fixed slope b, the value which minimises 4.15 is

$$a = median\{y_i - bx_i\} \tag{4.17}$$

The local M-estimate for parameter b is

$$0 = \sum_{i=1}^{N} x_i sign(y_i - a - bx_i) \tag{4.18}$$

Replacing a by the implied function $a(b)$ of 4.17 then 4.18 is an equation in a single variable which may be solved by bracketing and bisection (Press et al., 1988; Sadovski, 1974).

4.2.5 Results of the median linear regression

The linear regression assumes that contributions of the anomaly field with respect to the horizontal gradients are linear and that any variation in amplitude is controlled by the altitude at which the observation was made. Thus the smaller the cell's window on which the algorithm is applied, the better the approximation. The median linear regression reduction was tested on the same synthetic data as that used for the surface quadratic function, that is, figure 4.9.

Results for a 160 by 160 km window moved in 60 km increments are given in figure 4.13. The results are provided for several interpolated altitudes and shows remarkable recovery of the original dipole field, both spatially as well as in amplitude. The reduction algorithm was tested with various window sizes and increments. There are marginal improvements in the statistics (least squares per cent fits and r.m.s.) with the increase in window size, which incidently, cannot be discerned qualitatively. The marginally improved statistics with

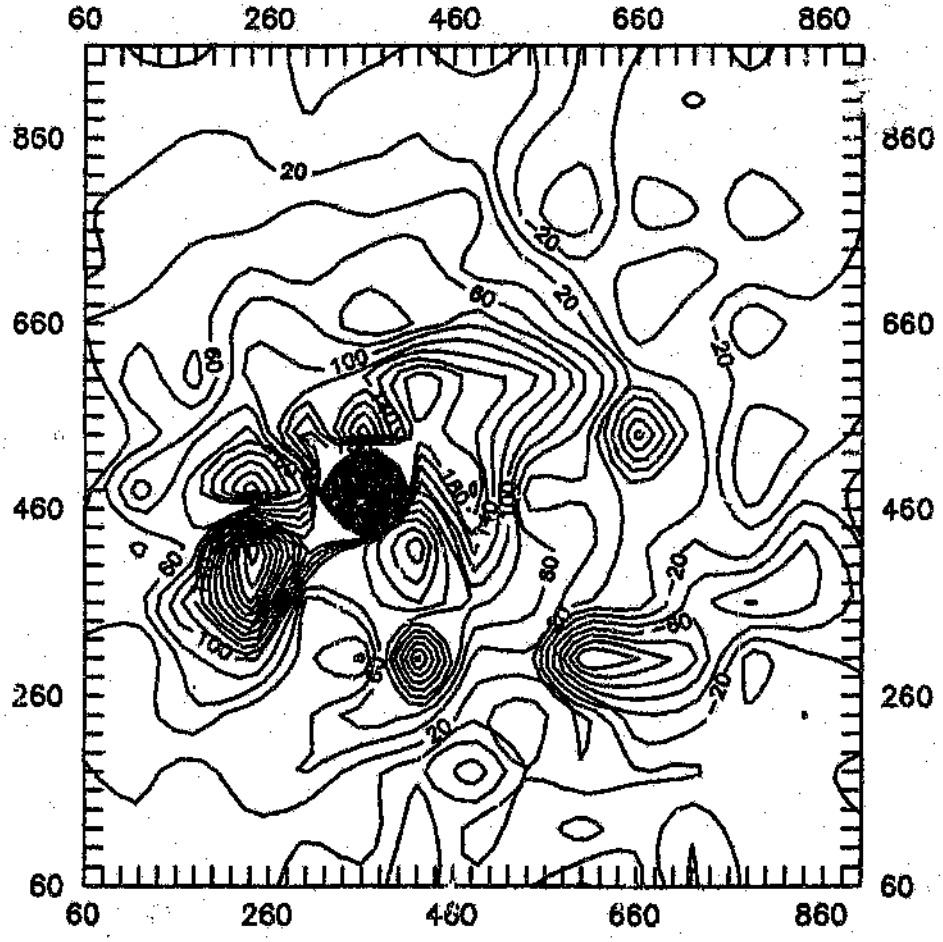

Figure 4.12: Results of the altitude reduction using the quadratic regression method. A window of 120 by 120 km was employed and moved in 60 km increments.

window size may be attributed to the increase in the data points rather than in the process. Intuitively the increase in window size should have an opposite effect because of the failing assumption of linearity of the horizontal gardients. The effect of increased window size is counteracted by an increase in data and thus maintains a constant statistical response.

The above example tests the ability of the algorithm to recover the randomly sampled (altitude) source field in a noise free environment. In order to test the algorithm's noise rejection capabilities zero-mean white noise is added to the same data set. A peak to peak noise amplitude of 100 nT and 200 nT is used; these amplitudes represent, respectively, approximately 100 per cent and 200 per cent of the dipole field value at an altitude of 400 km. Results are given in figures 4.14 and 4.15 and, illustrate the remarkable recovery of the dipole source field even with extreme signal corruption.

These results demonstrate the ability of the median linear regression technique to reduce a variably sampled (in space) dataset to any selected datum accurately. Inherent in the technique is also an effective noise rejection capability. It is thus possible to apply the method immediately after the core and ring current corrections at the preprocessing stage of the equivalent source techniques, for example. The application of the algorithm also results in a gridded dataset. The median linear regression technique encapsulates the following desirable properties, viz.: (1) the modelling is implicit, i.e. no *a priori* information of magnetisation is required, (2) effective noise rejection, (3) simplicity of use and (4) computational efficiency.

An immediate extension of the median linear regression method would be to develop the altitude-dependent surface quadratic, which was unsuccessfully implemented here, using L_1 norms.æ

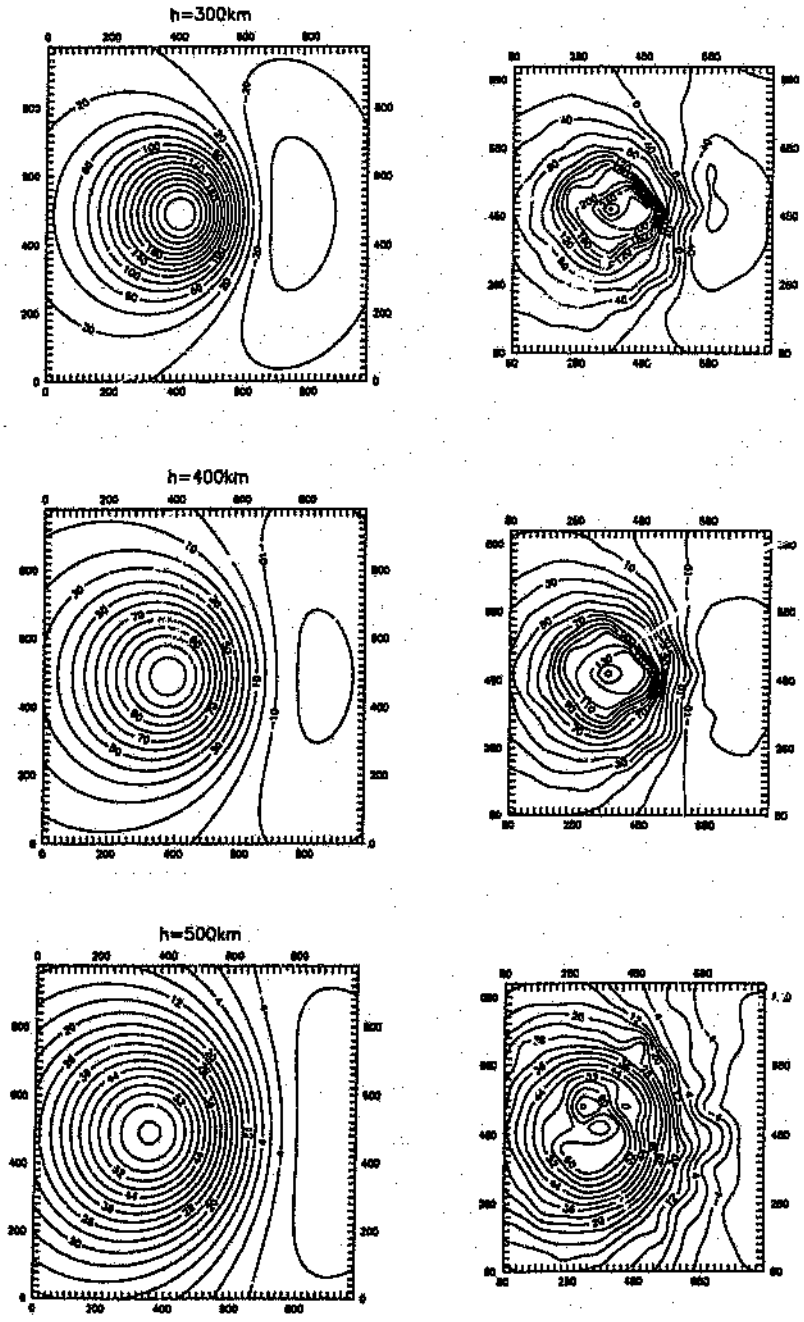

Figure 4.13: Altitude reduction for several reference datums using the median linear regression algorithm on the variable altitude data set of figure 4.10. A cell size of 160 by 160 km was used and moved in 60 km increments. The left hand column presents the expected dipole field for the respective altitudes while the right hand column is the recovered dipole field.

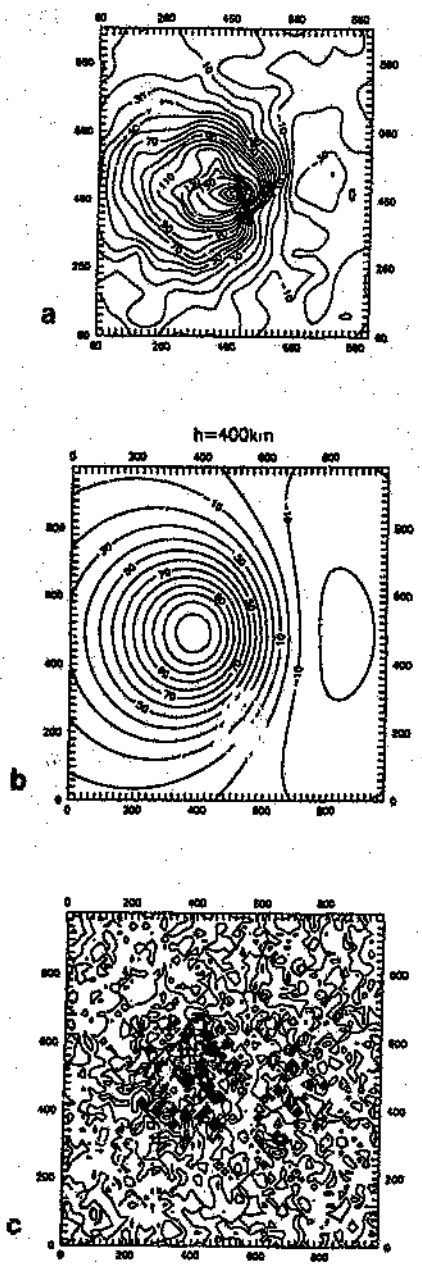

Figure 4.14: Altitude reduction to 400 km (a) recovered from variable altitude data with zero-mean noise (peak to peak 100 nT) (c). A residual analysis of the recovered dipole with respect to the expected field (b) results in a least squares per cent fit of 89% and an r.m.s. of 13 nT (peak to peak anomaly amplitude is 150 nT).

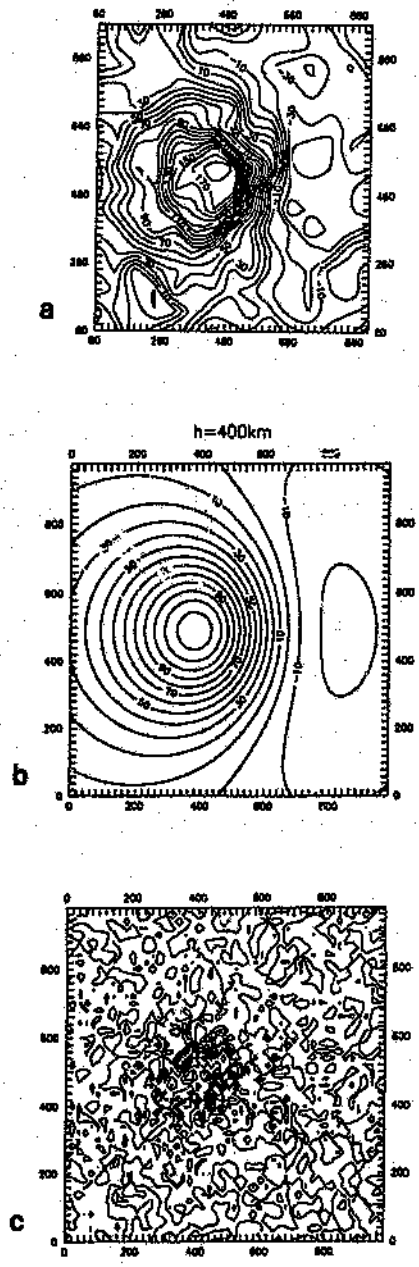

Figure 4.15: Altitude reduction to 400 km (a) recovered from variable altitude data with zero-mean noise (peak to peak 200 nT) (c). A residual analysis of the recovered dipole with respect to the expected field (b) results in a least squares per cent fit of 75% and an r.m.s of 21 nT (peak to peak anomaly amplitude is 150 nT).

Chapter 5

Ionospheric field correction

The removal of ionospheric field contributions from the total magnetic field as measured by a near-earth satellite magnetometer is not standardised and varies widely amongst investigators. With the exception of the work of Yanagisawa and Kono (1985) the effects of the various ionospheric current systems are removed subjectively. Magsat's twilight, sun-synchronous, polar orbit was designed to minimise and possibly exclude effects of the Sq current system. Sugiura and Hagan (1979) anticipated that strong ionospheric field effects would be present in Magsat data and that due consideration should be given to correct for these effects. It soon became clear that the effects were present at both dawn and dusk meridians (see e.g. Maeda et al., 1982).

Ionospheric field corrections are made after the main field and the external ring current and induction reductions have been applied. The effect of the ionospheric fields has been noted mainly as a path-to-path inconsistency. The correction comprises fitting and removing an arbitrary low-order function from each pass (trend removal) which is commonly refered to as the path-to-path correction (e.g. Mayhew, 1979; Singh et al., 1986; Kühn and Zaaiman, 1986).

The first attempt towards a more rigorous procedure for correcting ionospheric field effects on dawn and dusk data for the purpose of generating anomaly maps is that of Yanagisawa (1983). He attempts to model the ionospheric field for dawn and dusk meridians and then uses this model as a correction (the mean ionospheric field correction, MIFC). In this Chapter a brief review is made of the mean ionospheric field correction. This is followed with the introduction of a new data adaptive filter as a means of improving the derivation of the

ionospheric field (IF) by the method of *converging operations* (Garner et al., 1956). The IF is separated from the Sq contaminated lithospheric signal in this process.

5.1 Mean ionospheric field correction

The mean ionospheric field correction was developed (Yanagisawa, 1983) in order to accommodate the morphology of the field in an objective manner rather than the more subjective approach of the track-to-track corrections. Incorrect application of any of these corrections will result in lithospheric pseudo-anomalies or in the distortion of genuine anomalies, making quantitative interpretations highly questionable. Yanagisawa (1983, 1984) demonstrates that the zonal harmonics describing the external ring current and induction fields are independant of the Dst and Kp disturbance indices above the first degree expansion. The latitude-dependent perturbations at 0600 and 1800 local times are therefore present as a result of persistent electric currents in the ionosphere.

Assuming that the ionospheric fields are zonal, the lithospheric anomaly field is randomised by stacking meridians (in the longitudinal range $\phi \pm 30^0$) for 0300 and 1800 local times as a function of latitude[1]. The result of this stacking provides a description of a mean ionospheric field (MIF), averaged over the satellite's altitude range, longitudes and time. This MIF is then used to reduce (MIFC) the dawn and dusk data sets to obtain the lithospheric anomaly map. The resultant dawn and dusk anomaly maps were shown by Yanagisawa (1984) to have good correlation and are an improvement on the other detrending methods.

In Chapter 4 an altitude correction algorithm (median linear regression) is developed with an effective, robust method to reject uncorrelated noise. The primary objective of that algorithm is to cancel, in addition to the altitude perturbations, uncorrelated noise resulting from survey acquisition, system, attitude control and disturbance effects. This same algorithm, in the author's opinion, could be used to correct for the ionospheric field by processing randomly (in time) the satellite passes over a selected geographic region. This approach is comparable to the procedure of randomising the lithospheric field to derive the MIF (Yanagisawa, 1983). The method of Yanagisawa is adopted in this study because Magsat's sun-synchronous orbit

[1] Yanagisawa and Kono (1984) define the MIF in terms of dip latitude. However, dip latitudes are anomalous in the southern African region and prove to be problematical if used as a coordinate system. The ionospheric field is neither a simple function of geographic latitude nor dip latitude but intermediate to the two systems (Parkinson, 1983; Maeda, 1953). Geocentric latitude is used to define the MIF here.

restricts data to a narrow local time window, resulting in a insufficient data spread needed to randomise local time. Instead, the median linear regression algorithm is exploited to derive the MIF and thereby introduce a necessary altitude correction. Yanagisawa and Kono (1985, 1984) averaged the MIF over the satellite's altitude range and made no correction for the altitude variation which was found to be significant. The approach adopted in this study is thus felt to be far more robust than any previous attempts at altitude and MIF corrections.

5.2 A data adaptive filter approach

The ionospheric field is independent of magnetospheric disturbance effects and has a well defined ambient morphology (Yanagisawa, 1983 and 1984; Yanagisawa and Kono, 1984 and 1985). Satellite magnetic data for a specific geographic region, after removal of core and magnetospheric field effects, may be viewed after separation for either 0600 or 1800 local times, as a deterministic signal (i.e. the lithospheric anomaly field, LF) corrupted by another deterministic signal (the ionospheric Sq current systems, IF); termed the *contaminated lithospheric field* (CLF). The IF may be regarded as a single deterministic signal while the Sq contaminated lithospheric field (CLF) may be viewed as two interfering deterministic signals. In addition, both datasets (i.e. the MIF and the CLF) are corrupted by minor white noise. The ionospheric signal, is correlated between data sets whereas the lithospheric signal is uncorrelated. The implementation of data adaptive filters is particularly suited to this form of signal corruption (Widrow and Stearns, 1985; Hattingh, 1988). By making use of a data adaptive filter it is possible to improve on the derivation of a noise free IF by extracting the correlated signal from two independantly derived data sets.

5.2.1 The adaptive least mean square algorithm

A data adaptive filter is one whose structure is adaptable in such a way that its performance improves with time (or space). The process of adaptation is achieved by a dynamic filter whose weights vary with time in response to the monitored error from a reference channel as depicted schematically in figure 5.1. The output is the required response resulting in the cancellation of uncorrelated noise.

The principal element of the data adaptive filter is the adaptive linear combiner which

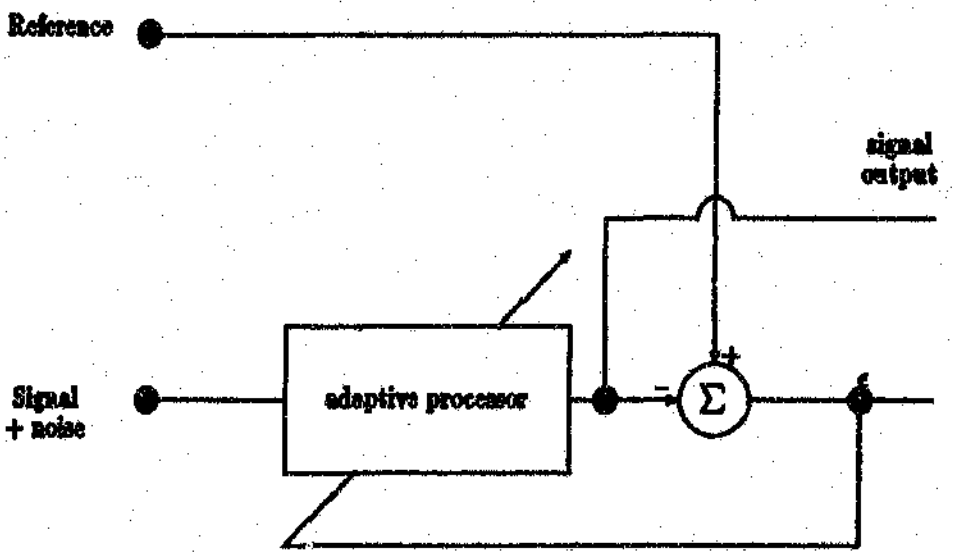

Figure 5.1: Schematic representation of an interference cancelling data adaptive structure.

is illustrated in figure 5.2 in the form of a single-input tapped delay line (TDL) structure (Widrow and Stearns, 1985). The signal may be represented by

$$x_k = s_k + n_k \tag{5.1}$$

where s_k is the information component and n_k the noise at the $k'th$ sampling instant. These quantities are assumed to be vector valued and the scalar output y_k is generated by

$$y_k = \sum_{l=0}^{L} W_{lk} x_{k-l} = W_k^T X_k \tag{5.2}$$

where

$$W_k = [W_{0k}, W_{1k}, \ldots, W_{Lk}]^T \tag{5.3}$$

is the weighting vector and

$$X_k = [x_{0k}, x_{1k}, \ldots, x_{k-L}]^T \tag{5.4}$$

the input vector.

The weighting vector is formed so as to minimise the mean square error between y_k and the scalar reference channel d_k. The error signal is

$$\varepsilon_k = d_k - y_k \tag{5.5}$$

Substituting 5.2 into 5.5 yields the expresssion

$$\varepsilon_k = d_k - W_k^T X_k \tag{5.6}$$

The mean square error is given by

$$\zeta = E\left[\varepsilon_k^2\right] = E[d_k]^2 - 2P^T W_k + W_k^T R W_k \tag{5.7}$$

where E is the expectation, $P = E[d_k x_k]$ is the cross correlation, and $R = E\left[x_k x_k^T\right]$ is the autocorrelation matrix. It is clear from the above expression that the mean square error describes a quadratic function of the weight vector W_k.

The optimum weight vector W_k^* is obtained by solving the gradient of 5.7 to find the global minimum of the performance surface,

$$\frac{\delta\zeta}{\delta W_k} = -2P + 2RW_k = 0 \tag{5.8}$$

and the optimum weight vector, sometimes called the Wiener weight vector, is

$$W_k^* = R^{-1}P \tag{5.9}$$

This optimum Wiener filter requires knowledge of the autocorrelation matrix R and cross correlation vector P. These quantities are seldom known *a priori*. To overcome this difficulty the unknown quantities are estimated from the observed data, or through the use of predetermined test signals. The least mean square (LMS) algorithm is a simple recursive implementation based on searching the performance surface by the method of steepest descent using estimated gradients. The LMS algorithm is expressed as

$$W_{k+1} = W_k + 2\mu\varepsilon_k X_k \tag{5.10}$$

where μ is a factor indicating the rate of convergence and stability (Widrow and Stearns, 1985; Widrow et al., 1976). Once the algorithm has converged the output, y_k, is the best least square estimate of the reference channel, d_k.

5.2.2 Two-dimensional median hybrid adaptive filter

Adaptive filters have desirable properties towards signal extraction. The adaptive filter structure is such that noise between two channels (one being the reference or desired response) may be cancelled. This noise may either be stochastic or may be a deterministic signal. We described above how the total magnetic field, after reduction for the main and magnetospheric field effects, may be processed to approximate this condition closely, yielding viz.: (1) a MIF map by randomising the lithospheric field contribution and (2) an ionospheric field map contaminated by the lithospheric anomaly field (CLF). Because the lithospheric anomaly field is not zonal it is necessary to consider implementation of the data adaptive filter in two-dimensions.

The pseudo two-dimensional adaptive median hybrid (2DAMH) filter presented here is the end product of numerous trials of various adaptive filter structures. The choice of the most appropriate algorithm was based principally on the best signal recovery from synthetic data sets. The central algorithm of the various adaptive filter structures tested is the LMS implemented in the form of a single-input TDL structure (see Fig. 5.2).

In order to implement an adaptive filter structure in two-dimensions, array structures were first considered (see e.g. Monzingo and Miller, 1980; Hudson, 1981; Justice et al., 1985) which generated poor results. A pseudo two-dimensional structure (as discussed below) was then attempted with improved results. The pseudo two-dimensional aspect is a simple implementation of the single-input linear combiner where first the rows of the grid are filtered followed by a second pass on the orthogonal columns. Outputs from this filter had some undesired 'herring bone'. To resolve this problem another approach was developed where the rows and columns are filtered alternately.

Nieminen et al. (1987) introduce an adaptive median hybrid (AMH) filter where the advantageous properties of median-type filters (makes for a more robust filter) are combined with the also advantageous properties of the adaptive filter structure. This structure is more suited for filtering signals with rapidly varying characteristics. The TDL filter can be used either as a forward adaptive predictor (FA) as illustrated in figure 5.2 or for backward prediction (BA). This median hybrid structure is exploited in the 2DAMH filter. The algorithm uses the FA predictor twice, i.e. in the forward direction and then in the reverse direction for the BA predictor. Both FA and BA predictor outputs are stored. The median is then obtained from the two FA and BA predictions and the original signal values.

A further modification to the 2DAMH filter was attempted by introducing an orthogonalisation scheme. Orthogonalisation of the inputs to the adaptive weights can result in a more rapid adaptation than is possible with LMS alone, particularly, when there is a wide eigenvalue spread of the data auto-correlation matrix (Narayan and Peterson, 1981; Widrow and Stearns, 1985). The orthogonalisation scheme that was used is based on the discrete Fourier Transform (DFT) of Narayan and Peterson (1981). The implementation is made by introducing on the TDL an FFT (see Fig. 5.3). Used in this manner the FFT may be considered as a bank of band-pass filters uniformly spaced in frequency between zero and

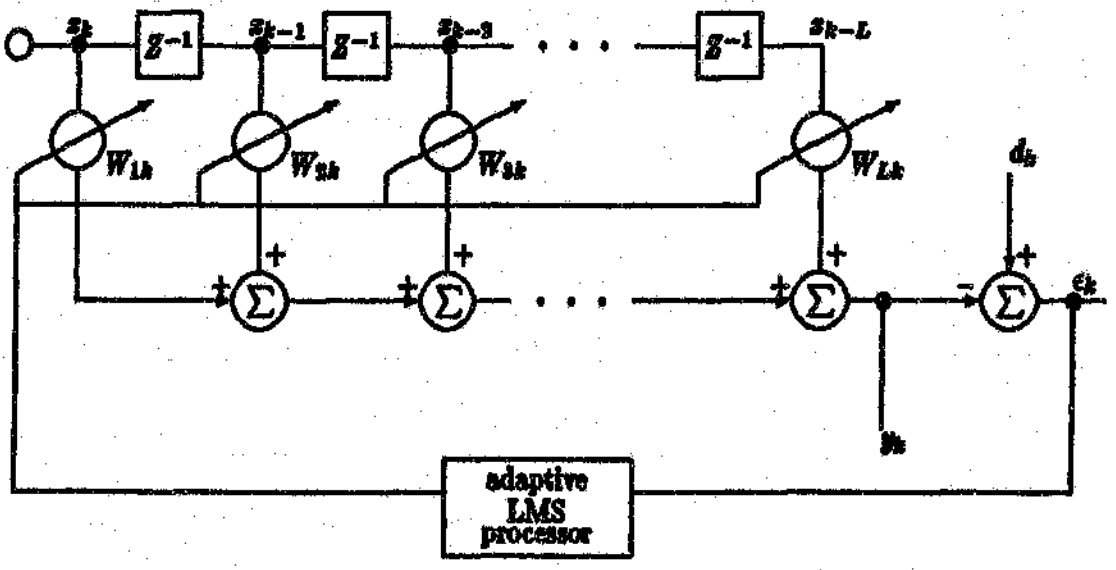

Figure 5.2: Structure of the adaptive tapped delay line (TDL) filter (also known as the adaptive transversal filter).

the Nyquist. The FFT outputs are complex discrete functions of the sampling index, k, and are approximately uncorrelated with each other, being in different frequency bands. These are weighted with complex adaptive weights to produce y_k which is also complex. The reference channel of the adaptive filter is treated as a real complex value and the resultant error is complex. Although y_k is complex its imaginary part will be small in general since the reference signal's imaginary part is zero. In the LMS algorithm the weights are adapted as complex weights.

Results of this wavenumber domain algorithm were virtually identical to the space domain algorithm. There are two main disadvantages in the implementation of the wavenumber domain algorithm compared with the space domain version (adopted in this study), viz.: (1) computationally intensive and (2) the filter's length (L) is constrained to a radix 2 value to accomodate the FFT requirements.

Although the LMS algorithm is numerically stable and converges to the true minimum mean square, this is strongly dependent on the the appropriate choice of the parameter μ (Cioffi, 1987). The convergence factor μ must be bounded by 0 and $\frac{1}{\lambda_{max}}$, where λ_{max} is the maximum eigenvalue of the input correlation matrix (Kang and Fransen, 1987). In the past μ was chosen empirically. Mikhael et al. (1984) demonstrate that an optimum convergence factor m be obtained by

$$\mu_k = 0.25/\sum_{l=1}^{L} d^2_{(k-l)} \tag{5.11}$$

This is used in the present 2DAMH algorithm. Further stability can be insured by introducing tap leakage (Long et al., 1987) such that 5.10 becomes

$$W_{k+1} = W_k\alpha + 2\mu_k\epsilon_k X_k \tag{5.12}$$

where $0 < \alpha < 1$; typically, $\alpha = 0.997 - 0.999$.

5.2.3 Computer simulations and discussion

Synthetic data representative of the MIF and of the IF contaminated lithospheric field (CLF) were generated to test the various adaptive filters. The computer simulations were adopted to approximate as realistically as possible the data and processing route. Several forms of

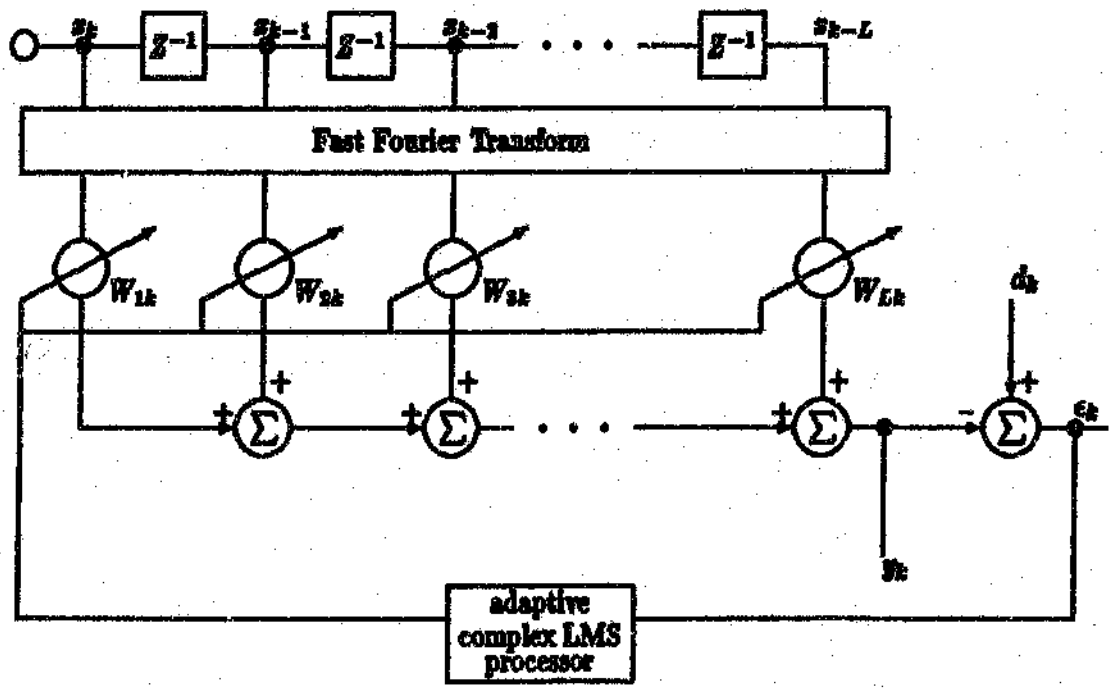

Figure 5.3: Structure of the wavenumber domain LMS adaptive filter.

corrupting signals were tested to ascertain the filter's limitations. In all cases the MIF is approximated by a zonal sinusoidal signal with some random line to line inconsistencies, viz.: (1) random phase shifts between lines (small) and (2) random signal amplitude changes (up to 40%). The lithospheric field was represented by a dipolar field.

Figure 5.4 is an example of the signal separation that is possible with the space-domain 2DAMH filter. A dipolar field is added to the MIF (see figure 5.4 b). The MIF is extracted from the combined fields of figure 5.4 b (see figure 5.4 c) using the MIF of figure 5.4 (a) as the reference signal. In this, worst case, example the MIF and the dipole fields are made to be of almost identical wavelength and are in-phase. The filter may be made to cancel white noise (typically -10 to -15 dB; see e.g. Mikhael and Hill, 1988) from a signal if the reference and signal channels are the same (Fig. 5.4 d).

Note that the filter was designed to cope with signals of varying characteristics such that data integrity is maintained. This important facet of the filter is exemplified in figure 5.4 where sharp features of small amplitude of the desired signal are preserved.

It was originally hoped that an adaptive filter structure could be designed such that the coherent signal (lithospheric) from two separate MIF contaminated lithospheric maps (for example, from the dawn and dusk meridian maps) could be extracted. This approach contrasts with that of Arkani-Hamed and Strangway (1985) where they extract the lithospheric signal by averaging band pass filtered dawn and dusk datasets. All data adaptive filter structures tested to date have been unable to achieve this goal. The use of the adaptive filter in deriving the MIF meets two objectives. Although the MIF is already isolated , it is preferable to extract the IF from two independent signal sources (i.e. the MIF and CLF); which is where this process differs funadmentally from Yanagisawa (1983). The data sets are derived by a similar procedure but assume different spatial and statistical definitions. Conclusions made from evidence from two independent experiments, i.e. the MIF and the IF contaminated lithospheric maps (for specific local times), is much less likely to be artifactual or rest on faulty assumptions than from one experiment only. The adaptive filter also serves as an independent means to verify the postulate that the IF is present in the Sq contaminated lithospheric maps. If the IF were not present then the filter output would be corrupt and would not approximate the reference signal.

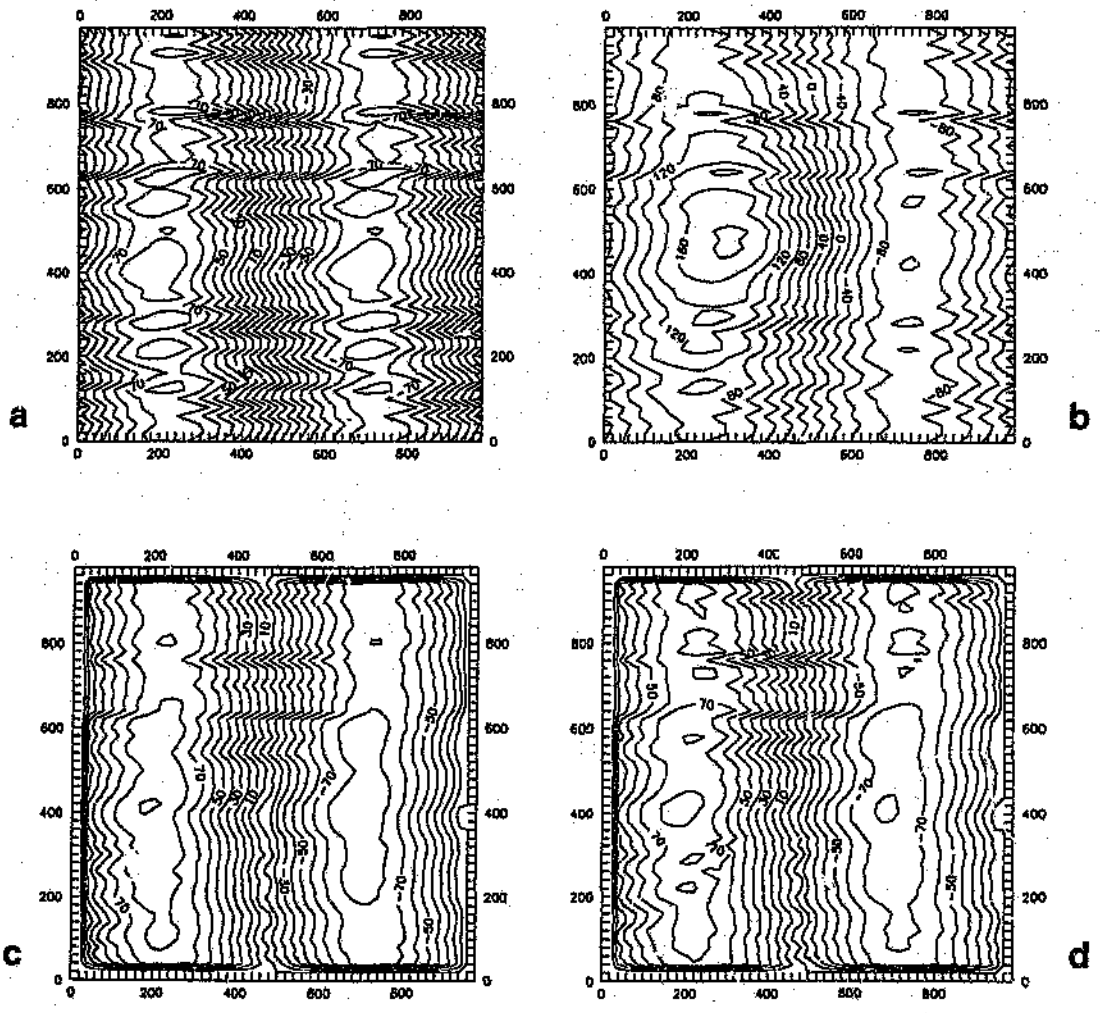

Figure 5.4: Results of computer simulations of the space-domain 2DAMH filter: (a) is the simulated MIF signal with minor white-noise, (b) is a dipolar field (400 km reference altitude) contaminated with the MIF and corrupted with minor white-noise, and (c) is the MIF extracted using the data aptive filter where (b) and (a) are the signal and reference channels, respectively. (d) serves as an example of noise cancellation on the MIF (a) (i.e. the MIF (a) is used as both reference and signal channels). Horizontal axes are in km and contours are in nT.

Chapter 6

Data processing

The southern subcontinent of Africa is selected to test the newly developed data reduction procedures. The objective, to reiterate, is to produce an anomaly map with the best possible resolution and data integrity. Only then can interpretation be contemplated with respect to correlations with known tectonic features. Procedures used to reduce the total-field measurements of a near-earth satellite for the purpose of generating lithospheric anomaly maps are not standard as is outlined in Chapter 1. Implementation of two new algorithms in this study, i.e. for altitude and ionospheric corrections, has led to a significant improvement on previously published lithospheric anomaly maps of the region thus meeting the above objective.

In summary, magnetic observations made from a near-earth satellite platform will comprise a total-field response from several contributing sources, viz.: (1) the main field, (2) the external ring current and induction fields, (3) the ionospheric field and (4) of particular interest in this study, the lithospheric field. In addition, the data will suffer from inherent survey noise. The processing route endeavours to separate the various contributing component magnetic fields observed by the satellite magnetometer. This Chapter details the procedures used to generate the lithospheric and ionospheric maps of southern Africa. Two new techniques, discussed in Chapters 4 and 5, have been introduced in the processing of satellite magnetometer data in favour of previously published algorithms, namely, the median linear regression algorithm as an altitude correction and the two-dimensional data adaptive algorithm for improved signal separation of the lithospheric field from the ionospheric field or, simply, noise cancellation from maps.

The results are presented as relevant ionospheric and lithospheric maps and a synopsis given.

6.1 Data selection

To begin with, the INV-B tapes were scanned for suitable data. Rejection of satellite passes in the region of interest (0^0E to 50^0 E and 0^0 S to 50^0 S) was based on, namely: (1) passes that had a magnetic activity index ,Kp , $\geq 3_-$ and (2) passes with local times outside the 0530-0630 and 1730-1830 meridians. Selected passes were stored, respectively, in dawn and dusk files. Data for each half orbit were retained over the latitude range 60^0N to 60^0S. Each such half orbit is corrected for the core, ring current and induction fields. Thereafter altitude and IF corrections are applied.

6.2 Main field correction

Separation of the main field is an unresolved problem as discussed in Chapter 2. Better, higher degree and order spherical harmonic models are being developed regularly as increased computing capabilities become available (see e.g. Schmitz et al., 1989; Cain et al., 1989b). However, the problem is manifest in the spectral separation which to-date remains unsolved. This problem is beyond the scope of this study. Since the most prominent Magsat investigators use the MGST 4/81 (Langel et al., 1981) model provided with the INV-B tapes it seems sensible to standardise the present work to that model.

The main field model values are obtained from a truncated (degree and order 13) spherical harmonic series and subtracted from the total-field response. This correction is applied immediately to all selected passes. Once the selected data are corrected for the core field contribution and filed into their respective dawn and dusk meridians, the magnetospheric and induction field effects are considered on a pass by pass basis.

6.3 Ring current correction

The geometry of the disturbance field may be expressed by a potential function of the form

$$V = a\left\{E_1(\frac{r}{a}) + I_1(\frac{a}{r})^2\right\}P_1(\cos\theta) \tag{6.1}$$

where a is the mean earth radius, r is the geocentric distance from the earth, θ is the magnetic colatitude and $P_1(\cos\theta)$ is the first degree Legendre polynomial (Langel and Sweeney, 1971). The coefficients E and I relate to the external and internal (inductive) components of the field, respectively. Magnetic field intensity can be expressed as the gradient of the scalar potential such that

$$\Delta\vec{B} = -\nabla V \tag{6.2}$$

Correction for the disturbing external and induced internal fields is made by fitting (in a least squares sense) the function 6.2 to the data and subtracting this model to obtain the residual. The coefficients E and I in the case of Magsat INV-B data are provided. However, in the southern African region a problem arises where the model fit is unacceptable if the given coefficients are used (Zaaiman and Kühn, 1986). The problem relates to an anomalous main field in this region which distorts dip latitudes. Zaaiman and Kühn (1986) demonstrate that this problem is almost entirely resolved if equation 6.2 is modelled using dip latitudes defined at an altitude of 3 R_E rather than at the observation altitude.

Figures 6.1 and 6.3 illustrate the poor model fits for dip latitudes calculated at satellite altitudes compared with those models where dip latitudes were calculated at equivalent ring current altitudes of 3 R_E (Figs 6.2 and 6.4). The effect is greatest on the dusk pass 211 (see figures 6.3 and 6.4). This higher altitude ring current correction is not entirely satisfactory on pass 211 but is an improvement. Note also that the 3 R_E model does not differ from the satellite altitude model other than in the region of anomalous dip latitudes.

The above results reaffirm the observations made by Zaaiman and Kühn (1986). Since the 3 R_E ring current model affects the anomalous region only and is an apparent improvement on the given INV-B model, it was decided to apply this model in the processing of the Magsat data in the southern African region. New E and I coefficients were calculated for the selected passes. The coefficients of the INV-B ring current model were calculated for the mid dip latitude range 0^0 to 45^0 to avoid effects from field-aligned currents in the polar

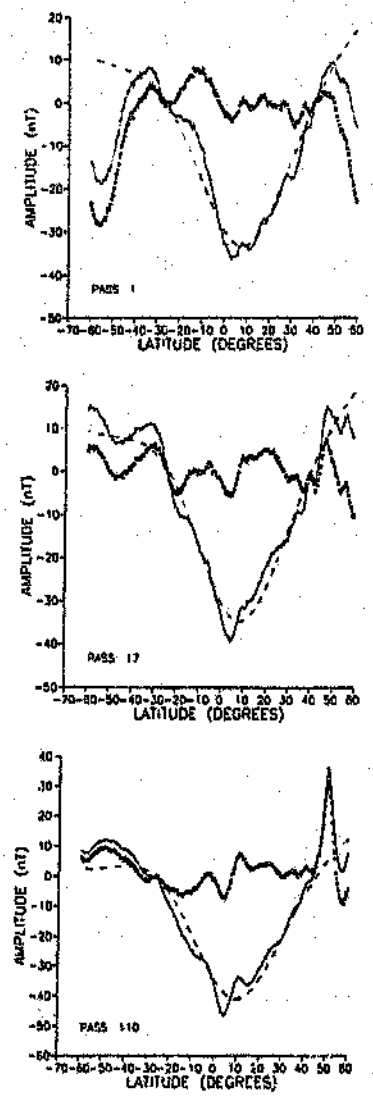

Figure 6.1: INV-B ring current model for selected dawn passes. The solid line represents the residual after core field subtraction, the dashed line the ring current model and the thick dotted line the residual from the ring current correction.

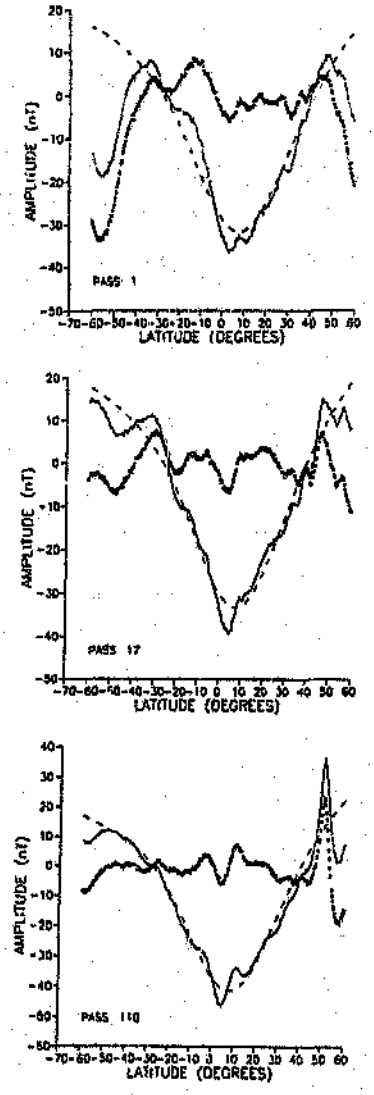

Figure 6.2: Ring current model for selected dawn passes using dip latitudes at altitude of 3 R_E. The solid line represents the residual after core field subtraction, the dashed line the ring current model and the thick dotted line the residual from the ring current correction.

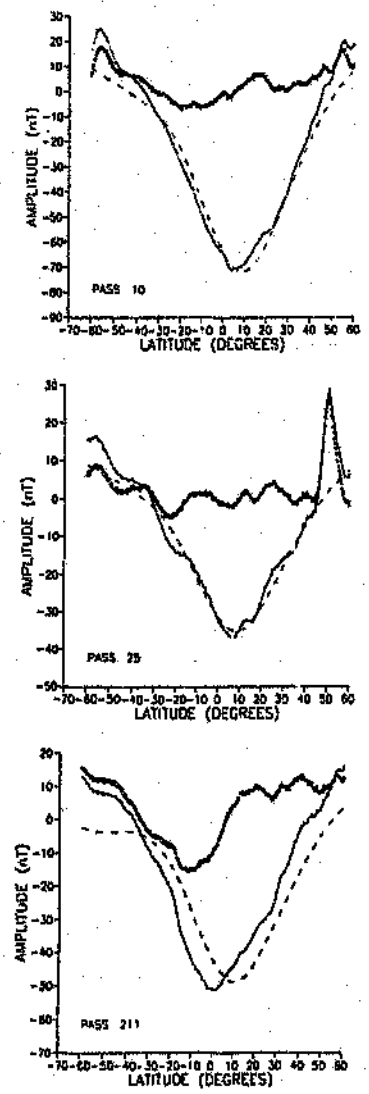

Figure 6.3: INV-B ring current model for selected dusk passes. The solid line represents the residual after core field subtraction, the dashed line the ring current model and the thick dotted line the residual from the ring current correction.

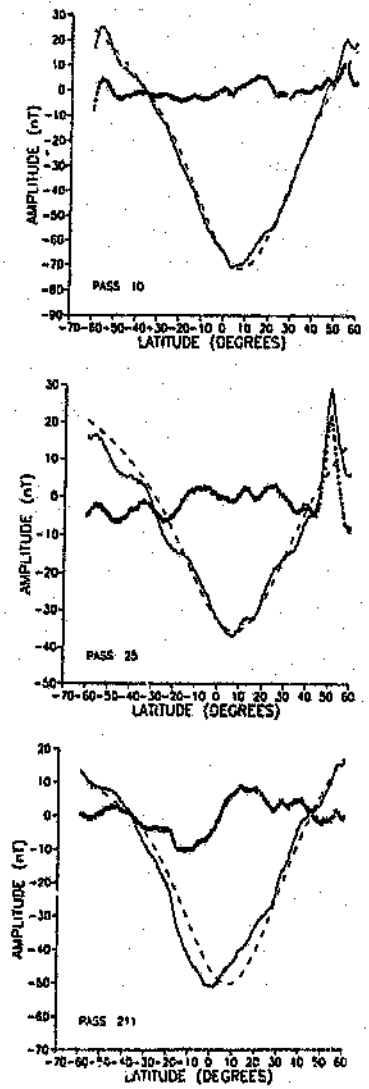

Figure 6.4: Ring current model for selected dusk passes using dip latitudes at an altitude of 3 R_E. The solid line represents the residual after the core field subtraction, the dashed line the ring current model and the thick dotted line the residual from the ring current correction.

regions. Extrapolating the model to higher latitudes results in divergences. Because the area of interest extends beyond the 45^0 latitudes the 3 R_E model was derived to 60^0.

Having removed the magnetospheric and related induction disturbance effects, the residual that remains represents the field responses from sources in the ionosphere and the lithosphere and, related altitude effects. The altitude effects are removed by applying the median linear regression algorithm with different parameters in order to define: (1) a mean ionospheric field (MIF) and (2) an ionospheric contaminated lithospheric field (CLF). The two fields (i.e. ionospheric and lithospheric) are then separated.

6.4 Mean ionospheric field and altitude reduction

The mean ionospheric field correction (MIFC) requires that a mean ionospheric field (MIF) be derived and separated from the combined ionosphere-lithosphere residual after the core, magnetosphere and induction field effects are removed. In Chapter 5 a means to derive the mean ionospheric field is developed from the work of Yanagisawa (1983). The MIF derived here differs from that work in that an altitude correction has been incorporated by making use of the median linear regression algorithm of Chapter 4. A MIF is derived by randomising the lithospheric field component. This was achieved by stacking data for given local times 0600 and 1800 $\pm$0030 in latitude and longitude cells of 2^0 by 60^0, respectively. These overlapping bins are moved in $0,5^0$ increments to produce an equirectangular projection grid of half degree centres.

Dip latitudes are commonly employed as a coordinate system in ionospheric studies. In the southern African region dip latitudes are anomalous (dip latitudes asymptote to 65^0). Using these as a coordinate system becomes problematic, if not unusable, because of extreme shape distortion of anomalies in the southwest Indian Ocean. All maps produced by Yanagisawa and Kono (1984) exclude data in this region probably for this reason. The coordinate system for the ionospheric field is neither geomagnetic nor geocentric[1] but intermediate. Consequently, a geocentric latitude, longitude coordinate system was used to derive the MIF.

The structure of the S_q field not only varies with respect to local time but also shows

[1]Maeda (1953) from a detailed spherical harmonic analysis of the S_q field introduced a new coordinate system that appeared to be more suitable for the S_q field, this being somewhat intermediate between the geomagnetic and geocentric systems.

seasonal variation. The ionospheric current system is not fixed relative to the ecliptic but moves slightly north and south in response to the tilt of the earth's rotational axis with respect to the ecliptic. Consequently, it was thought prudent to derive MIFs on a seasonal basis. Magsat data covers a period of seven months which spans the southern hemisphere's summer solstice and autumn equinox. The data were processed over two periods of approximately three months duration.

6.5 Contaminated lithospheric field and altitude reduction

Stacking data into small longitude-latitude bins (i.e. for a fixed geographical position) for a specific local time will yield a lithospheric field value contaminated by the S_q field, together with altitude variation effects and inherent survey noise. The median linear regression algorithm is used to obtain an altitude corrected value. Because of the small periods used to derive the fields it was necessary to increase the bin size to 4^0 by 4^0 in order to obtain a sufficient number of data points for reliable results. These 4^0 by 4^0 overlapping bins were moved in $0,5^0$ increments to produce a half degree equirectangular grid compatible with that of the MIF. The process is the same as that applied for the MIF and differs in the statistical and physical definitions discussed in section 6.4.

Both the MIF and the contaminated lithospheric field (CLF) were derived for two three-month periods for their respective 0600 and 1800 local times. The MIF and the CLF are used to obtain an improved ionospheric field separation with the use the adaptive filter discussed in Chapter 5.

6.6 Ionospheric and lithospheric field separation

In Chapter 4 an improved ionospheric field separation was motivated by the method of converging operations using data adaptive filters. Figure 6.5 illustrates the adaptive filter structure employed to derive the ionospheric field (IF) for the different seasons and local times.

The IFs are separated from the CLFs to derive the respective lithospheric signals. These signals are free from the ionospheric field components but contain white noise which differs for

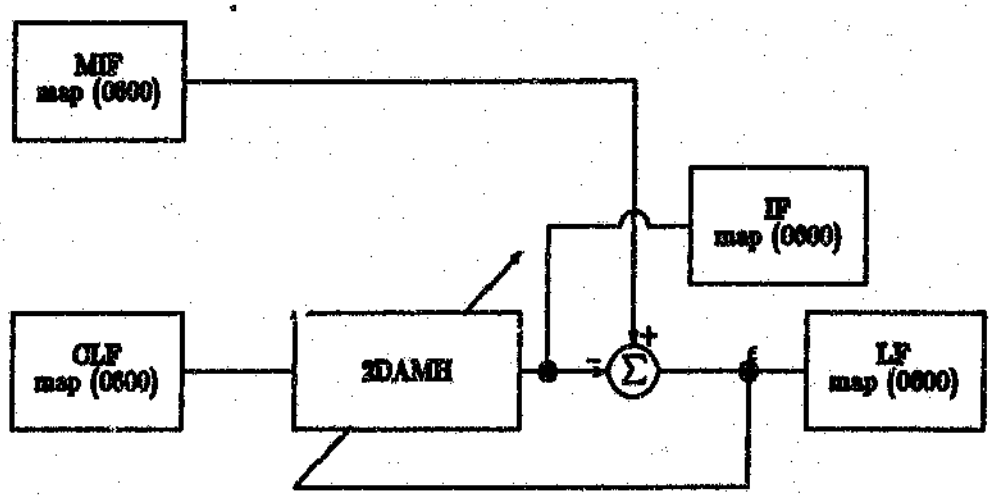

Figure 6.5: Schematic illustration of the adaptive filter structure used to separate the ionospheric field from the contaminated lithospheric field maps.

each map produced. Adaptive noise cancellation from the two lithospheric maps is achieved by the method of converging operations. The final seasonal lithospheric maps were produced with the adaptive filter structure sketched in figure 6.6.

6.7 Results and discussion

Figure 6.7 saliently summarises the data reduction route and procedures. Results of maps for the various processing steps after the core, magnetosphere and induction field components have been removed are given in detail for the first season (i.e. summer). Thereafter, the relevant ionospheric and lithospheric field maps are presented for the autumn season. The MIF and CLF for the summer solstice period at the respective local times (dawn and dusk) are presented as figures 6.8 and 6.9.

Figures 6.10(a) and (b) are the dawn and dusk ionospheric fields extracted using the adaptive filter structure of figure 6.5. The MIFs of figures 6.8 and 6.9 have had noise cancellation applied for presentation purposes. It is encouraging to note that the respective MIFs and IFs are nearly identical (see figures 6.8, 6.9, 6.10). This reinforces the original postulate of Yanagisawa (1983) that the IF is present as a contaminant within the contaminated lithospheric signal (CLF) as defined here.

The ionospheric field maps are interesting in several respects, viz.:

- There is evidence for some non-zonal structure within these maps.
- More structure is present in the dusk map than in the equivalent dawn map.
- The ambient amplitude of the dawn map is substantially higher (by approximately 3 nT) than that of the dusk map.
- Several almost identical responses are present in both dawn and dusk maps.

These aspects will be discussed below in the synopsis. The ionospheric fields of figure 6.10 are separated from the CLFs of figures 6.8 and 6.9 to produce the lithospheric maps of figure 6.11. These two, are in turn, used to produce the final lithospheric map of figure 6.12 using the adaptive filter structure depicted in figure 6.6.

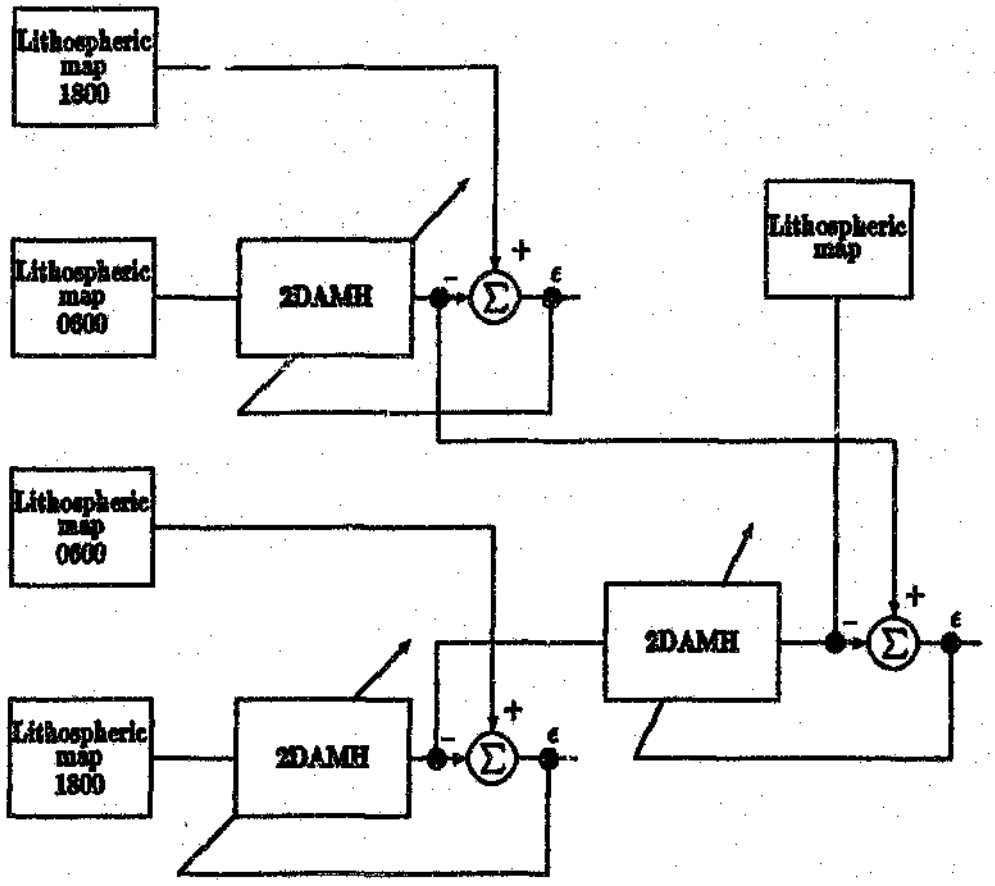

Figure 6.6: Sketch of adaptive filter structure by method of converging operations to obtain seasonal lithospheric anomaly map.

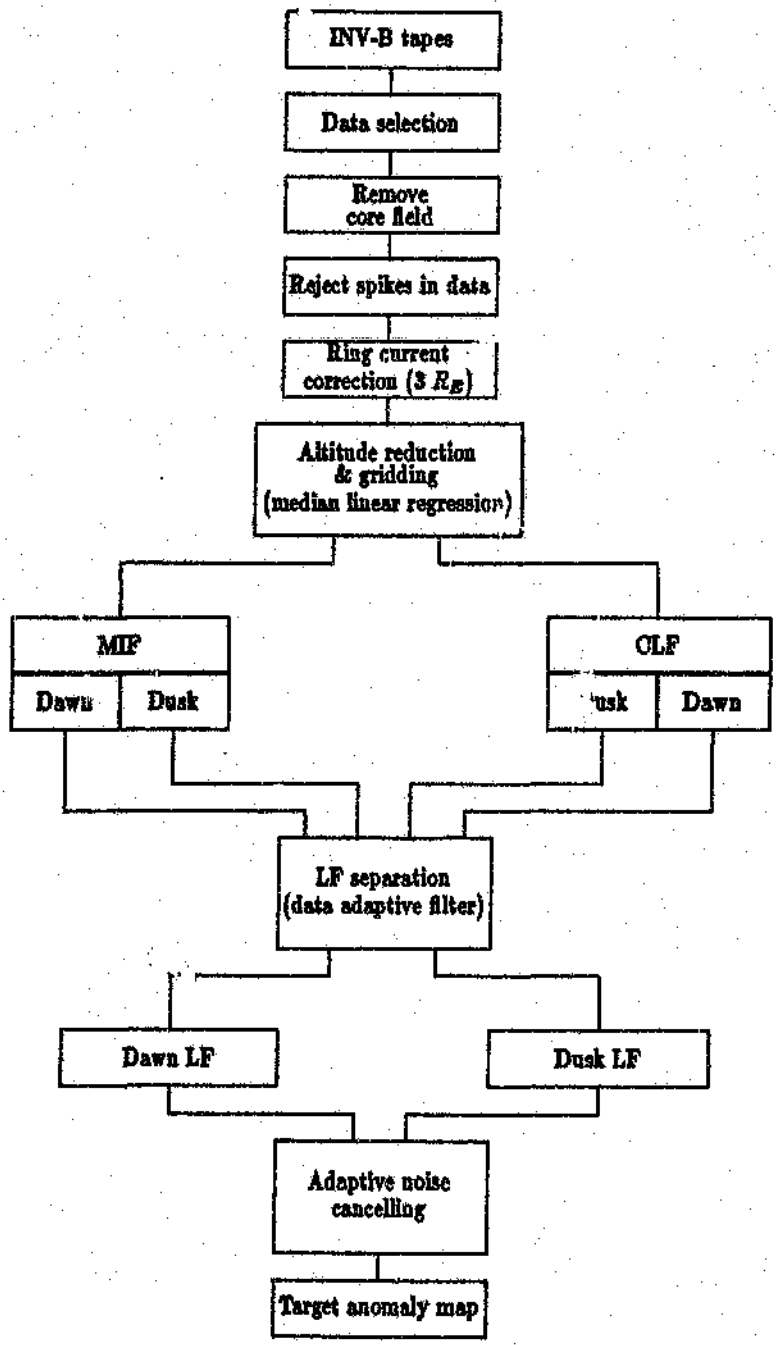

Figure 6.7: Flow chart summarising the data reduction route.

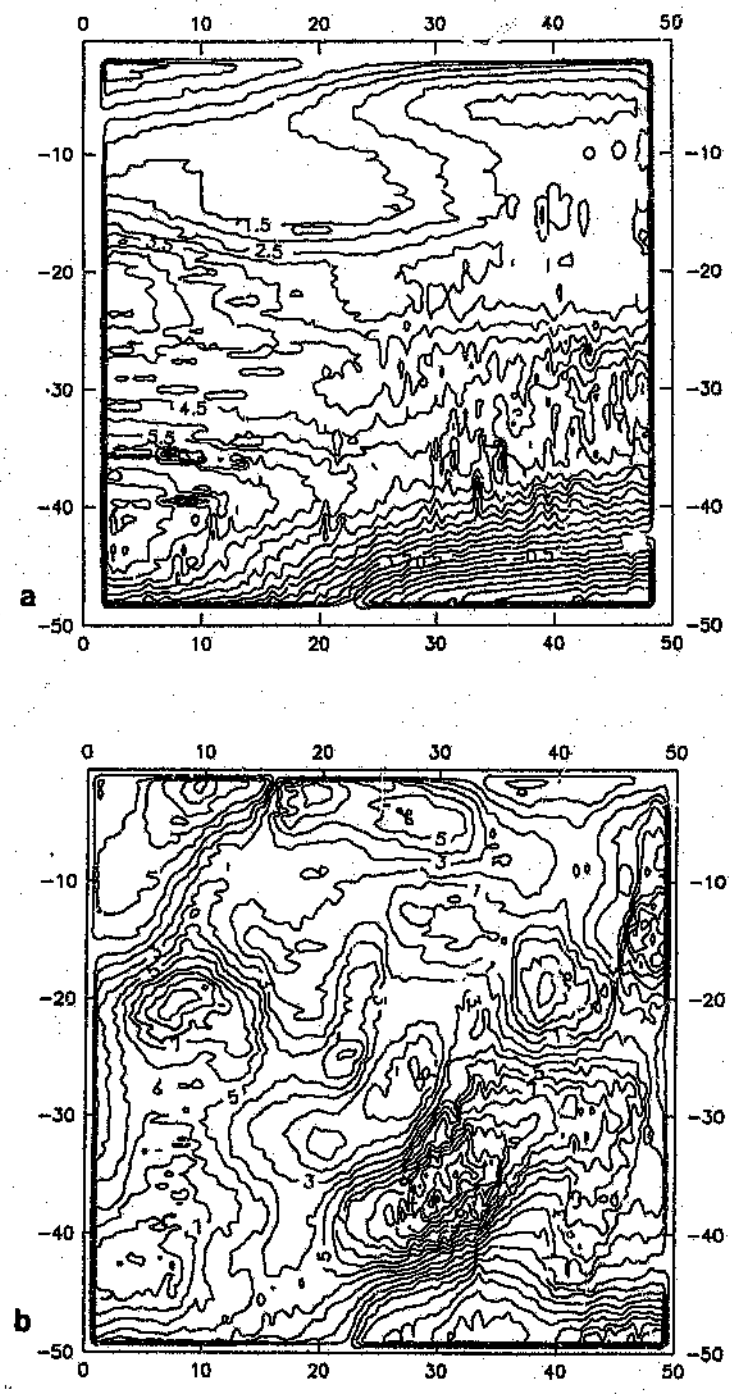

Figure 6.8: Mean ionospheric field (a) and contaminated lithospheric field (b) dawn maps for the summer solstice

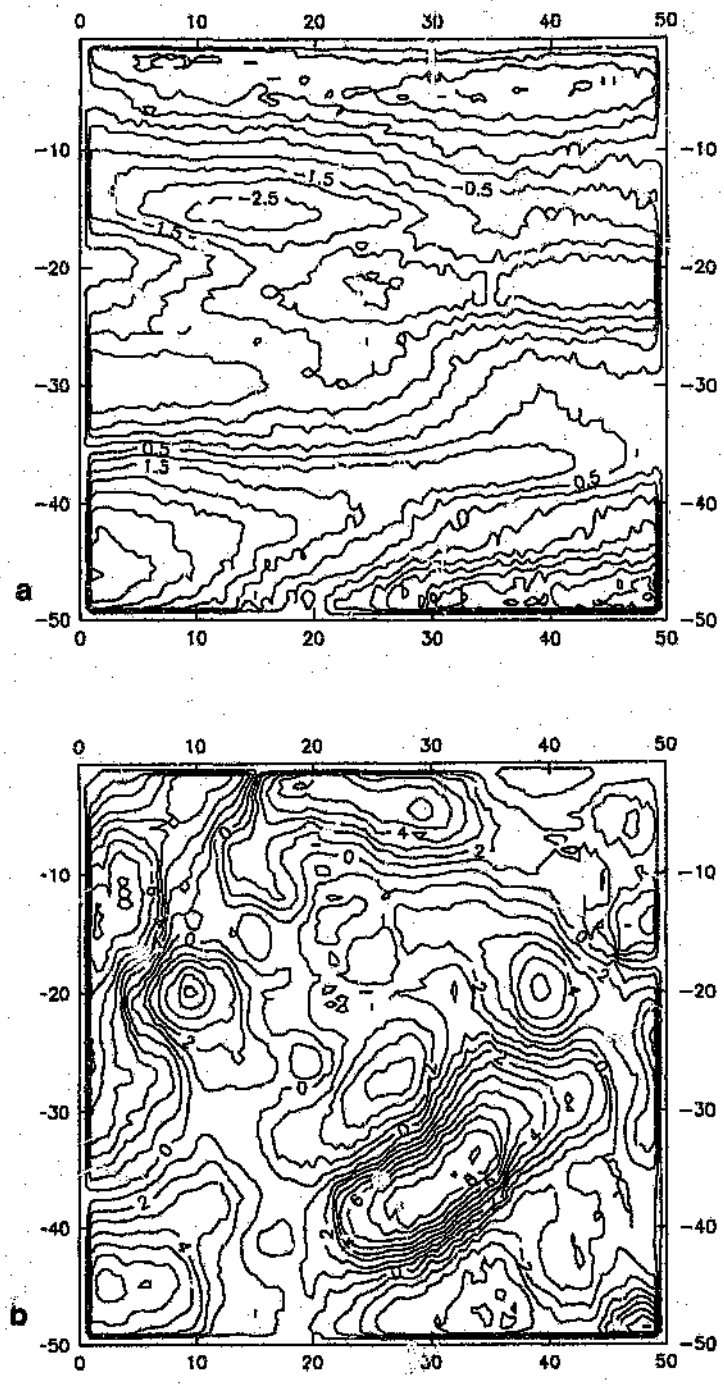

Figure 6.9: Mean ionospheric field (a) and contaminated lithospheric field (b) dusk maps for the summer solstice

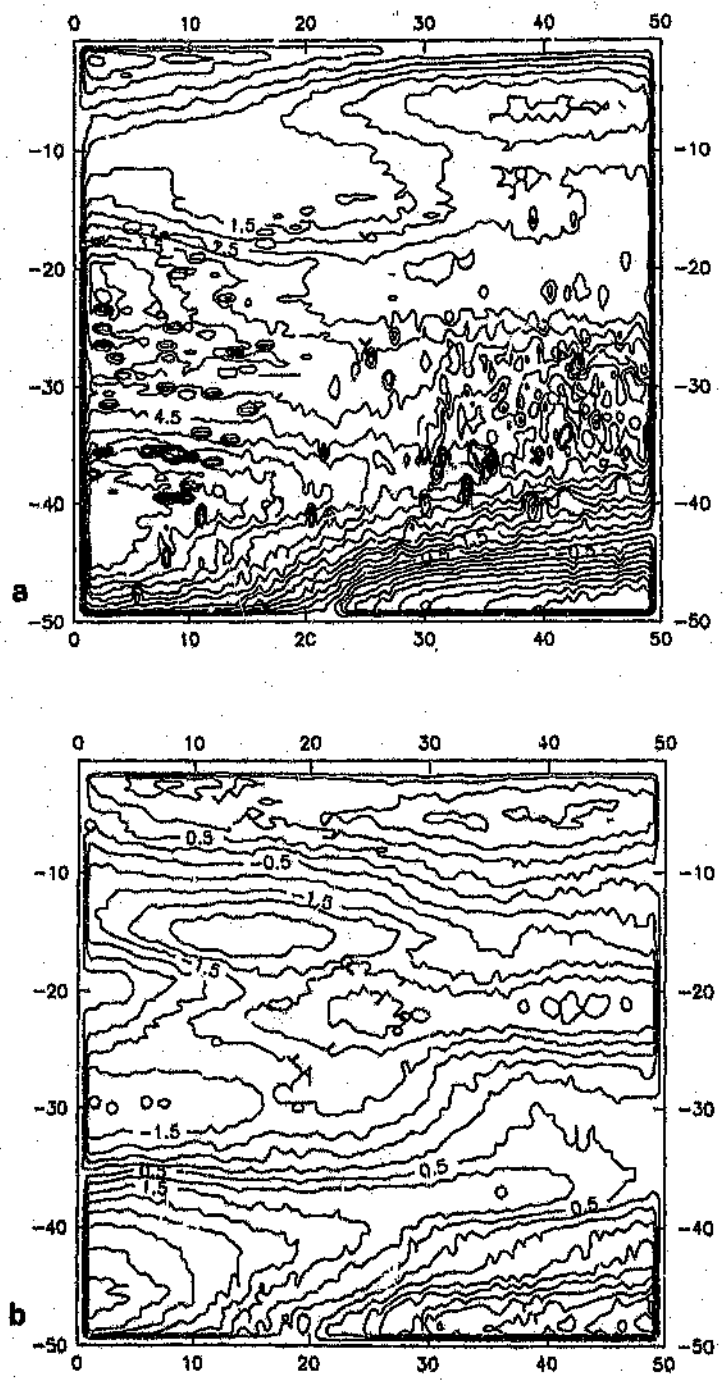

Figure 6.10: Separated dawn (a) and dusk (b) ionospheric field maps after adaptive filtering.

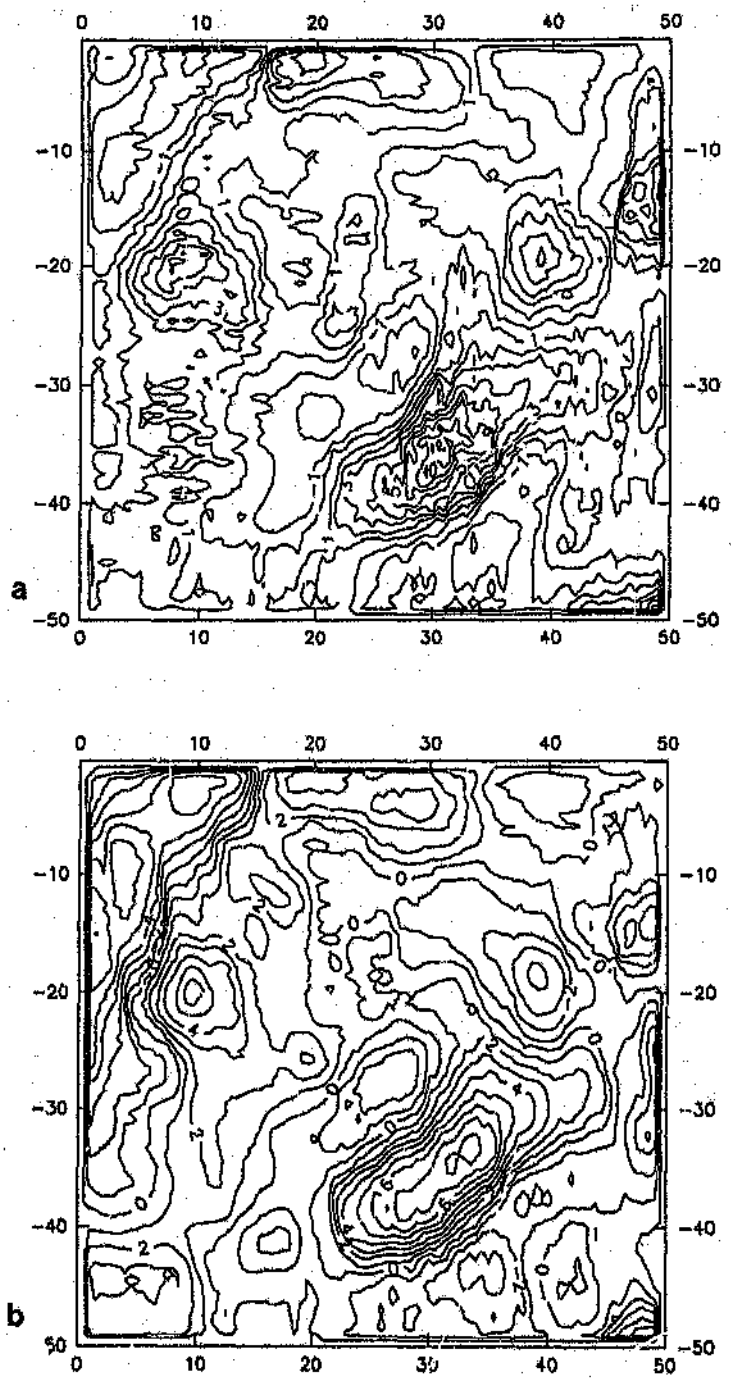

Figure 6.11: Dawn (a) and dusk (b) lithospheric maps separated from the contaminating ionospheric field.

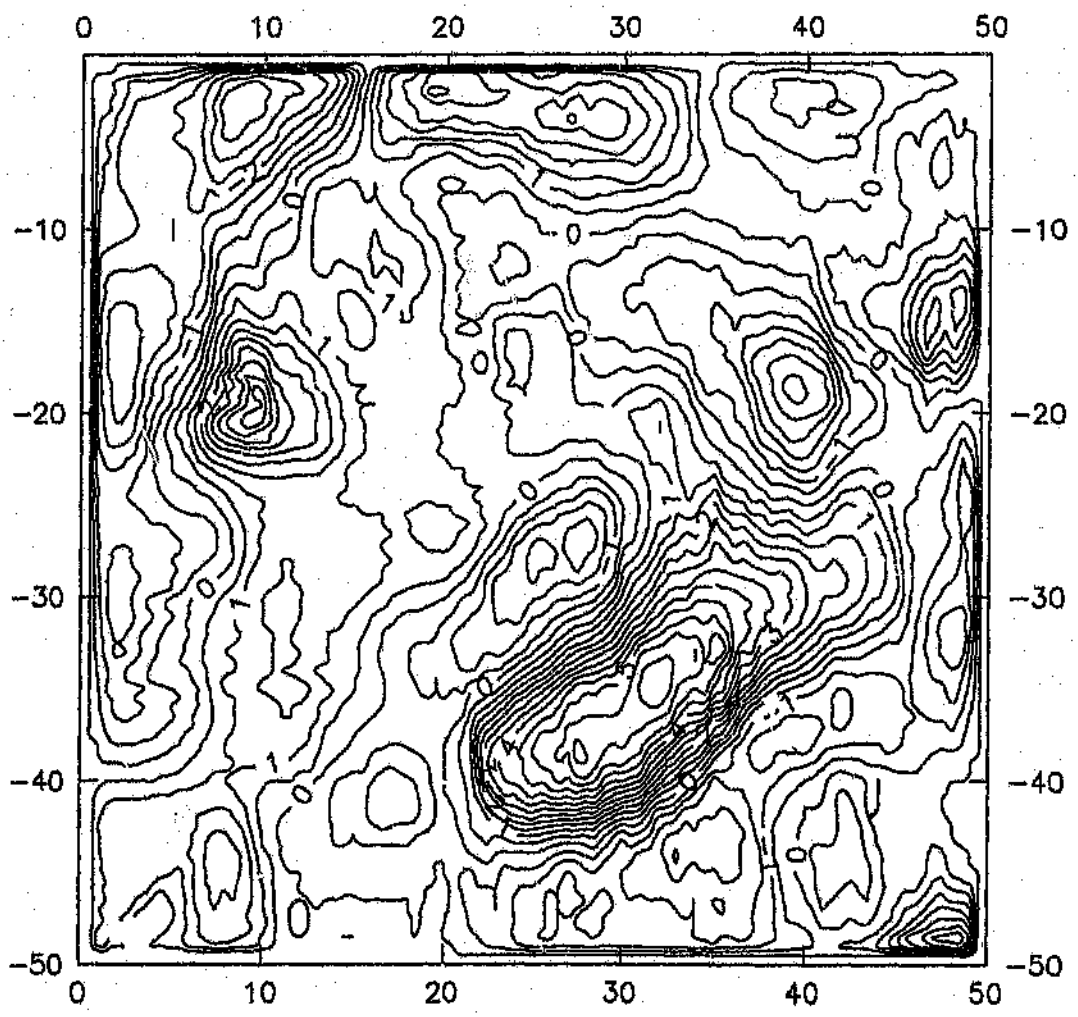

Figure 6.12: Lithospheric field map produced by the method of converging operations for the summer solstice.

Both dawn and dusk ionospheric field maps for the autumn equinox are presented in figure 6.13. It is interesting to note that the topology of these Sq magnetic field maps is almost identical. The lithospheric map for this season (Fig. 6.14) is, as required, a close approximation to the summer version (Fig. 6.12).

6.7.1 Synopsis of the ionospheric fields

Results of ionospheric field maps for dawn and dusk meridians for both seasons are compelling. Both the summer solstice and autumn equinox, have produced very similar ionospheric field maps for the respective local times. The ionospheric fields however, differ in regard to local time. In detail, there is some strong correlation of features between the dawn and dusk maps, particularly, in the south.

These long-wavelength correlating ionospheric field signatures in the dawn and dusk maps are suggestive of a non-ionospheric contributing source. If we assume that the method of deriving the MIF does effectively randomise the lithospheric field component then these correlating features represent residuals from the ring current model. The process of deriving the MIF is primarily based on the zonal behaviour of the IF and so is the ring current. The ring current model is inadequate in the high latitudes ($> 45^0$) where the effects of the polar field aligned current system are present (see e.g. Figs 6.1, 6.2, 6.3 and 6.4). That these signatures represent residuals from the ring current correction is supported by the fact that the strongest effects are mostly manifested in the high southern latitudes. Although, these ring current residuals are detrimental to Sq field analysis, their incorporation in the MIF provides a useful means of extracting these from the *target* lithospheric field maps.

From the above arguments it seems reasonable to assume that the MIF preserves, in addition to the ring current residuals, residuals from the core field separation. Thus, in principle, the anomaly maps presented here are free from residuals from inaccuracies of the ring current and core field models.

6.7.2 Synopsis of the lithospheric anomaly field

The lithospheric anomaly maps of figures 6.12 and 6.14 are almost identical and differ only in minor contour details. These two maps can be used as a measure of experimental precision.

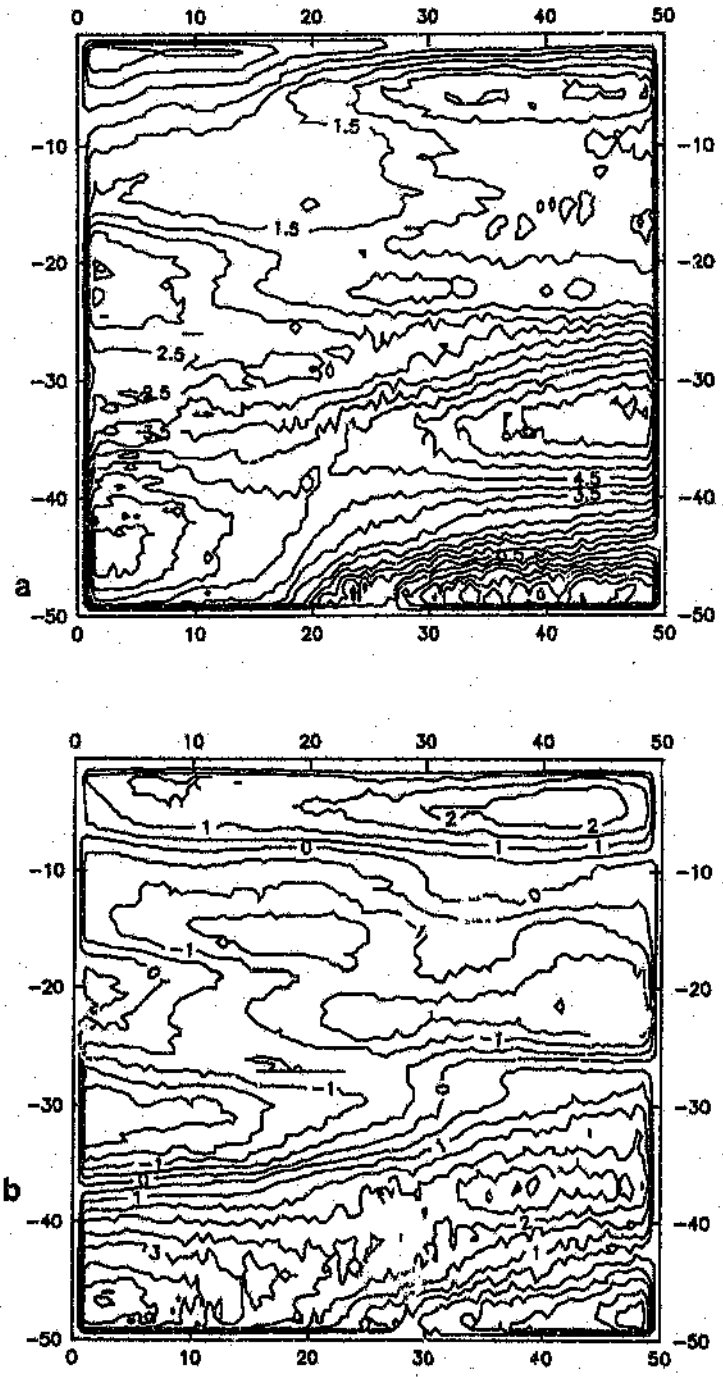

Figure 6.13: Dawn (a) and dusk (b) ionospheric field maps for the autumn equinox.

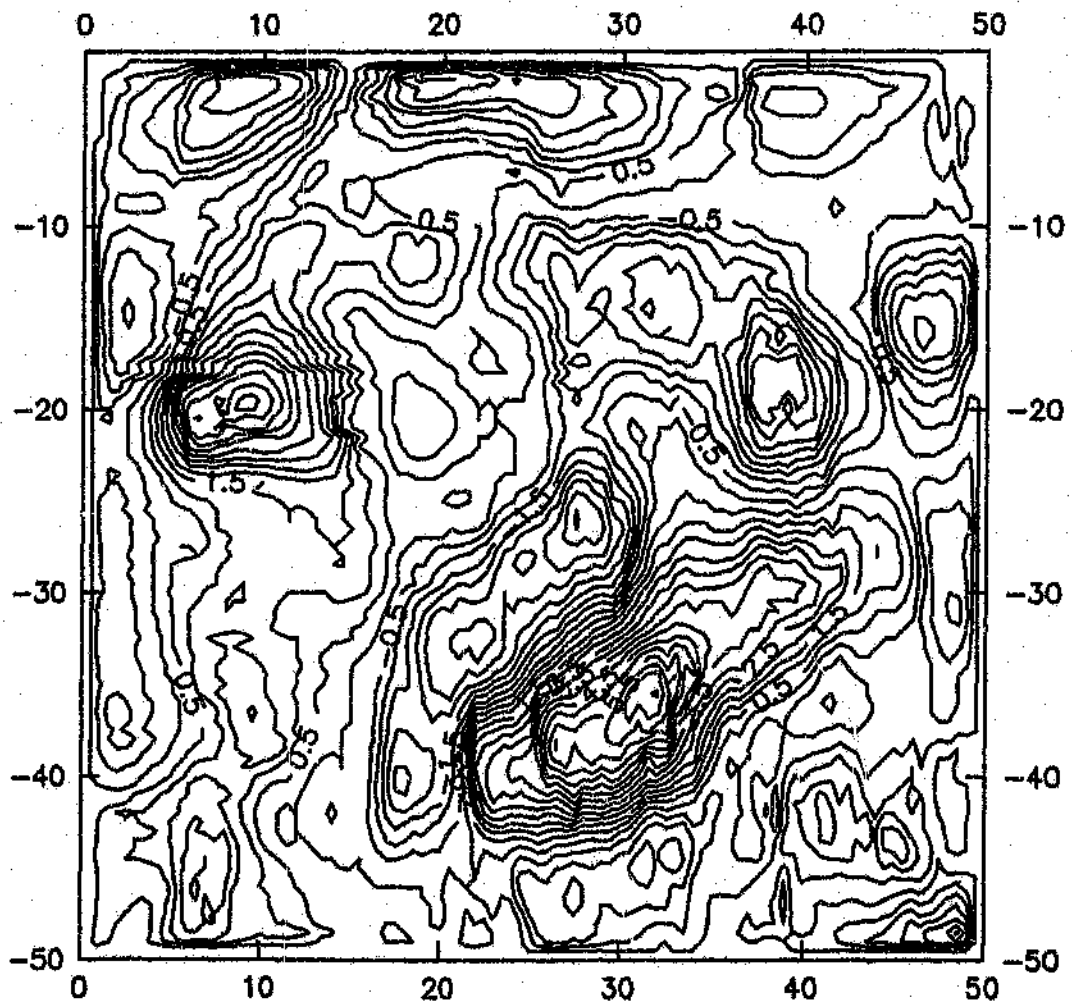

Figure 6.14 Lithosheric field map for the autumn equinox.

The r.m.s. between the two maps is 0,94 nT which is substantially smaller than the system's data accuracy of 5.8 nT (Langel et al., 1982).

The most dominant feature of the anomaly map is the northeast trending 'high' with a contiguous (to the northwest) 'low' in the southeast quadrant of the map. This anomaly (the Agulhas anomaly) is the focus of a detailed interpretation in Chapter 7. Another prominent feature is the isolated 'high' situated in the northwest quadrant. This high coincides with the Walvis Ridge and has recently been used as evidence for remanent magnetisation in Magsat data (Fullerton et al., 1989a).

Anomaly amplitudes (i.e. the Walvis Ridge and the Agulhas) are somewhat reduced from other published maps (e.g. Langel et al., 1982; Fullerton et al., 1989a; Lötter, 1989). The amplitude reduction is of the order of 3 nT with respect to Lötter (1989) and Langel et al. (1982) maps. These discrepencies are possibly related to processing residuals removed with the IF correction.

Chapter 7

Anomaly map of southern Africa

A long-term objective of this study is to compile satellite altitude magnetic anomaly data for large continental reconstructions such as Gondwana. An important consideration in the magnetic palaeo-reconstruction is whether or not magnetic responses should be incorporated in that reconstruction. Since some magnetic anomalies are considerably younger than others and are of oceanic origin. The southern African region was selected for the purpose of assessing the new processing techniques and for interpretation, for two reasons, viz.: (1) it is a focal point in a Gondwana reconstruction and (2) it is bordered by oceanic satellite-altitude magnetic anomalies, such as the Walvis Ridge (Fullerton et al., 1989a), and the Agulhas Plateau (Fullerton et al., 1989b; Antoine, 1989).

Magnetic signatures of continental southern Africa have been studied on several occasions with differing results. For example, Lötter (1989) derived a crustal magnetisation model from the total-field satellite anomaly measurements. This magnetisation map was compared with the subcontinental geology and in particular with tectonic provinces. A high degree of correlation was noted, although this was not ubiquitous. Where disagreement occured, it was attributed to an effective change in the magnetisation model due to variation in the depth of the Curie isotherm, which was assumed constant in the model. Arnott (1989) compared the total-field satellite anomaly map with the heat flow regime deduced from silicate geothermometry. Correlation between the heat flow data for southern Africa (which is presumed to be an indirect measure of the Curie isotherm; Mayhew, 1985; Johnson et al.,

1986) and the Magsat anomaly map is not definitive. The most notable correlation between datasets was noted between the heat flow data and a geanticlinal structure identified as the Vredefort axis; which itself is inferred from regional aeromagnetic data (Corner et al., 1990). It is thus apparent that agreement between previously processed Magsat anomaly data, geology and other geophysical parameters such as heat flow distribution are tenuous in detail.

The most prominent oceanic anomalies bordering southern Africa are the Walvis Ridge and Agulhas anomalies. The Walvis Ridge anomaly has been studied through forward modelling by Fullerton et al. (1989a). This anomaly is explained by the presence of substantial thermal remanent magnetisation (3 A/m) in a crust thickened during Cretaceous Quiet Times. Fullerton et al. (1989b) in studying the Agulhas anomaly and its geomorphic conjugate, the Maud Rise (situated in the South Atlantic), propose that they are both oceanic structures and correlate well with the areal extent of Cretaceous Quiet Zone ocean floor. Antoine (1989) interpreted the positive Agulhas anomaly to be the result of a reversely magnetised oceanic source because of the strong contiguous low situated to the north; the two anomalies were interpreted to originate from a single body giving rise to a reversed polarity pair. In order to explain the size of the source and the distinctive palaeomagnetic signature a model was postulated in which a large volume of melt is generated in a geologically short time span. Partial melting by decompression due to passive upwelling of hotter than normal asthenosphere in a rifted continental lithosphere was postulated as an appropriate mechanism.

7.1 The data set

The data reduction route and procedures are considered in the preceeding Chapters. The summer solstice total-field dataset (Fig. 6.12) was selected for the interpretation. To obtain maximum benefit from the dataset, it is displayed and enhanced using an I^2S image processor. Bathymetry and Seasat data were co-registered with the Magsat data. Figures 7.1, 7.2, 7.3 and 7.4 represent the Magsat, bathymetry and Seasat data, respectively. To enhance the short-wavelength aspects of the image the horizontal gradients are sun-shaded to create a shadowgram which, in turn, is coded as the intensity of the image while the hues of the image

represent field amplitude (see e.g. Antoine et al., 1990). Figures 7.1 and 7.2 differ in that the total-field values of figure 7.1 are coded linearly whereas those of figure 7.2 are coded using a stretched histogram.

As an additional interpretation aid, the Magsat data were combined with those of the bathymetry and Seasat. Two images were produced in which image intensity is coded with: (1) the bathymetry (Fig. 7.5) and, (2) the Seasat (Fig. 7.6) shadowgrams; while the hues are coded with Magsat's total magnetic field. Several shadowgrams were tested, the best results were obtained for an illumination azimuth from the north with an elevation of 40^0.

7.2 Interpretation

The principal features of figures 7.1 & 7.2 are: (1) the intense rectangular-shaped Agulhas anomaly off the southeastern coast of Africa, (2) the intense Walvis Ridge anomaly situated off the west coast of Africa at the 20^0S latitude and, (3) the northerly trending lower-intensity high off the southwestern coast of Africa. These features are clearly oceanic and will be the focus of this interpretation. Several isolated, low intensity responses occur within the southern African subcontinent and are also considered. The features in the extreme north of the image are excluded because they are outside the area of interest. The northern most anomaly is located over the Congo basin and constitutes the southern positive polarity shoulder of the Bangui anomaly (see Hastings, 1982; Frey, 1982). The positive anomaly in the northeast occupies the Comores-Seychelles region of the Indian ocean. It has not been the focus of specific interpretation although its response is used to support Frey's (1982) generalisation that positive Magsat oceanic anomalies coincide with oceanic rises or plateaux.

7.2.1 Modelling

Several profiles were selected for forward modelling purposes, the results of which are given in figures 7.7a,b and c. Because of the 3-D nature of the continental magnetic anomalies the profiles were primarily selected to approximate principal profiles to the most prominent oceanic features. A 2-D program, based on the Talwani algorithm (Talwani, 1965), was used for the forward modelling. The shape and amplitude of the magnetic field may not be perfectly represented by a model that uses a 2-D assumption of a body of limited strike length.

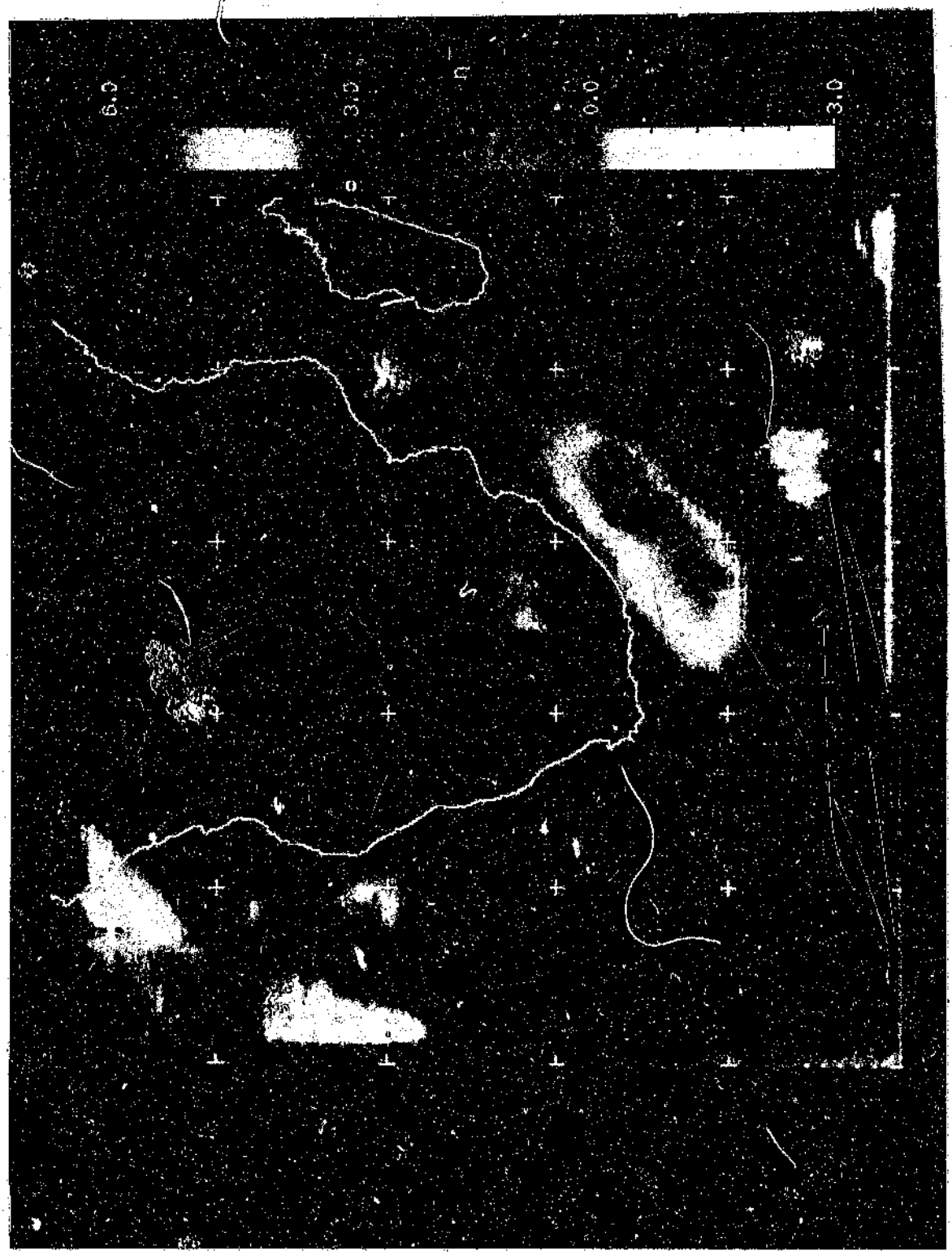

Figure 7.1: Sunshaded image of Magsat total magnetic anomaly field. Hues are coded linearly.

Figure 7.2: Sunshaded image of Magsat total magnetic anomaly field. Hues are coded using a stretched histogram. The transparent overlay may be used to identify magnetic anomalies and traverses that were extracted for modelling purposes. Anomalies are annotated as follows: Walvis Ridge (WR), Cuanza (C), Zambezi (Z), Mozambique (MZ), Kalahari (K), Southern Cape (SC), Southeast Atlantic (SEA), Agulhas (AG).

Figure 7.3: Sunshaded image of ocean floor bathymetry and continental topography.

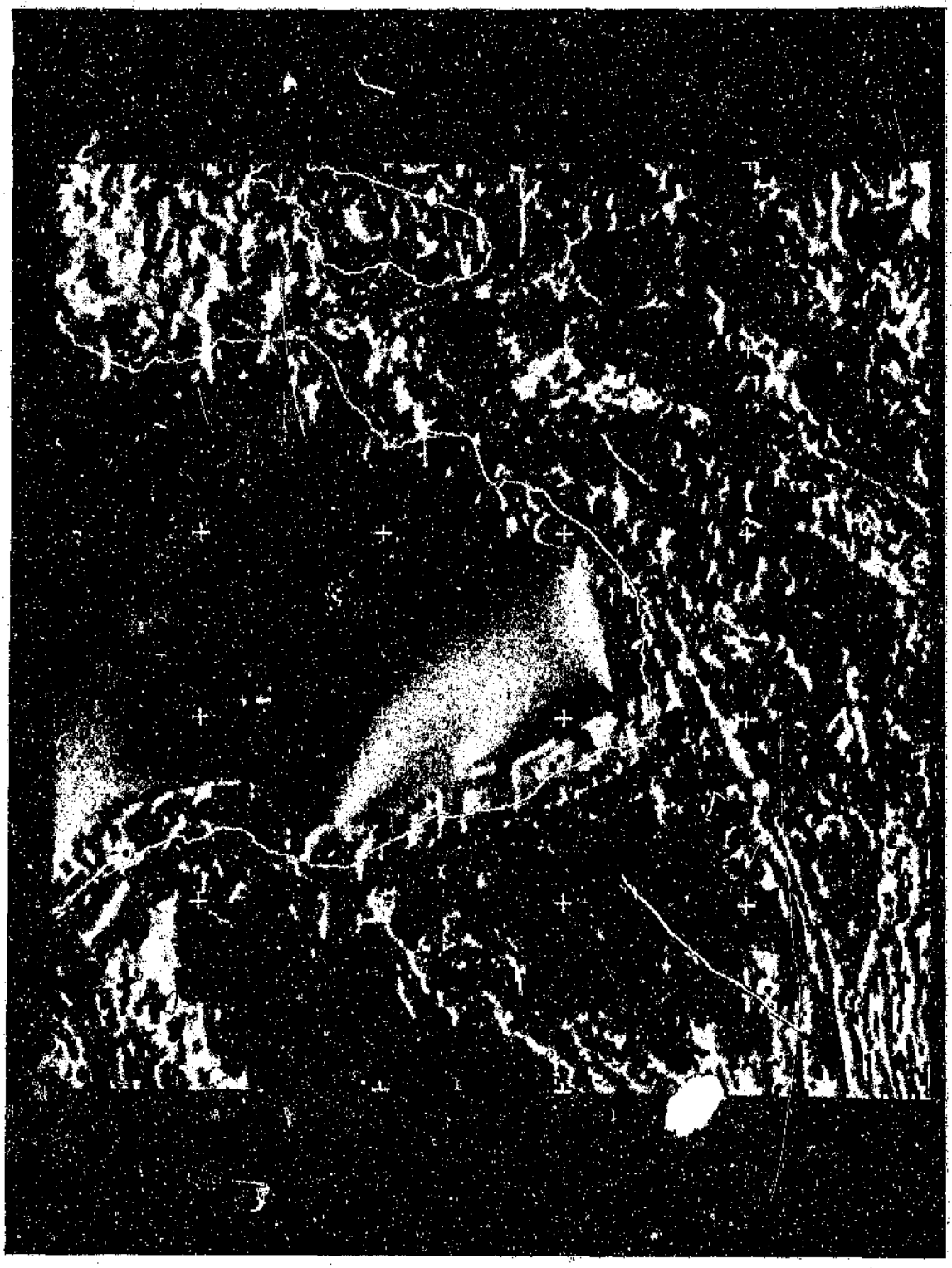

Figure 7.4: Sunshaded image of Seasat gravity field.

Figure 7.5: Sunshaded composite bathymetry-Magsat image. Image intensity is the bathymetry and topography shadowgram; hues represent Magsat magnetic total-field. The transparent overlay outlines first order orogenic provinces.

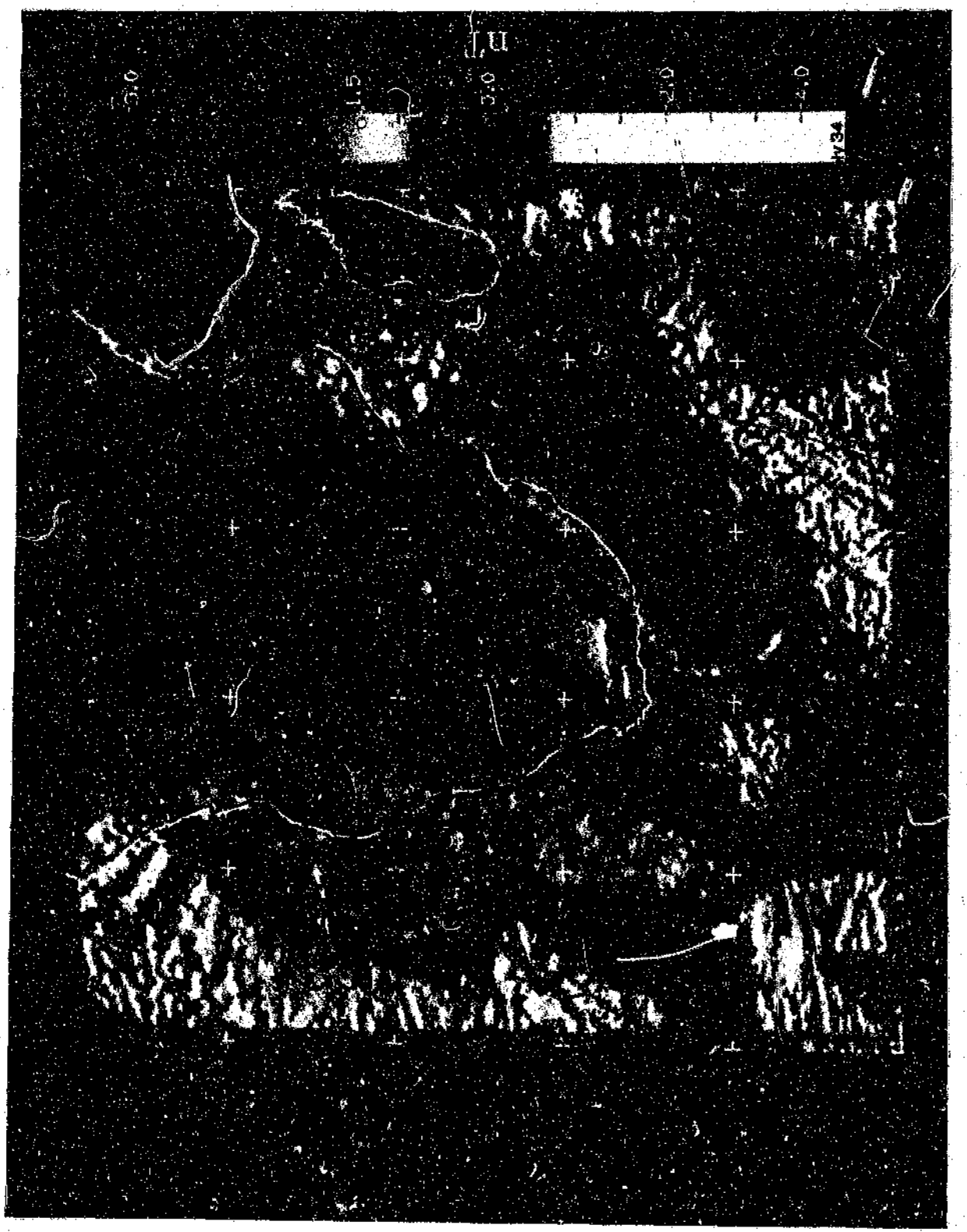

Figure 7.6: Sunshaded composite Seasat-Magsat image. Image intensity is the Seasat gravity field shadowgram; hues represent Magsat magnetic total-field. The transparent overlay delinertes ocean floor geomorphic and geophysical features.

Generally, the amplitudes are the most affected. Amplitudes are strongly underestimated with strike lengths below approximately 3 times the source to sensor separation, at which point the amplitude attains a value of 80% of the true amplitude (Nettleton, 1976). For the reference datum of 400 km used in this study the 2-D assumption fails for bodies of strike lengths below 1200 km. The Walvis Ridge anomaly (WR, Fig. 7.7c) has an anomaly half-width of approximately 1200 km and is thus reasonably represented using the 2-D assumption. The variable declination and inclination of the ambient polarising field along the profile is taken into consideration in the models. The inclination over this region (i.e. from the Walvis Ridge southwards) varies marginally from -56^0 to -64^0 while the declination varies over a range of some 15^0, i.e. from -15^0 to 30^0 (see Parkinson, 1983; p72).

Magsat anomaly data cannot resolve the depth to top of causative sources in the range of typical crustal depths which represents, at a maximum, 10% of the sensor altitude. Similarly, the depth extent, within this range, is an ambiguous parameter that cannot be resolved from these data. The most diagnostic information available from Magsat anomaly data are the lateral changes in magnetisation. Although, attempts have been made to generate magnetic crustal type-sections, for both continental and oceanic crust (e.g. Hahn, et al., 1984; Hayling and Harrison, 1986), the inverse problem remains ambiguous. For this reason it was decided to model the profiles using 10km tabular slabs for both continental and oceanic sources. The resultant volume-integrated magnetisation may then be interpreted in context with the local geology; this may require thining the slab with a resultant increase in magnetisation or *vice versa*.

7.2.2 Continental anomalies

The continental anomalies, viz.: the Mozambique (MZ), Zambezi (Z), Cuanza (C) and the Kalahari (K) (Fig. 7.2); are localised responses. These anomalies represent a lateral change in the total integrated lithospheric magnetisation. This could represent an increase in magnetic mineral assemblages or a variation in thickness of the lithosphere; not necessarily mutually exclusive. As a generalisation, the continental anomalies appear to be localised within tectonic provinces (e.g. the Southern Cape, Kalahari, Zambezi and Mozambique anomalies). This correlation may be seen by using the transparent overlay, to figure 7.5, on which the orogenic

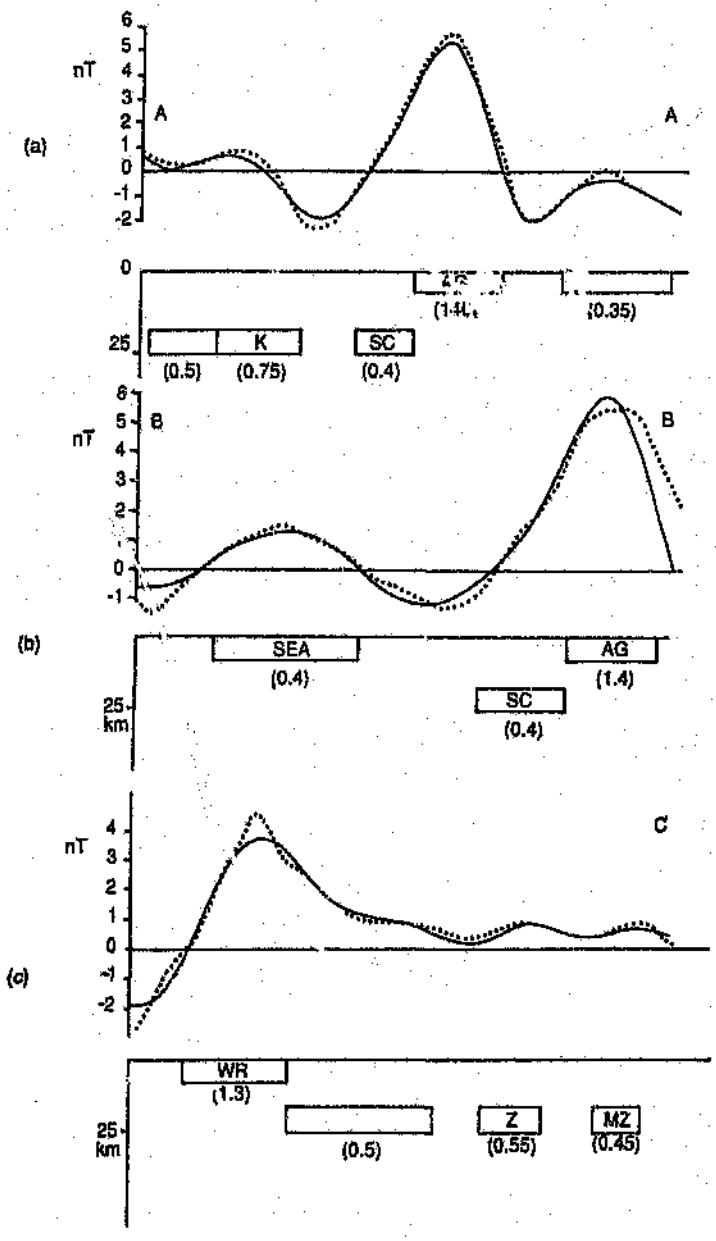

Figure 7.7: Forward modelling of selected profiles A-A'(a), B-B'(b) and C-C'(c). The solid line is the modelled field, the dashed line the observed field. The location of the profiles is shown in figure 7.2 and 7.5. Bracketed values are the apparent magnetisation contrast (A m^{-1} in a 30000 nT field) and are within the ranges as given by Hayling (unpublished reprint). All polarisation vectors are parallel to the ambient inducing magnetic field with the exception of the Agulhas anomaly which yields a remanent inclination of -72^0 (cf. -64^0). Magnetic anomalies are annotated as follows: Walvis Ridge (WR), Kalahari (K), Southern Cape (SC), Agulhas (AG), Southeast Atlantic (SEA), Zambezi (Z), Mozambique (MZ).

provinces are delineated. The local geology of the continental areas underlying the satellite magnetic anomalies differ considerably with respect to lithological assemblages, metamorphism and deformation. These areas are described, in brief, in order to ascertain whether or not there is a local or a common source for the apparent local increase in lithospheric magnetisation.

It must be borne in mind, when viewing the magnetic anomaly images, that these are representative of a 400 km reference altitude. The spatial influence of a single magnetic dipole source at this reference altitude is equivalent to an area of 4^0 by 4^0. Because of the inherent errors of data acquistion and processing, the interpreted anomaly boundaries should be viewed, in consequence, as being 'fuzzy'. The best possible spatial resolution given by Sailor et al. (1982) is 250 km (approximately 2^0 at these mid-latitudes).

Southern Cape anomaly

In order to model the positive southeastern Agulhas anomaly (profile A-A'; see Figs 7.2 and 7.7a) satisfactorally, two contiguous sources were required, i.e. a unit of low magnetisation contrast in the north (the Southern Cape anomaly, SC) and a unit of high apparent magnetisation contrast in the south (the Agulhas anomaly, AG). The high contrast source (AG) required a polarisation vector with a remanent inclination of approximately -72^0 whereas all other sources could be modelled for normal inducing field inclinations. An acceptable fit could be obtained, in the modelling of the intense positive Agulhas anomalous signature, only by incorporating the lower-contrast induced magnetisation immediately to the north (SC)[1]. Because the signature of the anomaly is manifested as a change of the northern gradient of the intense positive Agulhas response, it is not possible to discern this response on the images and therefore indeterminable other than through modelling along the profile. This modelling is in contrast to earlier preliminary interpretations of Antoine (1989), where remanence was used to model both the positive and the northern contiguous negative response as an anomaly pair.

The Southern Cape anomaly occurs in the eastern region of the Cape Fold Belt and the

[1]The uncertainties inherent in the anomaly map (see section 6.7.2) make alternative models possible although the author is of the opinion that the remanent inclination required by the modelling is evident, to a first order, in the data.

Namaqua-Natal Belt. The Namaqua-Natal Belt borders the south and southwestern Kaapvaal Craton. Most of the southern central portion of this tectonic province is overlain by Karoo sediments. It is exposed in the northwest and in the east. Basement rocks consist of gneisses, schists and granitoids of amphibolite to granulite facies metamorphism. Contiguous to, and south of the Namaqua-Natal Belt is the Pan-African Damara-Gariep-Malmesbury Belt which is associated with the Cape Fold Belt (a highly folded sequence of supra-crustal rocks) (De Beer and Meyer, 1984). The basement rocks comprise metasediments, metavolcanics and granites of low metamorphic grade.

Although the boundary of the Namaqua-Natal Belt is mostly unexposed it is mapped by means of a distinct gravity signature (De Beer and Meyer, 1984). This tectonic province is distinguished by an anomalous electrical conductivity belt (Southern Cape Conductive Belt) and by a strong regional magnetic anomaly (Beattie anomaly). De Beer and Meyer (1984) interpreted several radial gravity profiles from the Kaapvaal Craton across the Namaqua-Natal Belt and consistently derived a thicker, denser crust for the tectonic province with respect to the adjacent Kaapvaal Craton.

Mozambique anomaly

The Mozambique anomaly extends in a northwesterly direction from the eastern end of the oceanic Agulhas anomaly. It overlies Mozambique and terminates within Zimbabwe at the northern domain of the Limpopo Belt. The anomaly appears to be strongest in the north over the mobile belt. The contribution to this source may be two fold, that is: (1) a contribution from the speculative Cretaceous Oceanic crust underlying Mozambique (J.D. Fairhead pers. comm.) and (2) an origin within the Limpopo Belt.

The Limpopo Belt separates the Kaapvaal and Zimbabwe Cratons. Three zones are recognised. The central zone contains large scale folding and interference structures and consists of medium- to high-grade gneisses, metasediments and metavolcanics. The northern and southern zones of the Limpopo Belt are characterised by high-grade, granulite facies, metamorphism of similar lithologies and by a consistent alignment of foliation of the gneisses (Hunter and Pretorius, 1981). The structure of the belt is asymmetric and has a large (400 g.u.) isostatic gravity anomaly over the southern marginal zone (Coward and Fairhead, 1980;

De Beer and Stettler, 1988). Geoelectrical and gravity modelling by De Beer and Stettler (1988) show that this isostatic anomaly is caused by dense middle- to lower-crustal material in the upper 10 km of the crust.

Results of refraction and reflection seismic surveys, and gravity modelling by Barker (pers. comm.) of a traverse from the Kaapvaal Craton across the Limpopo Mobile Belt suggests that the data are consistent with a Moho depth of 45 km.

The western border of Mozambique has a distinctive, 700 km, north-south trending volcanic belt (Lebombo line) which is associated with a pronounced isostatic gravity anomaly. Darracott and Kleywegt (1974) interpreted gravity profiles across the Lebombo volcanic line into Mozambique. In their interpretation they show that only part of the anomaly can be accounted for by the basal basalts of the Lebombo monocline, and the remainder of the signal to the east must be a crustal effect.

Kalahari anomaly

Another region of elevated apparent magnetisation occurs at the intersection of the Irumide and Namaqua-Natal orogenic belts. The anomaly is termed Kalahari because it is situated at the edge of the Kalahari basin which extends eastwards into Botswana. In detail, the anomaly is located at a complex intersection of several subprovinces, namely: Gordonia, Richtersveld and Kheis (Stowe, 1986). The region comprises low metamorphic grade, metasediments and metavolcanics. No geophysical studies of regional significance have been undertaken over this anomaly. One of the radial gravity profiles studied by De Beer and Meyer (1984) intersects this region. This profile shows no apparent change of the regional Namaqua-Natal Belt signature.

Zambezi anomaly

Bordering the western edge of the Zimbabwe Craton, the Zambezi anomaly parallels the Lomagondi Province and extends northward into the Zambezi Belt (at the intersection with the Irumide) and into the Lufilian arc (Cahen et al., 1984). The assemblage of rocks comprising the Zambezi tectonic Belt are broadly described by Cahen et al. (1984) as high grade metamorphites. Within the Lufilian arc a sequence of strongly folded sediments become pro-

gressively metamorphosed and intruded by granites southward. This palaeo-thermal increase is reflected in northern Zimbabwe (Clifford, 1970). This region bears the imprints of several late Precambrian tectono-thermal events.

Cuanza anomaly

The most prominent of the southern African continental anomalies is the Cuanza anomaly in north Angola. This anomaly is located over the southern extension of the West Congolian Belt. The Cuanza anomaly occurs over a granulite facies metamorphic terrain comprising enderbrites, charnockites, kinzingites and granulite gneisses preserved in younger granite-gneissic rocks (Cahen et al., 1984).

Damara anomaly

North of the Kalahari anomaly, partially overlying the Damara Belt, and bordering the Namibian west coast, is a region of elevated magnetisation contrast. The Damara Belt is a complex orogenic unit comprising a coastal and an intracratonic branch. The coastal branch is described as the Koakoveld orogen by Cahen et al. (1984), which extends along the coast of northwest Namibia into Angola. The central zone of the northeasterly trending intracratonic belt is the site of high-temperature medium pressure metamorphism, granitisation and anatexis (Coward, 1983; Hartmann et al., 1983). The lithologies within the Damara and Kaokoveld orogens consist mostly of metasediments and metavolcanics. Metamorphism in the east of the Kaokoveld orogen is low-grade and increases westerward towards the coast where it is high-grade.

Seismic refraction profiles indicate that the Damara orogen shows local crustal thickening up to approximately 50 km (Green, 1983). Aeromagnetic data over the central zone record strong elevated magnetic responses from near surface supracrustal sources (Corner, 1983). Electrical sounding studies in the area have confirmed observations of an earlier magnetometer array study that a prominent conductive structure coincides with the Damara Belt. This conductive structure has a probable minimum thickness of 20 km and occurs at a depth of approximately 10 km (Van Zijl and De Beer, 1983).

7.2.3 A tentative model for the continental anomalies

The broad picture that emerges from the above observations is that the positive Magsat lithospheric apparent magnetisation contrasts are localised to orogenic belts. In detail the individual areas are quite diverse in local lithological assemblages, tectonic history and structure. Their metamorphic grades are, in general, high.

Because the magnetisation contrast as observed by Magsat is representative of the total volume-integrated magnetisation, any model for increased magnetisation must reflect either an increase in the thickness of a uniformaly magnetic crust, or an increase in the concentration of magnetic mineral assemblages, or both. Since the modelling required neither excessive magnetisations for the causative sources nor large regional contributions, it can be argued that these results are congruent with the postulate of Wasilewski (1987), that the magnetic and seismic Mohos are equivalent, other than in regions where the Curie isotherm is shallower. Further, it follows that an increase in crustal thickness and in magnetisation may be responsible for the observed continental Magsat anomalies for the reasons given below.

Generally, the crustal thickness of young orogenic belts is considerably greater than that of old Cratons (see e.g. Green and Durrheim, in press; Green, 1983; De Beer and Meyer, 1984; Reeves, 1985; Tanner and Gibb, 1979). For example, the average Moho depths are in the order of 32 km for the Kaapvaal Craton and 42 km for the surrounding mobile belts (Durrheim, 1990). In addition to the increased crustal thickness, these tectonic belts have a higher heat flow than the Cratons, the ambient values being around 60 and 40 m Wm^{-2}, respectively (M.Q.W. Jones pers. comm.; Jones, 1988 and 1987). It can be hypothesised that there is a direct correlation between heat flow (crustal temperature gradient), crustal thickness and crustal magnetisation through the Hopkinson effect[2]. This relationship is illustrated in figure 7.8. Several typical geotherms from the Namaqua-Natal Belt and from the Kaapvaal Craton (Jones, 1987) are represented. As indicated in the figure the maximum Hopkinson effect occurs in the 100^0 C broad region below the Curie isotherm. Moho depths for the craton and for the mobile belts are also indicated, they serve to define an effective

[2]The effect of temperature on rock magnetism is to increase the magnetic susceptibility. With increasing temperature the magnetic susceptibilty increases, reaches a maximum (Hopkinson peak, approximately 50^0 – 100^0C below the Curie isotherm) and falls off rapidly just before the Curie temperature is attained. The width and shape of the peak is related to the blocking temperature spectrum of the magnetic minerals. A modest enhancement of susceptibility by a factor of 2 for crustal rocks is entirely feasible (Dunlop, 1974).

increased magnetisation window as a result of the Hopkinson effect.

In addition to the postulated Hopkinson effect as a possible contribution to crustal magnetisation of tectonic belts there may be an additional contribution from serpentinisation of the crust; which may be mutually exclusive. Some mobile belts have middle- to lower-crust electrical conductivity anomalies (De Beer and Meyer, 1984; De Beer and Stettler, 1988; Miller, 1983; Gough, 1989). These electrical conductivity zones are an indication of an increase, at depth, in water con ent within orogenic belts (see e.g. Hyndman and Shearer, 1989; Vanyan and Shilovski, 1989). The presence of water may result in serpentinisation and consequently an increase in magnetite content (Winkler, 1974; Turner, 1968). Serpentinisation reaction curves from Winkler (1974) are indicated on figure 7.8. Because experimental data do not extend into the high pressure regimes these curves are extrapolated in the diagram.

7.2.4 Oceanic anomalies

Oceanic anomalies bordering southern Africa are the Walvis Ridge (WR), the Southeast Atlantic (SEA) and the Agulhas (AG) anomalies (Fig. 7.6). The Walvis Ridge anomaly is three-dimensional in appearance, relatively intense (4,5 nT in amplitude) and is located just off the Namibian coast at latitude 20^0S where the Walvis Rise meets the African continent. The Southeast Atlantic anomaly is located off the west coast of southern Africa, South of the Walvis Ridge anomaly and although parallels the coast, has a slight but persistent trend that is some 10^0E away from that of the continental margin southwards. Located off and contiguous to the southeast coast of southern Africa, in the Southwest Indian Ocean, is an intense and extensive positive magnetic response, the Agulhas anomaly.

The two profiles of figure 7.7(a) and (b) are an interpretation of the Agulhas and Southeast Atlantic anomalies. In the case of the Agulhas anomaly a total magnetisation vector with an inclination of -72^0 was required by the modelling. Assuming a normal induced magnetisation component of inclination -64^0 at 0,4 A/m (Hayling and Harrison, 1986) and a steeper resultant vector of magnetisation 1,4 A/m (assuming the same declination for both vectors), a remanent vector of inclination -76^0 and ~1,0 A/m intensity is estimated (for a 10 km thick crust in a ~ 30000 nT field). It is not possible to establish the inclination of any remanent magnetic vector from the Southeast Atlantic anomaly since the profile is essentially magnetic

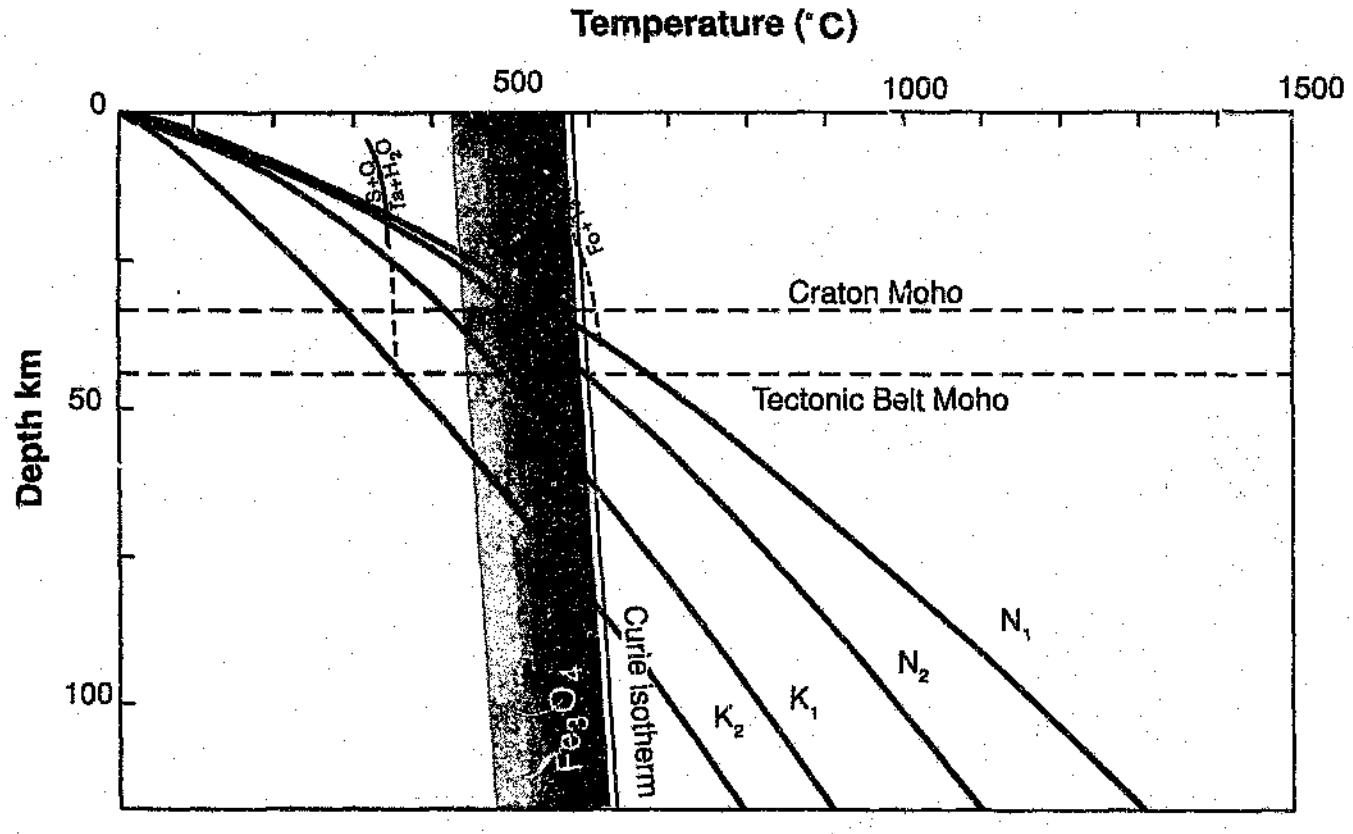

Figure 7.8: Graph showing the Hopkinson effect in relation to typical southern African geotherms for the Kaapvaal Craton (K_1, K_2) and Namaqua Mobile Belt (N_1, N_2) (after Jones, 1988) and their typical Moho depths. The grey shading, light to dark, represents the relative increase in magnetic susceptibility. Serpentinisation reaction curves are included; the dashed portions of these curves are extrapolated (after Winkler, 1974).

East-West; the presence of remanence can only be inferred from anomaly amplitudes and from its location in the ocean floor.

Magnetisation of the oceanic crust differs considerably from that of the continents. Models of oceanic crustal magnetisation comprise predominantly an average induced component of some 0,4 A/m (over the entire 6 km thick crust) and a TRM (which may be as high as 6 A/m) of the 2 km basal plutonic units and the top 0,5-1,0 km basalt layer (Hayling and Harrison, 1986; Arkani-Hamed, 1988; Hayling, unpublished preprint; see also Chapter 2). With the exception of the Jurassic and Cretaceous normal polarity epochs, the sea floor has recorded TRM as a regular and continuous alternation of polarity reversals of the geomagnetic field. As a working approximation, it may be argued that, the total TRM contribution of the total anomaly field for the magnetically striped ocean floor will be zero at satellite altitudes. In contrast, the periods of prolonged normal polarity of the geomagnetic field should be manifested in the satellite total field anomaly data (Hayling and Harrison, 1986). In this respect, the southern African continent is bordered by the Cretaceous Quiet Zone (KQZ) on the west and southeastern coasts. In essence, the three magnetic oceanic anomalies (SEA, AG and WR) correlate closely with the KTZ (Cande et al., 1989).

The Southeast Atlantic anomaly

In detail, the anomalies differ considerably. The Southeast Atlantic anomaly has an amplitude response that is consistent with a magnetisation contrast of 0,4 A/m. This must either reflect a thickening (100%, assuming induced magnetisation) of the oceanic crust or an increase in remanent magnetisation from the KQZ. The latter option seems more appropriate, since there is no geophysical evidence (seismic or gravity) for crustal thickening in this part of the Atlantic ocean (Chave, 1979; Detrick and Watts, 1979). An aspect of the Southeast Atlantic anomaly that is enigmatic at present, is the NNE gross trend. The anomaly, in the extreme South, terminates approximately at the Agulhas fracture zone; beyond which it appears to branch.

The Walvis Ridge anomaly

The Walvis Ridge anomaly has a magnetisation of 1,3 A/m and contrasts strongly with the Southeast Atlantic anomaly. The Walvis Ridge is an aseismic oceanic rise and is composed mostly of basalts (Detrick and Watts, 1979). It is generally accepted that such ridges (e.g. Walvis, Rio Grande and Ninetyeast) are formed over 'hot spots' centered on or near mido-cean ridges (Morgan, 1971). Chave (1979), studied the lithosphere structure along the Walvis Ridge and neighbouring Cape basin using Rayleigh wave group velocity dispersion. He found that the results for the Walvis Ridge were consistent with a crustal thickening to 12,5 km and with an anomalous upper-mantle low shear-wave velocity (4,25 - 4,35 km/s to depths of 45 km). The seismic ray path adjacent to the ridge (south) showed no crustal thickening; supporting the above postulate that the SEA results primarily from increased KQZ remanence. Detrick and Watts (1979) support this crustal thickening below the Walvis Ridge from an analysis of isostasy. They also observe a difference in isostasy between the East and West Walvis Ridge. The eastern Walvis Ridge is locally compensated by an overthickening of the crust in the order of 15-25 km. The western end of the rise was found to be morphologically and structurally different having an effective elastic plate thickness of 5-8 km. Fullerton et al. (1989a) argue that the Walvis Ridge Magsat anomaly is the result of TRM (3 A/m, for the entire layer 3) acquired during Cretaceous Quiet times (KQT). Assuming that the 0,4 A/m magnetisation of the Southeast Atlantic anomaly (of this dataset) is representative of KQZ TRM, the Walvis Ridge magnetisation of $\sim 1,3$ A/m (Fig. 7.7c) is consistent with the observed crustal thickening of a factor of 2.

The Agulhas anomaly

The Agulhas anomaly is the largest and most intense Magsat anomaly within the southern African region. This anomaly is delineated by several ocean floor features, for example: (1) the northern boundary coincides with the Agulhas Fracture Zone (in the west), which follows the continental shelf in the east, into the Maputo embayment; (2) the eastern spur (of the almost rectangular-shaped Agulhas anomaly) coincides with a similarly shaped Seasat depression which is truncated in the extreme east by the Davie Ridge and; (3) the western and southern perimeters roughly delineate the western and southern limits of the bathymetry

and Seasat highs of the Agulhas and Mozambique Plateaux.

Qualitatively, the Agulhas anomaly appears to have internal structure, namely, the eastern spur is of lower intensity; the truncation of this spur occurs at the Prince Edward Fracture Zone. Fullerton et al. (1989b) believe that TRM , acquired during KQT, explains the large magnetisation contrast of the Agulhas anomaly. The modelled profile (A-A' Fig. 7.7a) confirms this postulate. The magnetisation contrast is 1,4 A/m as compared with 1,0 and 0,4 A/m for the Walvis Ridge and Southeast Atlantic anomalies, respectively. The Agulhas magnetisation contrast is of the same order as the Walvis Ridge anomaly. By analogy, therefore, it can be argued that the Agulhas Magsat anomaly reflects a thickened oceanic crust. The lower-intensity spur of the anomaly may reflect, by comparing with the SEA, that part of the KQZ ocean floor of normal thickness.

An increase in thickness of the oceanic crust in the Southwest Indian Ocean is consistent with free-air gravity interpretations along a 21 km traverse by Graham and Hales (1965) over the Agulhas Plateau (north-south profile), and along a 27-31 km traverse by Doucoure and Bergh (unpublished preprint) over the Mozambique Ridge (east-west profile). Tucholke et al. (1981) comment, from refraction lines over the Agulhas Plateau, that no mantle refractions could be observed from refraction spreads as large as 72 km. This approximates a depth of investigation of 17 km for average oceanic crust and upper-mantle velocities, i.e. 17 km is a lower limit for the crustal thickness of the Agulhas plateau.

7.2.5 Implications to continental break-up of Gondwana

Although, the dispositions of the three oceanic Magsat anomalies broadly correlate with the Cretaceous Quiet Zone, in detail these can be focussed to correlate with a zone within KQT that is older than anomaly 34 (Fig. 7.6) (Cande et al., 1989). These magnetisation anomalies delineate oceanic floor for Aptian-Albian reconstructions (Fig. 7.9) (Unternehr et al., 1988; Rabinowitz and LaBrecque, 1979). To account for the lack of magnetic anomalies in the KQZ of the equatorial Atlantic, Hayling and Harrison argue that KQZ would not be observed from satellite altitudes because of the amplitude and inclination of the polarising geomagnetic field. This is not valid, because: (1) at the geographic equator inclinations are -25^0 (Parkinson, 1983, p72) and (2) the oceanic anomalies terminate abruptly north of the Walvis Ridge.

The distribution of magnetic ocean floor is consistent for an Aptian-Albian reconstruction. The interpreted remanent magnetisation vector (-76^0) for the Agulhas anomaly would also be consistent for the southerly palaeolatitudes during KQT (see e.g. Smith et al., 1981; Weijermars, 1989; Piper, 1988).

It follows, from the above, that these oceanic Magsat anomalies arise from a time frame, between pre-fragmented Gondwana and the end of early Cretaceous, recorded as a contrast in magnetisation of the oceanic crust. This contrast in magnetisation is attributed, in the first instance, to remanent magnetisation acquired during the Cretaceous normal polarity epoch and, in the second, due to local thickening of the crust.

It is opportune to view the Agulhas anomaly here within the framework of a reconstruction of Gondwana (Fig. 7.10). This reconstruction is based on de Wit et al. (1988) but is cognisant of the controversial nature of such reconstructions, particularly for West Antarctica. The configuration of microplates in figure 7.10 is presented as a compromise and is not intended to imply preferred orientations at this stage. For example, the fit of southern Africa, South America and the Agulhas Plateau is based upon the model of Martin and Hartnady (1986), whereas East Antarctica and southern Africa are juxtaposed in a manner similar to that proposed by Lawver and Scotese (1987). The overlap of western Dronning Maud Land and the coastal area of Mozambique is based on geophysical and geological constraints (Grantham et al., 1988; Corner, 1989; Hodgkinson, 1990). The position and orientation of the Ellsworth-Whitmore Mountains microplate is probably the most contentious issue currently being addressed in West Antarctica, and is shown here as a compromise between that proposed by Watts and Bramall (1981) and Storey et al. (1988a). Haag Nunatak has been fitted in a position similar to that of de Wit et al. (1988). It is based on the geological comparison of these rocks with other areas of East Antarctica and its apparent anomalous position within West Antarctica (Storey et al., 1988a).

In the above reconstruction, the Agulhas anomaly apparently underlies a large portion of Gondwana, encompassing part of Western Dronning Maud Land, the Falklands and Agulhas Plateaux and, the microplates of West Antarctica (South Georgia, Ellsworth-Whitmore Mountains, Haag Nunatak, Berkner and Filchner plates). Magmatism is widespread in this region and overlaps widely, in time, with the fragmentation history of Gondwana. For ex-

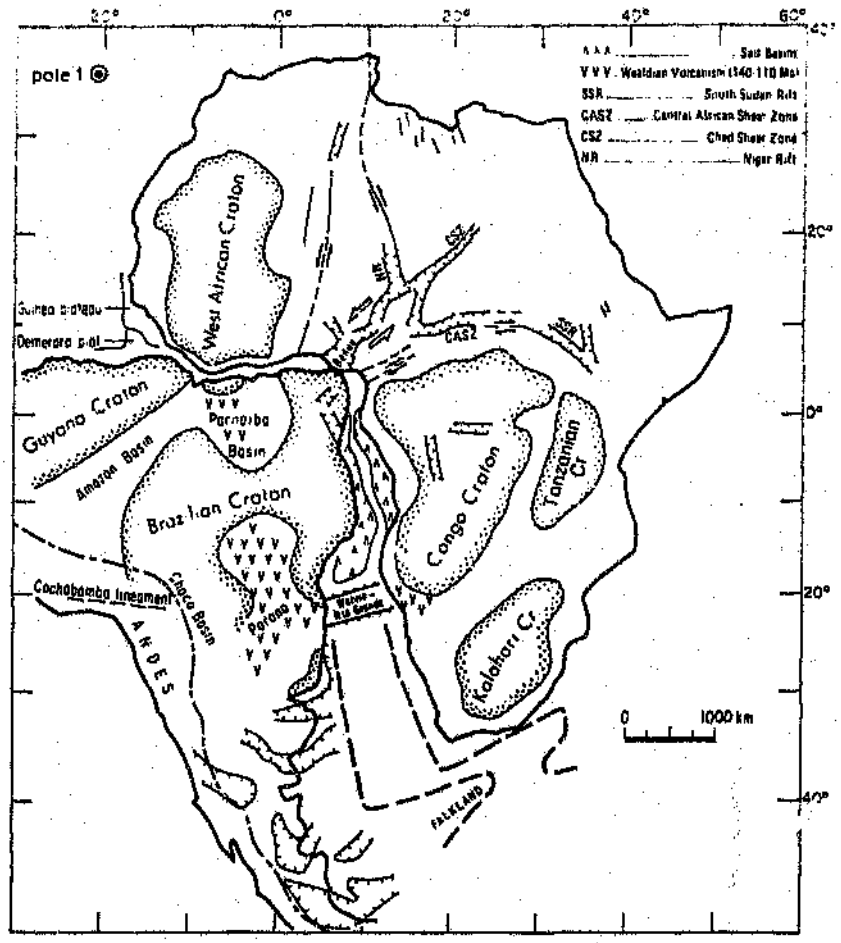

Figure 7.9: Palaeoreconstruction for the end of the Aptian (~ 100 Ma). (After Unternehr et al., 1988).

ample, the extensive Karoo basalts of South Africa spanning a period of 220-130 Ma with a peak at ca 190-180 Ma (de Wit et al., 1988). The Dufek intrusion (Fig. 7.10) has been associated with the voluminous basaltic rocks of the Ferrar Group, which occur throughout the Transantarctic Mountains and are of middle Jurassic age (170-180 Ma) (Ford and Kistler, 1980). Mafic magmatism of similar age occurs in the Theron Mountains in Coats Land (Brewer and Clarkson, 1987), and in western Dronning Maud Land in the Kirwanveggen (Harris et al., 1987) and Vestfjella areas (Peters, 1989). In this region the topographically defined Pencksökket is commonly interpreted as a failed rift (Barton et al., in press). Mid-to late-Jurassic rift-associated magmatism is also present in South Georgia, where the Drygalski Fjord complex has been interpreted to result from continental thinning and the formation of oceanic-type crust (MacDonald et al., 1987). Granitic rocks in the Ellsworth-Whitmore Mountains area have been dated at between 180-170 Ma and, have chemical signatures characteristf within-plate granite types (Storey et al., 1988b). He ascribes these granites to have an origin from "large-scale underplating of mafic magma and crustal melting in response to thermal disturbance in the Gondwanaland lithosphere related in some way to break-up of the supercontinent".

Antoine (1989), from previous Magsat data processed by the staff of the Hermanus Magnetic Observatory, interpreted the causative source of the Agulhas anomaly as an extensive slab of reversely magnetised ocean crust (based on the northern negative, southern positive anomaly pair). In order to explain the size of the magnetic source, together with its distinct palaeomagnetic signature, a geological model was required to generate a large volume of melt in a very short geological time span. The maximum reversed interval in the marine palaeomagnetic record (last 180 Ma and excluding the normal polarity epochs) is around 4 Ma (Harrison et al., 1986). Recent work by White et al. (1987) and White and McKenzie (1989) has suggested that a model of partial melting due to decompression during upwelling of hotter than normal asthenosphere may provide just such a mechanism. This model has been used by White and McKenzie (1989) to explain the occurence of large volumes of rift associated magmatism extruded over short (punctuated) time intervals. For example, the Deccan flood basalts in India and the flood basalts on the flanks of the North Atlantic Ocean.

The above model was favoured by Antoine (1989) as an appropriate mechanism in order

to explain an almost spontaneous geological event required to model the inferred distinct reversed palaeomagnetic signature of the causative source. That interpretation was consistent with independent geological, geomorphological (Cox, unpublished preprint) and geochemical evidence. Modelling in the present study contests the previously postulated reversely magnetised source of Antoine (1989).

An alternative remanent magnetisation vector compatible with KQZ inclinations is now modelled. The Southeast Atlantic anomaly is a newly recognised feature in Magsat anomaly data. An analysis of the inter-relationship between the magnetisation contrasts of these oceanic magnetic anomalies suggest that the Walvis Ridge and Agulhas anomalies may be ascribed to thickening of oceanic crust. The postulate that the Walvis Ridge was created by a hot spot or plume is generally accepted (see e.g. Morgan, 1971). The eastern Walvis Ridge is isostatically compensated at depth with a body of almost 2950 kg m^{-3}, possibly layer 3 (Goslin and Sibuet, 1975). Detrick and Watts (1979) believe that the presence of the Airy-type compensation (with similar observations made on the Ninetyeast Ridge) are a consequence of their formation on a lithosphere with little or no long-term bending strength; on a hot spot, for example. The similarities between the Walvis Ridge and the Agulhas Magsat anomalies suggest a common genesis.

It follows that the Agulhas Magsat anomaly may be the remnant 'scar' of an extensive region of the lithosphere with 'hotter' than normal asthenosphere, which initiated the break-up of Gondwana in this region. It seems rather fortuitous that the anomaly on a reconstruction of Gondwana underlies the most fragmented region at the triple junction of the South America, Africa and Antarctica plates. A model based on partial melting by decompression due to passive upwelling of hotter than normal asthenosphere in a rifted continental lithosphere is still favoured by the author as an appropriate mechanism. Such a model can account for: (1) the basaltic origin of the oceanward dipping reflectors off the continental margin of Queen Maud Land (Hinz and Krause, 1982), (2) the abundance of mafic and felsic magmatism (de Wit et al., 1988), (3) anatexis of continental crust (Storey et al., 1988b), (4) uplift in this region (unpublished apatite fission track ages 140-100 Ma from Dronning Maud Land and southern Africa, R.L. Brown and A.B. Moyes pers. comm.), (5) presence of continental fragments such as the southern Agulhas Plateau (Tucholke et al., 1981) and the Mozambique

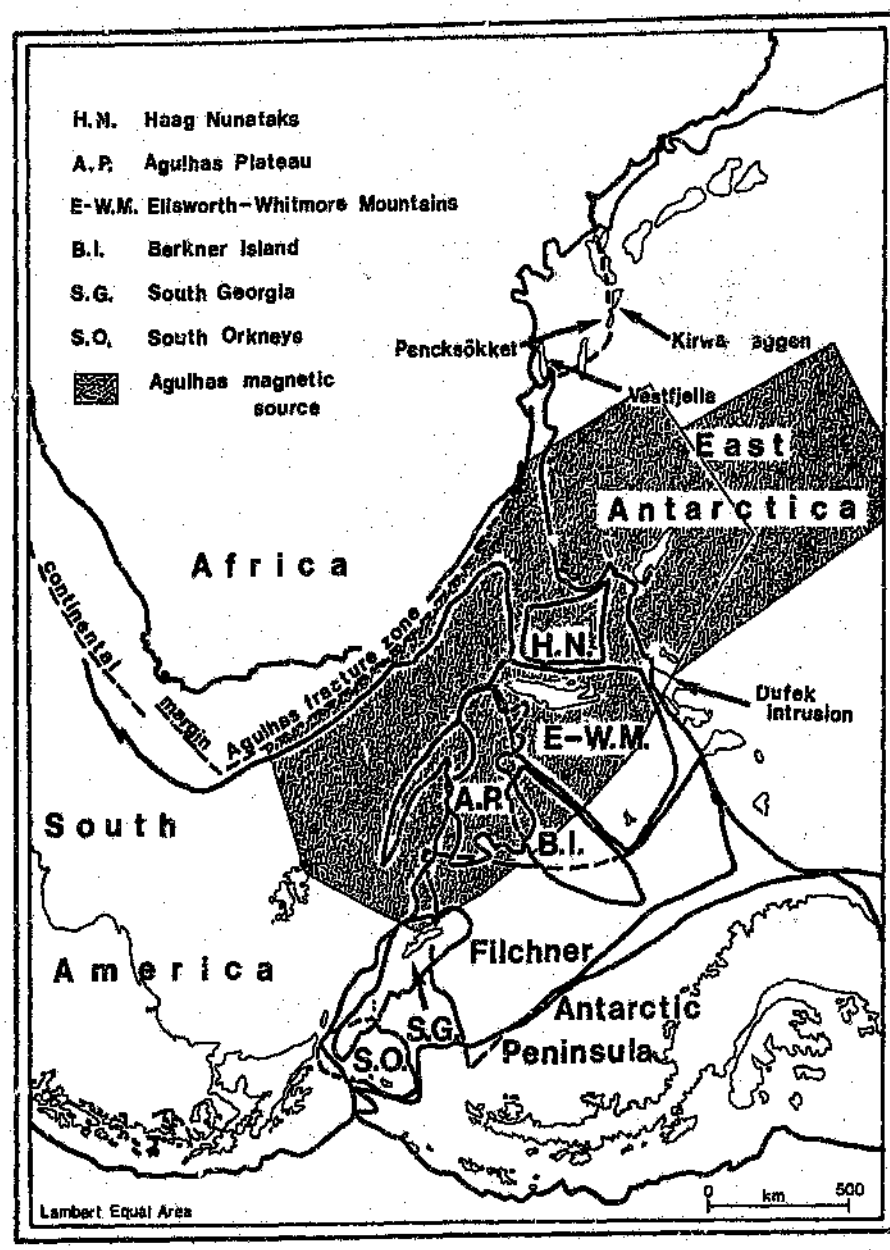

Figure 7.10: The Agulhas magnetic source in relation to prefragmented Gondwana.

Ridge (Doucoure and Bergh, 1990) and, (6) the thickening of the oceanic crust (Airy-type compensation).

Although the age of the Agulhas anomaly cannot be established directly, it has been shown to represent early Cretaceous oceanic crust. Rifting began at approximately 120-130 Ma (e.g. Cande et al., 1989; Martin and Hartnady, 1986; Rabinowitz and LaBrecque, 1979; Norton and Sclater, 1979) possibly as a consequence of uplift from a hotter than normal asthenosphere disturbing continental lithosphere at around 170 Ma, which is expressed as a major phase of magmatism, in this region, at that time. Smith and Drewry (1984) infer from fission track data that crustal uplift attains a maximum, 50 Ma after a thermal disturbance. This delayed response is consistent with the peak phase of magmatism in the region at ca 170 Ma and the begining of the separation of Gondwana at ca 120 Ma. It has also been shown in section 7.2.3 that the perimeters of the anomaly approximate an age of $\sim$ 100 Ma, a period just before the eastern tip of the Falkland Plateau passed beyond southern Africa. It is postulated that the Southwest Indian Ocean floor was created, from initial fragmentation to approximately 100 Ma, from a mantle that had little to no elastic strength and in consequence underwent Airy-type compensation. After $\sim$ 100 Ma the Southwest Indian oceanic crust no longer thickens and appears to maintain elastic strength.

The trend of the Southeast Atlantic anomaly may have some implications of relative motion between the South American and African plates during the early Cretaceous. It is proposed that the slight NNE trend of this anomaly, and the lack of a magnetic anomaly to the north of the Walvis Ridge anomaly, is consistent with a scissor-like opening of the South Atlantic fulcrumed on the Walvis ridge (Fig.7.9). This motion terminated at the end of the Albian (98 Ma) and assumed the present poles of rotation (see e.g. Norton and Sclater, 1979). A ridge jump is postulated by Barker (1979) at that time. Also, the Walvis Ridge shows its first discontinuity at approximately that period (Goslin and Sibuet, 1975) and it is congruent with the age of the perimeter of the Agulhas anomaly.

Chapter 8

Conclusions

The principal objectives of this thesis are (1) to research the processing of satellite magnetometer data towards extracting an improved lithospheric signal and, (2) to interpret the derived lithospheric anomaly map for the southern African region and surrounding oceans. To achieve the first objective, two aspects of the data reduction that have traditionally strongly compromised data quality are considered, viz.: (1) the variable altitude of the sensor and, (2) extracting the ionospheric field effects. The new methods are developed on synthetic data and later tested on Magsat data. The southern African region was selected for this purpose, and the resultant anomaly map interpreted in order to achieve the second objective.

Processing

Removal of the main and ring current field components of Magsat data is almost standard amongst investigators. Although these are not entirely satisfactory, they are adopted with some modification while attention is focussed on the more subjective aspects of the data reduction.

The main field component was removed using the truncated spherical harmonic model MGST 4/81 (Langel et al., 1981) provided with the INV-B tapes. The reduction adopted for the ring current effect was a first degree zonal spherical harmonic function (Langel and Sweeney, 1971) but modified (after Zaaiman and Kühn, 1986) by using dip latitudes calculated for altitudes of $3R_E$ rather than at the satellite's altitude. This approach was necessary to improve the model in the southern African region where dip latitudes asymptote to 65^0. The $3R_E$ model was an improvement but could be further improved. Coefficients for the

ring current model are based on a least squares solution. Solving for the ring current coefficients using a robust technique would, in the writer's opinion, improve the model and should constitute a basis for future research.

A solution has been found for the problem of the variable altitude and ionospheric field reductions. A procedure based on a robust linear regression (median linear regression) of amplitude versus altitude is developed (linearisation of the decay is achieved by taking the logarithm of an assumed exponential decay). The method assumes data redundancy for a given geographical location. This is achieved by considering a fairly large cell within which it is assumed that the horizontal gradients are negligible. At satellite altitudes this approximation is reasonable and is exploited. Computer simulations show that the algorithm is able recover the orginal signal in a large variable altitude range of 400 km (i.e. 200 - 600 km) even with additional severe signal corruption. This algorthim is utilised twice in data reduction procedures, using different latitudinal and longitudinal filter constraints. The two resultant maps are then used to remove ionospheric field effects using a two-dimensional data adaptive filtering technique. The method is based on the mean ionospheric field correction of Yanagisawa (1983) and is now extended to incorporate an altitude correction. Because the ionospheric field is time dependent it is defined by using a time constraint in data selection. The data are selected for two specific local times (0600 and 1800 hours). The lithosphere signal in comparison is defined geographically. Thus two sets of maps are generated, viz.:

- An ionosphere-contaminated lithospheric field. Achieved by applying the median linear regression algorithm for a specific geographical location and local time.
- A mean ionospheric field. Obtained by using the median linear regression algorithm for a specific local time without a geographical constraint. The procedure essentially randomises the lithosphere signal.

A new two-dimensional data adaptive filter is developed to extract the dawn or dusk lithosphere signals. The ionosphere-contaminated lithosphere and the ionosphere signals are input to the data adaptive filter. To optimise noise rejection the resultant two lithospheric field maps (i.e. dawn and dusk maps) are input to a data adaptive filter structure which results, by a method of converging operations, in a final lithospheric map.

The resultant dawn and dusk ionospheric field maps show unexpected correlation. This correlation is of long-wavelength features and is interpreted to represent residuals from an incomplete ring current correction. An added gain of the adopted processing procedures is that the inadequacies of the ring current correction become manifested in the ionospheric field map and are thus also removed from the contaminated lithosphere signal. The resultant lithospheric signal is technically improved from previous products in that: (1) the data are corrected to a common altitude datum by a procedure that makes no *a priori* assumptions of magnetisation, (2) the ionospheric field correction is objective, repeatable and, in addition, removes inadequacies of the ring current correction and, (3) greater structural detail and new north-south trending features are now evident. Also, an added gain is that the MIF preserves residuals from the core field separation, therefore, allowing removal of partially uncorrected core field effects. The reason for the lack of north-south structures in previously published satellite altitude magnetic anomaly maps may be linked to the arbitrary track-to-track corrections.

Interpretation

Southern Africa is surrounded by oceans and is a focal point in any reconstruction of Gondwana. For these reasons, this region was selected for analysis of the new processing techniques and for interpretation. The interpretation of the southern African continental Magsat anomalies shows a strong coincidence between these and tectonic provinces. The common geological factors of the tectonic provinces that could account for an increase in the volume-integrated crustal magnetisation, with respect to the Cratons, are: (1) an increase in crustal thickness (typically 32 to 42 km) and, (2) an increase in heat flow. Because the magnetic anomalies could be modelled without necessitating excessive crustal magnetisation contrasts at depth, being more consistent with expected values, the postulate of Wasilewski (1987), that the seismic Moho is also approximately the magnetic Moho other than where the Curie temperature is shallower, was adopted. The increase in crustal magnetisation by crustal thickening is insufficient to account for the observed magnetisation increase. However, crustal thickening coupled with a high heat flow places a large portion of the lower-crust into an effective window of magnetisation increase by the Hopkinson effect. Furthermore, these continental

tectonic provinces typically have deep-crustal electrical conductivity belts possibly due to deep crustal fluids. These fluids are likely to invoke serpentinisation of the mafic crustal rocks, hence an increase in magnetite.

The oceanic anomalies have provided an insight into the fragmentation history of Gondwana. To date there has been no evidence for an ocean to continent crustal magnetic contrast on the southwestern African coast where, because of the presence of KQZ ocean floor, it would be expected. This has been an artifact of past processing. The present anomaly map is now able to confirm the presence of such a magnetisation contrast, which coincides with the early Cretaceous ocean floor. The Walvis Ridge and the Agulhas anomalies are interpreted to represent remanent magnetisation of a thickened oceanic crust (20-30 km) assuming Airy-type compensation. It is proposed that the Agulhas anomaly is the remnant 'scar' of the process that led to the fragmentaion of Gondwana. A model of continental rifting in response to an upwelling of hotter than normal asthenosphere is consistent with the geophysical, geological and geochemical evidence.

Lastly, the trend of the Southeast Atlantic anomaly is believed to reflect a scissor-like opening of the South Atlantic, fulcrumed on the Walvis Ridge anomaly, which ended at ~100 Ma at which time poles of rotation between the South American and African plates changed abruptly.

Recommendations

The outcome of any research is, all too often, more work. Although, the processing of near-earth satellite data to extract the lithospheric signal has been improved, further improvements are possible, for example:

- An altitude correction using a median quadratic surface technique should improve the method further.
- Modelling of the ring current could be further improved by using an alternative to the least squares method.

More work is needed towards the problem of extracting the ionosphere signal. This can be achieved with an improved ring current model and by further work with data adaptive filters.

It must be emphasised that this study has focused on the scalar data and that some significant information is contained within the vector component data which could be exploited by data adaptive filter structures.

Further geophysical investigations of the Agulhas and Southeast Atlantic anomalies, in the form of surface wave dispersion and isostasy analyses (using long-wavelength filtering of Seasat data), is recommended. This information is necessary to test the postualte that a hotter than normal asthenosphere, centred on the Agulhas anomaly is responsible for the fragmentation of Gondwana.

In conclusion, the results of this thesis have made a small but important contribution both to the processing of near-earth satellite magnetometer data and towards understanding crustal magnetisation in the southern African region from such data. It must be reiterated that the resolution of magnetic data is a direct function of the source to sensor altitude. Magsat has been an entirely successful mission for both the liquid- and solid-earth geophysicists and has provided significant new input into the understanding of crustal magnetisation, geological processes and geodynamics. A decade has past since Magsat was launched. The detail that could be achieved by a lower altitude Magsat would revolutionise the geological sciences in terms of an understanding of geodynamic processes. Motivations for another lower altitude Magsat must continue unabated.

References

Abrams R., Gilson B., 1982. Magsat Investigator-B tape user's guide. NASA Technical Memorandum CSC/TM-82/6058.

Antoine L.A.G., 1989. A preliminary interpretation of the Agulhas Magsat anomaly. IAGA 6th Scientific Assembly, 24 July - 4 August, 1989, Exeter (UK).

Antoine L.A.G., Nicolaysen L.O., Niccol S.L., 1990. Processed and enhanced gravity and magnetic images over the Vredefort structure and their interpretation. Tectonophysics; 171: 63-74.

Arkani-Hamed J., 1988. Remanent magnetization of the oceanic upper mantle. Geophysical Research Letters; 15: 48-51.

Arkani-Hamed J., Strangway D.W., 1985. Intermediate-scale magnetic anomalies of the earth. Geophysics; 50: 2817-2830.

Arkani-Hamed J., Strangway D.W., Teskey D.J., Hood P.J., 1985. Comparison of Magsat and low-level aeromagnetic data over the Canadian Shield: implications for GRM. Canadian Journal of Earth Science; 22: 1241-1247.

Arnott F.W., 1989. New heat flow estimates for Australia and South Africa. South African Geophysical Association, First Technical Meeting, 29-30 June, 1989, Johannesburg.

Auzende J-M., Bideau D., Bonatti E., Cannat M., Honnorez J., Lagabrielle Y., Malavieille J., Mamaloukas-Frangoulis V., Mevel C., 1989. Direct observation of a section through slow-spreading oceanic crust. Nature; 337: 726-729.

Barker P.F., 1979. The history of ridge-crest offset at the Falkland-Agulhas fracture zone from a small-circle geophysical profile. Geophysical Journal of the Royal Astronomical Society; 58: 1-15.

Barker W., personal communication. Department of Geophysics, University of the Witwatersrand, Johannesburg, South Africa.

Barton J.M., Auret S.H., Copperthwaite Y.E., Elworthy T.P., in press. The Pènck-Jutulstraumen trough system, western Dronning Maud Land, Antarctica. In: Global Tectonics Through Time, Sychanthavong S.P. (editor).

Barrodale I., 1968. L_1 approximation and the analysis of data. Applied Statistics; 17: 51-57.

Benton E.R., Alldredge L.R., 1987. On the interpretation of the geomagnetic energy spectrum. Physics of the Earth and Planetary Interiors; 48: 265-278.

Bhattacharyya B.K., 1977. Reduction and treatment of magnetic anomalies of crustal origin in satellite data. Journal of Geophysical Research; 82: 3379-3390.

Bhattacharyya B.K., Chan K.C., 1977. Reduction of magnetic and gravity data on an arbitrary surface acquired in a region of high topographic relief. Geophysics; 42: 1411-1430.

Brewer T.S., Clarkson P.D., 1987. Mesozoic magmatism of Greater Antarctica: implications for Precambrian plate tectonics. 5th International Symposium on Antarctic Earth Sciences, 23-28 August, Cambridge.

Buddington A.F., Lindsley D.H., 1964. Iron-Titanium oxide minerals and synthetic equivalents. Journal of Petrology; 5: 310-357.

Cahen L., Snelling N.J., Delhal J., Vail J.R., Bonhomme M., Ledent D., 1984. The geochronology and evolution of Africa. Clarendon Press, Oxford.

Cain J.C., Sweeney R.E., 1973. The POGO data. Journal of Atmospheric and Terrestrial Physics; 35: 1231-1247.

Cain J.C., Wang Z., Schmitz D.R., Meyer J., 1989a. The geomagnetic spectrum for 1980 and core-crustal separation. Geophysical Journal; 97: 443-447.

Cain J.C., Wang Z., Kluth C., Schmitz D.R., 1989b. Derivation of a geomagnetic model to n=63. Geophysical Journal; 97: 431-441.

Campbell W.H., 1987. Some effects of quiet geomagnetic field changes upon values used for main field modeling. Physics of the Earth and Planetary Interiors; 48: 193-199.

Cande S.C., LaBrecque J.L., Larson R.L., Pitman W.C., Golorchenko X., Haxby W.F., 1989. Map of: Magnetic lineations of the world's ocean basins. American Association of Petroleum Geologists, Tulsa.

Chave A.D., 1979. Lithospheric structure of the Walvis Ridge from Rayleigh wave dispersion. Journal of Geophysical Research; 84: 6840-6848.

Cioffi J.M., 1987. Limited-precision effects in adaptive filtering. IEEE Transactions on Circuits and Systems; CAS-34: 821-833.

Clifford T.N., 1970. The structural framework of Africa. In: African magmatism and tectonics, T.N. Clifford and I.G. Gass (editors). Oliver and Boyd, Edinburgh.

Cohen Y., Menvielle M., Le Mouel J.L., 1986. Magnetic measurements aboard a stratospheric balloon. Physics of the Earth and Planetary Interiors; 44: 348-357.

Coles R.L., Haines G.V., Van Beek G.J., Nandi A., Walker J.K., 1982. Magnetic anomaly maps from 40 N to 83 N derived from MAGSAT satellite data. Geophysical Research Letters; 9: 281-284.

Corner, B., 1989. The Beattie anomaly and its significance for crustal evolution within the Gondwana framework. South African Geophysical Association, First Technical Meeting, 29-30 June, 1989, Johannesburg.

Corner B., 1983. An interpretation of the aeromagnetic data covering the western portion of the Damara orogen in South West Africa/Namibia. Special Publication of the Geological Society of South Africa; 11: 339-354.

Corner B., Cooper G., 1989. Crustal magnetite enrichment: a new dimension in mapping regional structure. SEG 59th Annual International Meeting and Exposition 29 October - 2 November, 1989, Dallas.

Corner B., Wilsher W.A., 1989. Structure of the Witwatersrand basin derived from interpretation of aeromagnetic and gravity data. Proceedings of Exploration '87, Ontario Geological Survey; Special Volume [illegible]

Corner B., Durrheim R.J., Nicolaysen L.O., 1990. [illegible]ish[illegible]een the Vredefort structure and the Witwatersrand basin wit[illegible]tectonic framework of the Kaapvaal craton as interpreted from regional g[illegible]ity and aeromagnetic data. Tectonophysics; 1[illegible] · 49-61.

Counil J-L., Achache J., 1987. Magnetization gaps associated with tearing in the Central America subduction zone. Geophysical Research Letters; 14: 1115-1118.

Coward M.P., 1983. The tectonic history of the Damaran belt. Special Publication of the Geological Society of South Africa; 11: 409-421.

Coward M.P., Fairhead J.D., 1980. Gravity and structural evidence for the deep structure of the Limpopo belt, southern Africa. Tectonophysics; 68: 31-43.

Cox K.G., (preprint). Mantle plumes and continental flood basalts: supporting evidence from drainage patterns. Submitted to Nature.

Dampney C.N.G., 1969. The equivalent source technique. Geophysics; 34: 39-53.

Darracott B.W., Kleywegt R.J., 1974. The structure of the southern portion of the Lebombo belt deduced from gravity data. Transactions of the Geological Society of South Africa; 77: 301-308.

De Beer J.H., Meyer R., 1984. Geophysical characteristics of the Namaqua-Natal belt and its boundaries, South Africa. Journal of Geodynamics; 1: 473-494.

De Beer J.H., Stettler E.H., 1988. Geophysical characteristics of the southern African continental crust. Journal of Petrology; Special Lithosphere Issue: 163-184.

Detrick R.S., Watts A.B., 1979. An analysis of isostasy in the world's oceans 3 aseismic Ridges. Journal of Geophysical Research; 84: 3637-3653.

De Wit M., Jeffrey M., Bergh H.W., Nicolaysen L.O., 1988. Geological map of sectors of Gondwana, reconstructed to their disposition - 150 Ma. American Association of Petroleum Geologists and University of the Witwatersrand, Johannesburg.

Didwall E.M., 1984. The electrical conductivity of the upper mantle as estimated from satellite magnetic field data. Journal of Geophysical Research; 89:537-542.

Doucoure M., Bergh H.W., (preprint). Crustal structure of the aseismic Madagascar and Mozambique Ridges from a geophysical profile along latitude 33^0 40' South. Submitted to Marine Geophysical Research.

Dunlop D.J., 1974. Thermal enhancement of magnetic susceptibility. Journal of Geophysics; 40: 439-451.

Durrheim R.J., 1990. A seismic investigation of the Kaapvaal craton. PhD thesis, University of the Witwatersrand, Johannesburg. pp.171.

Fairhead J.D., personal communication. Department of Geophysics, University of Leeds, Leeds.

Ford A.B., Kistler R.W., 1980. K-Ar age, composition and origin of Mesozoic mafic rocks related to the Ferrar Group in the Pensacola Mountains, Antarctica. New Zealand Journal of Geology and Geophysics; 23: 371-390.

Frey H., 1982. MAGSAT scalar anomaly distribution: the global perspective. Geophysical Research Letters; 9: 279-281.

Fullerton L.G., Frey H.V., Roark J.H., Thomas H.H., 1989a. Evidence for a remanent contribution in Magsat data from the Cretaceous Quiet Zone in the South Atlantic. Geophysical Research Letters; 16: 1085-1088.

Fullerton L.G., Roark J., Frey H., Thomas H., 1989b. Further evidence for a Cretaceous Quiet Zone TRM contribution to Magsat data over some Oceanic plateaus. Transactions of the American Geophysical Union; 70: 1065.

Garner W.R., Hake H.W., Eriksen C.W., 1956. Operationalism and the concept of perception. Psychological Review; 63: 149-159.

Goslin J., Sibuet J.C., 1975. Geophysical study of the easternmost Walvis Ridge, South Atlantic: deep structure. Geological Society of America Bulletin; 86: 1713-1724.

Gough D.I., 1989. Magnetometer array studies, earth structure, and tectonic processes. Reviews of Geophysics; 27: 141-157.

Graham K.W.T., Hales A.L., 1965. Surface-ship gravity measurements in the Agulhas Bank area, South of South Africa. Journal of Geophysical Research; 70: 4005-4011.

Grantham G.H., Groenewald P.B., Hunter D.R., 1988. Geology of the northern H.U. Sverdrupfjella, western Dronning Maud Land, and its implications for Gondwana reconstructions. South African Journal of Antarctic Research; 18: 2-10.

Green R.W.E., 1983. Seismic refraction observations in the Damara orogen and flanking craton and their bearing on deep seated processes in the orogen. Special Publication of the Geological Society of South Africa; 11: 355-367.

Green R.W.E., Durrheim R.J., (in press). A seismic refraction investigation of the Namaqualand metamorphic complex, South Africa. Journal of Geophysical Research.

Griffin W.L., O'Reilly S.Y., 1987. Is the continental Moho the crust-mantle boundary? Geology; 15: 241-244.

Gunn P.J., 1975. Linear transformations of gravity and magnetic fields. Geophysical Prospecting; 23: 300-312.

Hahn A., Ahrendt H., Meyer J., Hufen J-H., 1984. A model of magnetic sources within the earth' crust compatible with the field measured by the satellite Magsat. Geol. Jb. Hannover; A75: 125-156.

Hargreaves J.K., 1979. The upper atmosphere and solar-terrestrial relations. Van Nostrand Reinhold Berkshire, England; pp.298.

Harris C., Marsh J.S., Erlank A.J., Duncan A.R., 1987. Jurassic basalts of Dronning Maud Land and their significance for Gondwana reconstruction. 5th International Symposium on Antarctic Earth Science, 23-28 August, Cambridge.

Harrison C.G.A., Carle H.M., Hayling K.L., 1986. Interpretation of satellite elevation magnetic anomalies. Journal of Geophysical Research, 91: 3633-3650.

Hartmann O., Hoffer E., Haack U., 1983, Regional metamorphism in the Damara orogen: interaction of crustal motion and heat transfer. Special Publication of the Geological Society of South Africa ; 11: 233-241.

Hastings D.A., 1982. Preliminary correlations of MAGSAT anomalies with tectonic features of Africa. Geophysical Research Letters ; 9: 303-306.

Hattingh M., 1988. A new data adaptive filtering program to remove noise from geophysical time- or space-series data. Computers and Geosciences; 14: 467-480.

Hayling K.L., (preprint). Magnetic anomalies at satellite altitude over continent-ocean boundaries. Submitted to Tectonopysics.

Hayling K.L., Harrison C.G.A., 1986. Magnetization modeling in the north and equatorial Atlantic Ocean using Magsat data. Journal of Geophysical Research; 91: 12423-12443.

Henderson R.G., 1970. On the validity of the use of the upward continuation integral for total magnetic intensity data. Geophysics; 35: 916-919.

Henderson R.G., Cordell L., 1971. Reduction of unevenly spaced potential field data to a horizontal plane by means of finite harmonic series. Geophysics; 36: 856-866.

Hermance J.F., 1982. Model simulations of possible electromagnetic induction effects at MAGSAT activities. Geophysical Research Letters; 9: 373-376.

Hinz K., Krause W., 1982. The continental margin of Queen Maud Land/Antarctica: seismic sequences, structural elements and geological development. Geol. Jb. Hannover; E 23: 17-41.

Hodgkinson G.K., 1990. Palaeomagnetic studies in western Dronning Maud Land, Antarctica. MSc thesis, University of the Witwatersrand, Johannesburg.

Hones E.W., 1986. The earth's magnetotail. Scientific American; 254: 32-39.

Hudson J.E., 1981. Adaptive array principles. Peter Peregrinus, Exeter.

Hunter D.R., Pretorius D.A., 1981. In: Developments in Precambrian Geology 2, Precambrian of the Southern Hemisphere, D.R. Hunter (editor), Elsevier, Amsterdam.

Hyndman R.D., Shearer P.M., 1989. Water in the lower continental crust: modelling magnetotelluric and seismic reflection results. Geophysical Journal International; 98: 343-365.

Johnson B.D., 1985. Viscous remanent magnetization model for the Broken Ridge satellite magnetic anomaly. Journal of Geophysical Research; 90: 2640-2646.

Johnson B.D., Mayhew M.A., O'Reilly S.Y., Griffin W.L., Arnott F., Wasilewski P.J., 1986. Magsat anomalies, crustal magnetisation and heat flow in Australia. Poster 4th International Kimberlite Conference, Perth.

Jones M.Q.W., personal communication. Bernard Price Institute for Geophysical Research, University of the Witwatersrand, Johannesburg, South Africa.

Jones M.Q.W., 1987. Heat flow and heat production in the Namaqua mobile belt, South Africa. Journal of Geophysical Research; 92: 6273-6289.

Jones M.Q.W., 1988. Heat flow in the Witwatersrand Basin and environs and its significance for the South African shield geotherm and lithosphere thickness. Journal of Geophysical Research; 93: 3243-3260.

Justice J.H., Owsley N.L., Yen J.L., Kak A.C., 1985. Array signal processing, S.H. Haykin (editor). Prentice-Hall, New Jersey.

Kang G.S., Fransen L.J., 1987. Experimentation with an adaptive noise-cancellation filter. IEEE Transactions on Circuits and Systems; CAS-34: 753-758.

Kühn G.J., personal communication. Hermanus Magnetic Observatory, Hermanus, South Africa.

Kühn G.J., Zaaiman H., 1986. Long wavelength magnetic anomaly map for Southern Africa from Magsat. Transactions of the Geological Society of South Africa; 89: 9-16.

Langel R.A., Benson B.J., 1987. The Magsat bibliography. NASA Technical Memorandum 87822.

Langel R.A., Estes R.H., 1982. A geomagnetic field spectrum. Geophysical Research Letters; 9: 250-253.

Langel R.A., Sweeney R.E., 1971. Asymmetric ring current at twilight local time. Journal of Geophysical Research; 76: 4420-4427.

Langel R., Berbert J., Jennings T., Horner R., 1981. Magsat data processing: a report for investigators. NASA Technical Memorandum 82160.

Langel R.A., Phillips J.D., Horner R.J., 1982a. Initial scalar magnetic anomaly map from MAGSAT. Geophysical Research Letters; 9: 269-272.

Langel R.A., Ousley G., Berbert J., Murphy J., Settle M., 1982b. The MAGSAT mission. Geophysical Research Letters; 9: 243-245.

Lawver L.A., Scotese C.R., 1987. A revised reconstruction of Gondwanaland. In: Gondwana Six: structure tectonics and geophysics, G.D. MacKenzie (editor). American Geophysical Union, Washington D.C., British Antarctic Survey, Cambridge; Geophysical Monograph 40: 17-23.

Long G., Shwed D., Falconer D.D., 1987, Study of pole-zero adaptive echo canceller. IEEE Transactions on Circuits and Systems; CAS-34: 765-769.

Lötter C.J., personal communication. Rand Mines LTD., Johannesburg.

Lötter C.J., 1989. An investigation of Magsat data over South Africa. Anglo American Corporation of South Africa Report Ref:12/000/291/89/1306.

Lötter C.J., Zaaiman H., Kühn G.J., 1986. Methods to reduce satellite magnetic anomaly data to a common altitude - a comparison. 31st SAIP Conference, July, 1986, Johannesburg.

Lowes F.J., 1966. Mean-square values on sphere of spherical harmonic vector fields. Journal of Geophysical Research; 71: 2179-2179.

Lowes F.J., 1974. Spatial power spectrum of the main geomagnetic field, and extrapolation to the core. Geophysical Journal of the Royal Astronomical Society of London; 36: 717-730.

MacDonald D.I.M., Storey B.C., Thompson J.W., 1987. South Georgia. BAS GEOMAP Series, sheet 1, 1:250 000, geological map and supplementary text, Cambridge.

Maeda H., 1953. On the residual part of the geomagnetic Sq field in the middle and lower latitudes during the Interantional Polar Year, 1932-33. Journal of Geomagnetism and Geoelectricity; 5: 39-51.

Maeda H., Iyemori T., Araki T., Kamei T., 1982. New evidence of a meridional current system in the equatorial ionosphere. Geophysical Research Letters; 9: 337-340.

Maher M.J., Pitts B.E., 1989. Interpretation of a potential field profile over the Cape Fold Belt. South African Geophysical Association, First Technical Meeting, 29-30 June, 1989, University of the Witwatersrand, Johannesburg.

Martin A.K., Hartnady C.J.H., 1986. Plate tectonic development of the South West Indian Ocean: a revised reconstruction of East Antarctica and Africa. Journal of Geophysical Research; 91: 4767-4786.

Mayhew M.A., 1979. Inversion of satellite magnetic anomaly data. Journal of Geophysics; 45: 119-128.

Mayhew M.A., 1985. Curie isotherm surfaces inferred from high-altitude magnetic anomaly data. Journal of Geophysical Research; 90: 2647-2654.

Mayhew M.A., Estes R.H., Myers D.M., 1985. Magnetization models for the source of the "Kentucky anomaly" observed by Magsat. Earth and Planetary Science Letters; 74: 117-129.

Mayhew M.A., Galliher S.C., 1982. An equivalent layer magnetization model for the United States derived from MAGSAT data. Geophysical Research Letters; 9: 311-313.

Mayhew M.A., LaBrecque J.L., 1987. Crustal geologic studies with Magsat and surface magnetic data. Reviews of Geophysics; 25: 971-981.

Mayhew M.A., Johnson B.D., Langel R.A., 1980. An equivalent source model of the satellite-altitude magnetic anomaly field over Australia. Earth and Planetary Science Letters; 51: 189-198.

M[illegible]ew M.A., Johnson B.D., Wasilewski P.J., 1985. A review of problems and progress in studies of satellite magnetic anomalies. Journal of Geophysical Research; 90: 2511-2522.

Meyer J., Hufen J-H., Siebert M., Hahn A., 1983. Investigations of the internal geomagnetic field by means of a global model of the earth's crust. Journal of Geophysics; 52: 71-84.

Mikhael W.B., Hill P.D., 1988. Performance evaluation of a real-time TMS32010-based Adaptive noise canceller (ANC). IEEE Transactions on Acoustics Speech and Signal Processing; 36: 411-412.

Mikhael W.B., Wu F., Kang G., Fransen L., 1984. Optimum adaptive algorithms with applications to noise cancellation. IEEE Transactions on Circuits and Systems; CAS-31: 312-315.

Miller R.McG., 1983. The Pan-African Damara orogen of South West Africa/Namibia. Special Publication of the Geological Society of South Africa; 11: 431-515.

Monzingo R.A., Miller T.W., 1980. Introduction to adaptive arrays. John Wiley and Sons, New York.

Morgan W.J., 1971. Convection plumes in the lower mantle. Nature; 230: 42-43.

Mörner N-A., 1986. The lithospheric geomagnetic field: origin and dynamics of long wavelength anomalies. Physics of the Earth and Planetary Interiors; 44: 366-372.

Moyes A.B., personal communication. Bernard Price Institute for Geophysical Research, University of the Witwatersrand, Johannesburg, South Africa.

Narayan S.S., Peterson A.M., 1981. Frequency domain least-mean-square algorithm. Proceedings of the IEEE; 69: 124-126.

Nettleton L.L., 1976. Gravity and magnetics in oil prospecting. McGraw-Hill, New York.

Nicolaysen L.O., 1985. Renewed ferment in the earth sciences - especially about power supplies for the core, for the mantle and for crises in the faunal record. South African Journal of Science; 81: 120-132.

Nieminen A., Heinonen P., Neuvo Y., 1987. Median-type filters with adaptive substructures. IEEE Transactions on Circuits and Sysytems: CAS-34: 842-846.

Norton I., Sclater J.C., 1979. A model for the evolution of the Indian Ocean and the breakup of Gondwanaland. Journal of Geophysical Research; 84: 6803-6830.

Pankhurst R.J., 1982. Rb-Sr geochronology of Graham Land, Antarctica. Journal of the Geological Society of London; 139: 701-712.

Parker R.L., Klitgord K.D., 1972. Magnetic upward continuation from an uneven track. Geophysics; 37: 662-668.

Parkinson W.D., 1983. Introduction to geomagnetism. Scottish Academic Press, Edinburgh.

Peters M., 1989. Igneous rocks in western and central Neuschwabenland, Vestfjella and Ahlmannryggen, Antarctica. Petrograhy, geochemistry, geochronology, palaeomagnetism, geotectonic implications. AWI Berichte Zur Polarforschung; 61: 181.

Piper J.D.A., 1988. Palaeomagnetic database. Open University Press, Stoney, Stratford.

Press W.H., Flannery B.P., Teukolski S.A., Vetterling W.T., 1988. Numerical recipes in C. Cambridge University Press, New York.

Rabinowitz P.D., LaBrecque J., 1979. The Mesozoic South Atlantic ocean and evolution of its continental margins. Journal of Geophysical Research; 84: 5973-6002.

Reeves C.V., 1985. The Kalahari desert, central southern Africa: a case history of regional gravity and magnetic exploration. In: The Utility of Regional Gravity and Magnetic Anomaly Maps, W.J. Hinze (editor), Society of Exploration Geophysicists, Tulsa; 144-153.

Regan R.D., 1979. The reduction and analysis of satellite magnetometer data. Geophysical Surveys; 3: 331-349.

Regan R.D., Cain J.C., Davis W.M., 1975. A global magnetic anomaly map. Journal of Geophysical Research; 80: 794-802.

Regan R.D., Davis W.M., Cain J.C., 1973. The Bangui magnetic anomaly. Transactions of the American Geophysical Union; 54: 242.

Regan R.D., Rodriguez P., 1981. An overview of the external magnetic field with regard to magnetic surveys. Geophysical Surveys; 4: 255-296.

Ritzwoller M.H., Bentley C.R., 1982. MAGSAT magnetic anomalies over Antarctica and the surrounding oceans. Geophysical Research Letters; 9: 285-288.

Sadovski A.N., 1974. L_1-norm fit of a straight line. A[illegible]tatistics; 23: 244-248.

Sailor R.V., Lazarewicz A.R., Brammer R.F., 1982. Spatial resolution and repeatability of Magsat crustal anomaly data over the Indian Ocean. Geophysical Research Letters; 9: 289-292.

Schlinger C.M., 1985. Magnetization of the lower crust and interpretation of regional magnetic anomalies: example from Lofton and Vesterålen, Norway. Journal of Geophysical Research; 90: 11484-11504.

Schmitz D.R., Meyer J., Cain J.C., 1989. Modelling the earth's geomagnetic field to a high degree and order. Geophysical Journal; 97: 421-430.

Schnetzler C.C., Allenby R.J., 1983. Estimation of lower crust magnetization from satellite derived anomaly field. Tectonophysics; 93: 33-45.

Sheriff R.E., 1984. Encyclopedic dictionary of exploration geophysics (2nd edition). Society of Exploration Geophysicists, Tulsa.

Singh B.P., Agarwal A.K., Rastogi R.G., 1986. On the nature of residual trend in Magsat passes after removal of core and external components. Annales Geophysicae; 4: 653-658.

Singh B.P., Basavaiah N., Rajaram M., Geetharamanan G., 1989. A method of obtaining solutions with only positive dipole moments on inversion of satellite magnetic anomalies. Physics of the Earth and Planetary Interiors; 58: 95-102.

Smith A.G., Drewry D.J., 1984. Delayed phase change due to hot asthenosphere causes Transantarctic uplift? Nature; 309: 536-538.

Smith A.G., Hurley A.M., Briden J.C., 1981. Phanerozoic paleocontinental world maps. Cambridge University Press, Cambridge.

Stern D.P., 1988. Physics of the quiet magnetosphere. Reviews of Geophysics; 26: 781-781.

Storey B.C., Dalziel I.W.D., Garrett S.W., Grunow A.M., Pankhurst R.J., Vennum W.R., 1988a. West Antarctica in Gondwanaland: crustal blocks, reconstruction and breakup processes. Tectonophysics; 155: 381-390.

Storey B.C., Hole M.J., Pankhurst R.J., Millar I.L., Vennum W.R., 1988b. Middle Jurassic within-plate granites in West Antarctica and their bearing on the break-up of Gondwanaland. Journal of the Geological Society London; 145: 999-1007.

Stowe C.W., 1986. Synthesis and interpretation of structures along the north-eastern boundary of the Namaqua tectonic province, South Africa. Transactions of the Geological Society of South Africa; 89: 185-198.

Sugiura M., Hagan M.P., 1979. Geomagnetic Sq variation at satellite altitudes: is Sq corrections important in Magsat data analysis? Geophysical Research Letters; 6: 397-400.

Talwani M., 1965. Computation with the help of a digital computer of magnetic anomalies caused by bodies of arbitrary shape. Geophysics; 30: 797-817.

Tanner J.G., Gibb R.A., 1977. Gravity method applied to base metal exploration. In: Geophysics and geochemistry in the search for metallic ores, P.J. Hood (editor), Geological Survey of Canada, Economic Geology Report 31; 105-122.

Taylor P.T., Frawley J.J., 1987. Magsat anomaly data over the Kursk region, U.S.S.R. Physics of the Earth and Planetary Interiors; 45: 255-265.

Taylor P.T., Keating T., Kahn W.D., Langel R.A., Smith D.E., Schnetzler C.C., 1983. GRM: Observing the terrestrial gravity and magnetic fields in the 1990's. Transactions of the American Geophysical Union; 64: 609-611.

Taylor P.T., Schnetzler C.C., Regan R.D., 1989. Satellite magnetic data: how useful in exploration?. Geophysics: The Leading Edge; 8: 26-28.

Toft P.B., Haggerty S.E., 1986. A remanent and induced magnetization model of Magsat vector anomalies over the West African Craton. Geophysical Research Letters; 13: 341-344.

Toft P.B., Haggerty S.E., 1988. Limiting depth of magnetization in cratonic lithosphere. Geophysical Research Letters; 15: 530-533.

Tucholke B.E., Houtz R.E., Barrett D.M., 1981. Continental crust beneath the Agulhas plateau, Southwest Indian Ocean. Journal of Geophysical Research; 86: 3791-3806.

Turner F.J., 1968. Metamorphic petrology, mineral and field aspects. McGraw-Hill, New York.

Unternehr P., Curie D., Olivet J.L., Goslin J., Beuzart P., 1988. South Atlantic fits and intraplate boundaries in Africa and South America. Tectonophysics; 155: 169-179.

Van Zijl J.S.V., De Beer J.H., 1983. Electrical structure of the Damara orogen and its tectonic significance. Special Publication of the Geological Society of South Africa; 11: 369-380.

Vanyan L., Shilovski A., 1989. Fluids in the lower crust inferred from electromagnetic data. In: Properties and processes of the earth's lower crust, R.F. Mereu, S. Meuller, D.M. Fountain (editors), American Geophysical Union, Geophysical Monograph 51, IUGG; 6: 243-246.

von Frese R.R.B., personal communication. Ohio State University Columbus, U.S.A.

von Frese R.R.B., Hinze W.J., Braile L.W., 1981. Spherical earth gravity and magnetic anomaly analysis by equivalent point source inversion. Earth and Planetary Science Letters; 53: 69-83.

Von Frese R.R.B., Hinze W.J., Olivier R., Bentley C.R., 1987. Satellite magnetic anomalies and continental reconstructions. In: Gondwana Six: structure tectonics and geophysics, G.D. MacKenzie (editor). American Geophysical Union, Washington D.C., British Antarctic Survey, Cambridge; Geophysical Monograph 40: 9-14.

Wasilewski P.J., 1987. Magnetic properties of mantle xenoliths and the magnetic character of the crust-mantle boundary. In: Mantle Xenoliths, P.H. Nixon (editor). John Wiley & Sons, Chichester.

Wasilewski P.J., Thomas H.H., Mayhew M.A., 1979. The Moho as a magnetic boundary. Geophysical Research Letters; 6: 541-544.

Wasilewski P., Mayhew M.A., 1982. Crustal xenolith magnetic properties and long wavelength anomaly source requirements. Geophysical Research Letters; 9: 329-332.

Watts D.R., Bramall A.M., 1981. Palaeomagnetic evidence for a displaced terrain in Western Antarctica. Nature; 293: 638-641.

Webster W.J., Taylor P.T., Schnetzler C.C., Langel R.A., 1985. The magnetic field of the Earth: performance considerations for space-based observing systems. IEEE Transactions on Geoscience and Remote Sensing; GE-23: 541-551.

Veijermars R., 1989. Global tectonics since the breakup of Pangea 180 million years ago: evolution maps and lithospheric budget. Earth-Science Reviews; 26: 113-162.

Wendorff L., personal communication. Institut Für Geophysik der Universität Göttingen, FRG.

White R.S., McKenzie D.P., 1989. Volcanism at rifts. Scientific American; 260: 44-55.

White R.S., Spence G.D., Fowler S.R., McKenzie D.P., Westbrook G.K., Bowen A.N., 1987. Magmatism at rifted continental margins. Nature; 330: 439-444.

Widrow B., McCool J.M., Larimore M.G., Johnson C.R., 1976. Stationary and nonstationary learning characteristics of the LMS adaptive filter. Proceedings of the IEEE; 64: 1151-1162.

Widrow B., Stearns S.D., 1985. Adaptive signal processing. Prentice-Hall, New Jersey.

Winkler H.G.F., 1974. Petrogenesis of metamorphic rocks. Springer-Verlag, New York.

Wilsher W.A., de Wit M.J., Marrao E., 1989. A GIS solution for Gondwana geoscientific data. Journal of African Earth Sciences; 9: 371-374.

Wyllie P.J., 1980. The origin of Kimberlite. Journal of Geophysical Research; 85: 6902-6910.

Yanagisawa M., 1983. Derivation of crustal magnetic anomalies from Magsat. DSc thesis, University of Tokyo, Tokyo.

Yanagisawa M., 1984. Derivation of crustal magnetic anomalies from MAGSAT. The Institute of Space and Astronautical Science Report 609.

Yanagisawa M., Kono M., 1984. Magnetic anomaly maps obtained by means of the mean ionospheric field correction. Journal of Geomagnetism and Geoelectricity; 33: 417-441.

Yanagisawa M., Kono M., 1985. Mean ionospheric field correction for Magsat data. Journal of Geophysical Research; 90: 2527-2536.

Yionoulis S.M., Piscane V.L., 1985. Geopotential Research Mission: status report. IEEE Transactions on Geoscience and Remote Sensing; GE-23: 511-516.

Zaaiman H., Kühn G.J., 1986. The application of the ring current correction model to Magsat passes. Journal of Geophysical Research; 91: 8034-8038.